1-1-2014

Prediction of Transitional Boundary Layers and Fully Turbulent Free Shear Flows, using Reynolds Averaged Navier-Stokes Models

Maurin Alberto Lopez Varilla

Prediction of transitional boundary layers and fully turbulent free shear flows, using Reynolds averaged Navier-Stokes models

By

Maurin Alberto Lopez Varilla

A Dissertation
Submitted to the Faculty of
Mississippi State University
in Partial Fulfillment of the Requirements
for the Degree of Doctor of Philosophy
in Computational Engineering
in the Bagley College of Engineering

Mississippi State, Mississippi

August 2014

Prediction of transitional boundary layers and fully turbulent free shear flows, using

Reynolds averaged Navier-Stokes models

By

Maurin Alberto Lopez Varilla

Approved:

_____

D. Keith Walters
(Major Professor)

_____

David S. Thompson
(Minor Professor)

_____

Ioana Banicescu
(Committee Member)

_____

Seongjai Kim
(Committee Member)

_____

Pasquale Cinnella
(Graduate Coordinator)

_____

Jason Keith
Interim Dean
Bagley College of Engineering

Name: Maurin Alberto Lopez Varilla

Date of Degree: August 10, 2014

Institution: Mississippi State University

Major Field: Computational Engineering

Major Professor: D. Keith Walters

Title of Study: Prediction of transitional boundary layers and fully turbulent free shear flows, using Reynolds averaged Navier-Stokes models

Pages in Study: 105

Candidate for Degree of Doctor of Philosophy

One of the biggest unsolved problems of modern physics is the turbulence phenomena in fluid flow. The appearance of turbulence in a flow system is regularly determined by velocity and length scales of the system. If those scales are small the motion of the fluid is laminar, but at larger scales, disturbances appear and grow, leading the flow field to transition to a fully turbulent state. The prediction of transitional flow is critical for many complex fluid flow applications, such as aeronautical, aerospace, biomedical, automotive, chemical processing, heating and cooling systems, and meteorology. For example, in some cases the flow may remain laminar throughout a significant portion of a given domain, and fully turbulent simulations may produce results that can lead to inaccurate conclusions or inefficient design, due to an inability to resolve the details of the transition process. This work aims to develop, implement, and test a new model concept for the prediction of transitional flows using a linear eddy-viscosity RANS approach. The effects of transition are included through one additional transport equation for v^2 as an alternative to the Laminar Kinetic Energy (LKE) framework. Here v^2 is interpreted as the energy of fully turbulent, three-dimensional velocity fluctuations.

This dissertation presents two new single-point, physics-based turbulence models based on the transitional methodology mentioned above. The first one uses an existing transitional model as a baseline which is modified to accurately capture the physics of fully turbulent free shear flows. The model formulation was tested over several boundary layer and free shear flow test cases. The simulations show accurate results, qualitatively equal to the baseline model on transitional boundary layer test cases, and substantially improved over the baseline model for free shear flows. The second model uses the SST $k-\omega$ fully turbulent model and again the effects of transition are included through one additional transport equation for v^2. An initial version of the model is presented here. Simplicity of the formulation and ease of extension to other baseline models are two potential advantages of the new method.

DEDICATION

To my mother, father and sister, thank you for believing in me; for allowing me to further my studies. Do not ever doubt my dedication and love for you.

To my wife, whose love and confidence is a constant source of inspiration and encouragement.

To all my family, I'm the first one but I hope not to be the last one.

ACKNOWLEDGEMENTS

I have to begin by expressing my deepest appreciation to my major professor, Dr. Keith Walters, any word will be short for expressing my gratitude and admiration for such a wonderful mentor. Thank you for all your help and support during these years.

I thank my committee members for their contributions on this dissertation. In addition, I would like to thank the Center for Advanced Vehicular Systems for providing financial support and facilities for this research effort.

I feel compelled to thank my friends in Starkville. They became family far from home.

Thanks to my family in Colombia for their invaluable love and support.

Finally, I want to thank my wife Katerine. Congratulations, because this accomplishment belongs to you as well.

TABLE OF CONTENTS

LIST OF TABLES

LIST OF FIGURES

LIST OF NOMENCLATURE

d = wall distance

p = Pressure

Re = Reynolds number

n = Number of mesh points per unit length of the large scales

τ_{ij} = Reynolds stress tensor

k_L = Laminar kinetic energy

k = Turbulent kinetic energy

ω = Inverse turbulence time-scale

ν = Kinematic viscosity

ν_T = Turbulent viscosity

τ = Turbulent time scale

t = time

CHAPTER I

INTRODUCTION

Introduction to turbulence modeling

One of the fundamental features of fluid mechanics in real world applications is the presence of turbulence. The appearance of turbulence in a flow system is usually determined by the Reynolds number which is defined by the characteristic velocity and length scales of the system, if those scales are small enough the motion of the fluid is laminar, but at larger Reynolds numbers, disturbances appear and grow, leading the flow field to transition to a fully turbulent state. The prediction of transitional flow is critical for many complex fluid flow applications, such as, aeronautical, aerospace, biomedical, and automotive. For example, in some cases the boundary layer may remain laminar throughout a significant portion of a given domain, and fully turbulent simulations may produce results that can lead to inaccurate conclusions or inefficient design, due to an inability to resolve the details of the transition process. In order to address this problem, it is first noted that the motion of Newtonian fluids in any engineering application is fully described by the Navier-Stokes equations together with the equation for conservation of mass. With **u** being the vector of velocities, p the pressure, t the time and ν the kinematic viscosity and assuming incompressibility the equations are

$$\frac{\partial u}{\partial t} + (u \cdot \nabla)u = -\nabla p + \nu \Delta u$$
$$\nabla \cdot u = 0 \tag{1.1}$$

This is a set of non-linear partial differential equations for which unfortunately there is not a closed form mathematical expression for the solution. This fact (together with the importance of turbulence in current engineering applications) is the engine of the exponential growing of computer simulations in this field. Computational fluid dynamics (CFD) is currently used in a wide variety of application areas such as chemical processing, heating and cooling systems, meteorology, and marine systems, providing good results in research and industrial processes. Despite significant progress in CFD regarding robust mathematical algorithms and computational power, the accurate and realistic prediction of transitional flows still remains as one of the principal weaknesses in CFD applications [39]. Simulations of fluid motion go from the simplest (computationally inexpensive) algebraic models to the most accurate results (computationally intensive) of Direct Numerical Simulations (DNS). The evolution of categories for the solutions of the Navier-Stokes equation can be summarized as follows (in order of decreasing complexity):

- DNS
- Large Eddy Simulations (LES)
- Reynolds Averaged Navier-Stokes Models (RANS)
    - Reynolds stress transport models
    - Non-linear eddy viscosity models
    - Linear eddy viscosity models

Direct Numerical Simulations (DNS), Large Eddy Simulations (LES), and Reynolds Averaged Navier-Stokes (RANS) are the most widely used techniques in CFD simulations. Of these three categories, each has advantages as well as limitations. For example, DNS provides the most accurate predictions but it is computationally intensive [40]. While LES is less expensive than DNS and performs well in separated flow regions, it requires immense computational resources in the near-wall region to get accurate results. RANS is the least expensive and generally shows good near-wall prediction capabilities but exhibits poor performance in regions of separated flow. Recent efforts to exploits the benefits of LES models far from the wall and the good near-wall results of RANS models have lead to a new set of hybrid RANS-LES models (HRL), examples of these types of models are presented in [41-44]

DNS and LES

Turbulent flow is dominated by instabilities and apparently random or chaotic motions. This behavior can be view as statistical fluctuations of all flow field variables (velocity, pressure, density, temperature, etc.) around their mean values. This random behavior makes turbulent flow difficult to predict. However, these fluctuations can be computed numerically using DNS or with some degree of approximation using LES. DNS involves a process where the equations (1.1) are computationally solved without any modeling (modifications) of their terms. With DNS all the spatial and time scales of the flow are solved, from the smallest (Kolmogorov) scales up to the largest scales of the flow field. This approach provides the most accurate results, which are in theory comparable with experimental data. DNS are of great value, because they can provide accurate numerical solutions (provided accurate numerical methods are used) of the

equations of fluid motion, which is also the final purpose of this project. However, when using DNS one needs to consider (besides the numerical accuracy) the accurate inclusion of boundary and initial conditions [29], but the most problematic aspect of this type of simulations is the large amount of computational power needed even for simple simulations due to the resolution of all scales of turbulence. To illustrate the problem, consider that the size of the smallest eddies (the Kolmogorov scales) is inversely proportional to $\mathrm{Re}^{3/4}$, also if n is the number of points per unit length of the smallest eddies, the total number of mesh points required, and the number of arithmetic operations per time step will scale with $n^3\,\mathrm{Re}^{9/4}$. Because integration in time is also required, with a time step determined by the smallest turbulent time scales, then, in the best cases, the computational effort for DNS simulations is proportional to Re^3. This means that increasing the Reynolds number by a factor of 10, requires an increase in the computational power of at least 1000 and by a factor $10^{9/4} = 178$ for the memory requirements [28].

In contrast to DNS, LES model belongs to the category of approximation models, which means that when using LES models, one is not actually solving the Navier-Stokes equations directly, but instead a modification or approximation of them. For LES, a new set of equations is obtained after applying a filtering operation to the original equations. The smallest scales, i.e., from the Kolmogorov scales to a certain threshold, are modeled and the remaining large-scale turbulent fluctuations are directly simulated. However, even though LES resolves only a part of the scale from the full cascade, it can be shown that if n is the number of points per unit length of the large scales directly simulated,

then the number of arithmetic operations will scale with $n^3 \, \mathrm{Re}^{3/4}$, and similar to above, due to the time integration, the total simulation effort scales with $\mathrm{Re}^{9/4}$. Despite the lower values of computational effort compared with DNS, LES is still computationally intensive for high Reynolds number flow. Due to the computational limitations, DNS and LES methods will not be feasible for industrial applications in the near future, moreover, according to Spalart [45] DNS and LES will be ready for realistic industrial applications around 2080 and 2045, respectively.

Reynolds averaged Navier-Stokes equations

From the previous sections, the advantages of using DNS and LES to attack a turbulence simulation problem are apparent. At the same time, it is clear that there are significant computational limitations when using those approaches, and because of that, DNS and LES are not always the best options to model complex applications. Fortunately there is a large family of RANS models, which have been proven to be reasonably accurate using very low computational resources compared with LES. Because of this balance between accuracy and computational cost, RANS models are the most used models in industry for practical CFD simulations. RANS models are based on the concept of decomposition of instantaneous flow variables into a combination of a mean (or average) component and a fluctuating component (Reynolds decomposition), which can be written as

$$\begin{aligned} u &= \bar{u} + u' \\ p &= \bar{p} + p' \end{aligned} \tag{1.2}$$

where the overbar represents the averaging operator, $\overline{m}$ is Reynolds averaged value and m' is the fluctuating component of the arbitrary representative variable m. Substituting equations (1.2) into equations (1.1), and applying the averaging operation to the equations, the Reynolds averaged equations of motion are obtained, which can be expressed in index notation as

$$\rho \frac{\partial \overline{u}_i}{\partial t} + \rho \overline{u}_i \frac{\partial \overline{u}_i}{\partial x_j} = -\frac{\partial \overline{p}}{\partial x_j} + \frac{\partial}{\partial x_j}(2\mu \overline{s}_{ij} - \rho \overline{u'_j u'_i})$$
$$\frac{\partial \overline{u}_i}{\partial x_j} = 0. \tag{1.3}$$

The previous set of equations is known as the Reynolds averaged Navier-Stokes equations (RANS), and they are completely written in terms of mean values, except for the term $-\rho \overline{u'_j u'_i}$ which is known as the Reynolds-stress tensor, and which is usually denoted by $\rho \tau_{ij}$ so that $\tau_{ij} = -\overline{u'_j u'_i}$. The Reynolds-stress tensor is a symmetric tensor, which is composed of six new unknown variables (due to symmetry) for three-dimensional flows. Therefore, as a result of the averaging process, for three-dimensional cases, there are ten unknowns for the four equations in (1.3). This discrepancy between the number of equations and the number of variables is known as the closure problem of turbulence.

Linear eddy viscosity models

It was stated in the previous section that DNS and LES are often not practical for simulations with high Reynolds numbers or complex geometries. Also, in the previous

section, the Reynolds decomposition was introduced, producing new unknowns to the system. This leads to the closure problem of turbulence model theory.

The purpose of RANS turbulence modeling is to produce approximations for the unknown quantities that inevitably appear after the averaging process due to the nonlinear nature of the Navier-Stokes equations. These approximations must be presented in terms of flow variables that are present already in the original set of equations. This closes the system.

One approach to develop models is based on the Boussinesq hypothesis, which states that the Reynolds stress tensor τ_{ij} is linearly proportional to the mean strain rate tensor. The mathematical formulation for this assumption is:

$$\tau_{ij} = 2\mu_T \bar{s}_{ij} - \frac{2}{3} k \delta_{ij} \tag{1.4}$$

where μ_T is a scalar quantity called eddy viscosity and k is the turbulent kinetic energy defined as

$$k = \frac{1}{2}\left(\overline{u'^2} + \overline{v'^2} + \overline{w'^2}\right) = \frac{1}{2}\overline{u_i' u_i'} \tag{1.5}$$

As a result, instead of the six unknown variables in the Reynolds stress tensor, the closure problem has been reduced to two scalar unknowns: the eddy viscosity and the turbulent kinetic energy. Moreover, it is possible to derive a transport equation for k and add this equation to (1.3), thus there is only one variable left to calculate in order to close the system. The exact derivation of the equation for k can be found in the open literature and is given by

$$\frac{Dk}{Dt} = \underbrace{-\overline{u_i' u_j'}\frac{\partial \bar{u}_i}{\partial x_j}}_{\text{Production } P} \underbrace{-\nu\overline{\frac{\partial u_i'}{\partial x_j}\frac{\partial u_i'}{\partial x_j}}}_{\text{Dissipation } \varepsilon} + \underbrace{\nu\frac{\partial^2 k}{\partial x_j^2}}_{\text{Molecular viscous trasnsport}} \underbrace{-\frac{1}{2}\frac{\partial \overline{u_j' u_j' u_i'}}{\partial x_i}}_{\text{Turbulent transport}} \underbrace{-\frac{1}{\rho}\frac{\partial \overline{p' u_i'}}{\partial x_i}}_{\text{Pressure diffusion}} \tag{1.6}$$

where the term in the left hand side of equation (1.6) is the mean-flow material derivative of turbulent kinetic energy. The terms in the right hand of equation (1.6) are the production P and dissipation rate of turbulent kinetic energy ε, the viscous diffusion, and two turbulent transport terms. Note that the last 2 terms in equation (1.6) are also unknown terms produced by fluctuating parts of the velocity and pressure. In practical applications those terms are also modeled by quantities that only include mean flow variables. The dissipation per unit mass ε and the turbulent kinetic energy k are the most common variables used in RANS turbulence models.

Finally, the eddy viscosity μ_T is the only quantity left in this set of equations which does not have a clear method of calculation or approximation, therefore, linear eddy viscosity models arise from the different ways to calculate μ_T, generally in terms of variables like k and ε for which model transport equations can be derived.

RANS turbulence models

Fully turbulent models

Two-equation models are the most commonly used for industry applications. They usually involve the variables k, ε and/or ω. The specific dissipation rate ω is usually defined in terms of the turbulence dissipation ε. A common expression is $\omega = \frac{\varepsilon}{Ck}$, where C is a constant which can changes from model to model. The landmark model in this category is the $k-\varepsilon$ model of Jones and Launder [67], followed by a

variety of two-equation models based on the k equation and an additional transport equation for a second turbulent quantity such as the $k-\omega$ [70], the $k-\tau$ [69] and the $k-\nu_T$ [68] models, where τ , the turbulent time scale, is defined as $\tau = \frac{1}{\omega}$, and $\nu_T = \frac{\mu_T}{\rho}$ is the kinematic eddy viscosity. The $k-\varepsilon$ and $k-\omega$ models, are the most used models by the scientific and industrial community. However, the basic $k-\varepsilon$ model has two major acknowledged problems associated with it: the lack of natural boundary conditions for the dissipation rate and the sensitivity to large adverse pressure gradients [69,29]. The $k-\omega$ model can alleviate these problems since the asymptotic behavior of ω is known in more detail. For the interested reader, detailed discussions of these models may be found in [29, 30].

Laminar-to-turbulent transitional models

Two-equation models were initially developed to predict only fully turbulent flows, but in recent years they have been improved to include transition-sensitive capabilities, an important feature in many practical applications. Transition-sensitive RANS models can usually be classified as either correlation-based [1], [31,32] or physics-based [4,5]. Correlations are obtained (for the first approach) from experimental data in simple geometries and flow conditions. Researchers also assume instantaneous flow transition in a particular location or they incorporate a transition zone, generally based on the universal intermittency profile of Dhawan and Narasimha [33]. However some of these models need additional information that make difficult their implementation into general purpose Computational Fluid Dynamics (CFD) codes,

especially for complex three-dimensional geometries. An example of this is the data correlation proposed in [31]

$$R_{\theta tr} = 163 + e^{6.91 - Tu} \tag{1.7}$$

where Tu , is the turbulent intensity. In this case transition is setup to initiate at the location where the local momentum thickness Reynolds number is larger than the above value. Therefore, in order to initiate transition, it is necessary to calculate the momentum thickness Reynolds number, which needs several mesh cells in the domain for its calculation. That feature makes the model more difficult to implement in general CFD codes.

Recent approaches use additional transport equations to include the transitional capability to the fully turbulent models using empirical correlations in a more general fashion, examples are presented in [1,2]. In this case, the models take advantage of the information given by the evolution of the flow field to predict transition zones.

Several new models have focused on the single-point approach, including the phenomenological models in [4,5] and [23]. Single-point models represent the easiest way to implement laminar, transition and turbulent flow prediction capability into general purpose CFD codes. One popular approach in this group of physic-based models is the adoption of an additional transport equation for laminar kinetic energy (LKE), used to represent pre-transitional, non-turbulent velocity fluctuations which lead to transition and fully turbulent flow [4].

Final remarks

The big picture is clear for CFD simulations of turbulent flow. There are three primary modeling techniques used in research and industrial problems involving turbulent flows.

In the DNS method [40], the Navier-Stokes equations are solved directly without using any turbulence modeling. As all spatial and time scales of turbulence must be resolved, the DNS method provides results theoretically as accurate as experiments but requires immense computational resources. Spatially, it requires resolving the smallest Kolmogorov scale up to the largest integral scale of flow domain. Hence, the computational cost increases with increasing Reynolds number. Due to its computational limitation, the DNS method will not be feasible for industrial applications in the near future [45].

LES models [46] apply filtering operations to the Navier-Stokes equations to achieve resolved solutions of the large turbulent scales most responsible for momentum and energy transfer. LES models perform well in separated flow regions as they are capable of resolving the largest scales of turbulence that dominate momentum and energy transfer in the flow field. Near wall performance of the LES model is poor and requires a large amount of computational resources in the near wall region. As LES only resolves the larger turbulent scales and models the smaller scales, it requires significantly less computational resources than the DNS; but, it is still computationally intensive for high Reynolds number flows [47].

In the RANS modeling approach [48], the Navier-Stokes equations are averaged and all turbulent scales are modeled. Only the mean values of the flow variables are

resolved in this approach. RANS is based on empirical or at least semi-empirical information and thus resolves, in theory, less physics in comparison to DNS and LES models. As it models all spatial and time scales, the RANS modeling approach requires the least computational resources, which is the primary reason that RANS models are the most widely used in industrial applications. RANS models perform well in the near wall region due to the universality of the flow physics in the boundary layer, but they have practical limitations in separated flow regions. In theory, the Reynolds averaging process does not produce a loss of information [22]. Wang and Perot in [22] consider that the Reynolds stress tensor contain all the necessary information to accurately resolve the mean flow field, thus, any turbulence model that can model correctly the different components of the Reynolds stress tensor, should provide accurate results, for the case of either fully turbulent or transitional flow.

CHAPTER II

MOTIVATION, CONTRIBUTIONS AND OBJECTIVES

Motivation

Due to the computational constraints inherent in DNS and LES, linear-eddy viscosity RANS models are still the preferred option for industrial applications; at the same time, our lack of knowledge about the underlying physics of turbulence impacts the accuracy and range of applicability of RANS models. For instance, there is no turbulence model generally considered by the research and applications communities as a superior alternative compared with the others. For example, models in [20] and [21] are capable of predicting fully turbulent flows, but unable to capture the transition process, but transitional models such as [4] and [5] do not perform as well as [20] for free shear flows as evidenced by [22].

RANS models remain popular as a result of the potential balance between accuracy and computational efficiency, therefore the number of RANS models that seek to incorporate more complex physics has increased in recent years. As more capabilities are added to RANS models in the form of enhanced methods for complex physical mechanisms (curvature, transition, etc.), they are likely to become even more useful to the industrial and scientific communities. While DNS and LES approaches will increasingly provide high-fidelity analysis capability, there seems little doubt that RANS model development will continue for the foreseeable future.

Objectives

Three main objectives are proposed in this research effort:

- The introduction and description of a new methodology to describe the transition process in the RANS framework, as an alternative to the laminar kinetic energy concept. In this methodology the energy in the wall normal fluctuation is used to initiate and control the transition process.
- In addition to the first item, two phenomenological RANS linear eddy-viscosity transitional models adopting the new methodology are developed:
  - The first model is an improved version of the $k_T - k_L - \omega$ transitional model developed by Walters and Cokljat in [5]. The baseline model [5] is modified to improve the behaviour of the model in [5] for free shear layer flows such as jets, wakes, and mixing layers.
  - The second model uses the fully turbulent shear stress transport (SST) $k - \omega$ model developed by Menter in [21] as a baseline and includes the effects of transition through an additional transport equation for the wall normal velocity fluctuations that represents the energy of the fully turbulent three-dimensional velocity fluctuations. The simplicity in its mathematical formulation is the main advantage of this model.

Contributions

One transition methodology is evaluated and reinterpreted in order to describe the laminar-to-turbulent transition process in a more physically correct sense than the one proposed by the laminar kinetic energy concept. Walters [5] states that one of the primary difficulties when developing phenomenological RANS turbulence models is that the physics of transition is not entirely understood and indeed is an active area of research in itself.

The new methodology described in this document seeks to improve the understanding and hence the implementation of new phenomenological RANS-based transitional models. It is expected that new models can be developed (in addition to the two models presented in this document) that make used of the proposed methodology.

The $k_T - k_L - \omega$ transitional model developed by Walters and Cokljat in [5] has achieved wide acceptance due to its easy to implement nature and reasonable accuracy in resolving transitional flows. Nevertheless, there are references such as [22] and [26] that have evidenced weaknesses of the transitional model for fully turbulent free shear flows. The model proposed in chapter V is designed to inherit all of the positive characteristics of the $k_T - k_L - \omega$ transitional model for transitional boundary layers, but to correct the behavior of the $k_T - k_L - \omega$ model described in [22] and [26] for fully turbulent free shear flows.

The new model presented in chapter V has been developed using a more physically correct methodology to include transitional capabilities to the model. It will be superior for fully turbulent free shear flows compared with the $k_T - k_L - \omega$ model, but it will exhibit the same characteristics in transitional boundary layers. This implies that the

range of applications of the new model is wider than the $k_T - k_L - \omega$ model, which is important for industrial applications.

The model in chapter V improves the accuracy of the $k_T - k_L - \omega$ model in [5] when the term that controls the behavior in the wake region is replaced by a more elaborated SST-like term. It is valid to say that the gain in accuracy was achieved by increasing the complexity of the model.

The second transitional model presented in chapter VI is a single-point, physics-based method that adopts the transition concept presented mention before and described in detail in chapter III. The version of the model presented here uses the SST $k - \omega$ model as the baseline, and includes the effects of transition through one additional transport equation for a new variable that represents the energy of fully turbulent, three-dimensional velocity fluctuations.

The new transitional model presented in chapter VI is an initial version of a model that is intended to be dramatically simpler in the formulation of the equations and with fewer model constants than the model presented in chapter V, but with at least the same accuracy. Simplicity of the formulation and ease of extension to other baseline models are two potential advantages of the new method.

Publications and presentations

A list of publication and presentations based on partial results of this research are given below

Journal publications

1. M. Lopez., D. K. Walters., "*Prediction of transitional and free shear flows using an alternative to the laminar kinetic energy approach*". In preparation.

2. M. Lopez., D. K. Walters., "*A Physics-Based Correction of the* $k_T - k_L - \omega$ *Transitional Model*". In preparation.

3. M. Lopez., D. K. Walters., "*A simpler phenomenological model formulation for RANS simulations*". In preparation.

Conference proceedings

1. M. Lopez. D. K. Walters. "*Laminar-to-Turbulent Boundary Layer Prediction Using an Alternative to the Laminar Kinetic Energy Approach*". Proceedings, ASME 2012 International Mechanical Engineering Congress & Exposition. 9-15 November 2012, Houston, Texas.

2. D. K. Walters. M. Lopez. "*Phenomenological RANS Modeling of Transitional Flow:An Alternative to the Laminar Kinetic Energy Approach*". Proceedings, 9th International ERCOFTAC Symposium on Engineering Turbulence Modelling and Measurements. 6 - 8 June 2012, Thessaloniki, Greece.

Presentations

1. M. Lopez. D. K. Walters. 2014 "*Prediction of transitional boundary layers and fully turbulent free shear flows, using Reynolds Average Navier-Stokes models*," 2014 Graduate research poster competition, organized by the college of engineering at Mississippi State University.

2. M. Lopez. D. K. Walters., 2013, "*Accurate resolution of laminar, transitional and turbulent regions using an improved RANS model*," Finalist in the Graduate paper competition. Society of Hispanic Professional Engineers national conference. Indianapolis, November, 2013

3. M. Lopez. D. K. Walters., 2013, "*A New Phenomenological RANS Model for the Prediction of Transitional Boundary Layers*," Poster presentation in the summer school: Flow, Geometric Motion, Deformation, and Mass Transport in Physiological Processes. IMA, Minneapolis.

4. M. Lopez. D. K. Walters., 2012, "*On the Development of a Simpler Phenomenological Linear eddy-viscosity RANS Model for Transitional Flow*," 9th Differential Equations & Computational Simulations Conference, Starkville, Mississippi.

5. M. Lopez. D. K. Walters., 2012, "*A New Phenomenological RANS Modeling of Transitional Flow*. 10th annual Graduate Student Research Symposium. Mississippi State University.

Organization

The following chapters of this document are organized according to the objectives. In Chapter III the new methodology to describe the transition process is discussed, this methodology is used in the two turbulence models presented in this document. Chapter IV includes a small modification perform over the original model presented by Walters and Cokljat [5]. This modification will be further used in the development of the model presented in chapter V. Chapter V contains the description of the first transitional model that improves the accuracy of the model proposed in [5] for free shear flows. Test cases covering transitional boundary layers and free shear flows are included to test the performance of the modified model. Chapter VI describes the initial development of a new transitional model. The model is intended to be simpler than existing RANS transitional models in terms of its description and complexity of the equations, but with at least the same accuracy. Chapter VII contains final conclusion about the complete research.

CHAPTER III

LAMINAR TO TUBULENT TRANSITION CONCEPT FOR RANS MODELS

Introduction

Transitional flow phenomena are observed in a wide range of engineering applications including aerospace, aeronautics, biomedical, wind turbines, etc. Transitional flow is of vital importance in aerodynamic simulations. For example, in some cases the boundary layer may remain laminar throughout a significant portion of the domain, and fully turbulent simulations may produce results that can lead to inaccurate conclusions or inefficient design. The inherent behavior of transitional phenomena is very complex and still not understood with respect to many physical aspects. Using CFD, extensive research has been performed in the areas of turbulence modeling with improvements over the years. However, transition sensitive CFD simulations is still a very active research field, where questions still remain about the true nature of the physics of transitional flows.

In recent years researchers have tried to predict boundary layer transition using several approaches that include Direct Numerical Simulations [49], low Reynolds number eddy viscosity turbulence models [50-53], incorporation of an empirical correlation to a fully turbulent RANS model [24, 54], or the addition of transport equations to fully turbulent models in order to control the transition process [1-5] etc.

Due to wide range of applicability and the balance between computational resources used and accuracy of RANS models, a number of researchers have developed transitional models based on the low Reynolds number eddy viscosity framework [50, 51]. In these types of models, the concept of "diffusion controlled" transition is employed, i.e., transition triggered by the diffusion of freestream turbulence into the boundary layer, [50]. In [51] a two-equation turbulence model to predict the transitional flow was proposed. In this model, two different transition specific closure coefficients were formulated using linear stability theory. Although this transitional flow prediction approach achieved some degree of success, it has been proved that the transitional mechanisms are highly dependent on initial conditions and flow solution methods instead of representing the inherent transitional flow physics [52, 53].

Some other models [33, 55] have attempted to predict transitional flow fields by coupling an empirical transition correlation to a fully turbulent RANS model. In this approach, correlations are obtained from experimental data in simple geometries and flow conditions. Generally, the correlations relate turbulence intensity to the critical momentum thickness Reynolds number at which transition occurs. In these approaches researchers usually assume instantaneous flow transition in a particular location or they incorporate a transition zone, generally based on the universal intermittency profile of Dhawan and Narasimha [33]. Although this approach provides sufficient accuracy, its implementation is problematic in modern CFD codes. Such correlation-based transition models require the comparison between the momentum thickness Reynolds number and transition onset momentum thickness Reynolds number. The calculation of such

quantities is generally difficult for parallel computations of complex three-dimensional geometries using unstructured meshes.

Recent transition modeling approaches employ additional transport equations with the RANS-based turbulence models. Additional model terms may also be used to address the transitional behavior in the simulation. Within this recent transitional modeling approach, they can usually be classified as either correlation-based [1, 2], [31-33] and [55] or physics-based [4, 5] and [56, 57]. Wang and Perot [33] applied additional equations for turbulence potential terms to formulate a single–point, physics based transition model. Walters and Laylek [4] developed a phenomenological RANS-based, single-point, transitional model that addresses in-depth transitional flow physics without intermittency factors. The newest version of this model was developed by Walters and Cokljat in [5]. Suzen and Huang [56] proposed a correlation-based transition model that includes a transport equation for an intermittency factor. Steelant and Dick [57] developed a transport equation for the intermittency factor and incorporated it into conditioned Navier-Stokes equations. The transport equation was based in the intermittency distribution of Dhawan and Narasimha [33]. Menter et al. [1] proposed a single-point, correlation-based transition model that includes two different transport equations: one for the intermittency factor and the other for the transition onset Reynolds number. To date, single-point transition models have been widely accepted by the scientific community because they do not require non-local information in the simulation; thus, they can be easily implemented in modern CFD codes. The single-point transition models of Wang and Perot [33], Walters and Cokljat [5], and Menter et al. [1] have achieved wide acceptance due to their easy to implement nature.

Among the physics-based transitional models, one popular approach is the adoption of an additional transport equation for laminar kinetic energy (LKE), used to represent pre-transitional, non-turbulent velocity fluctuations which lead to transition and full turbulence [6]. The models presented by Walters and Laylek [4] and Walters and Cokljat [5] are examples of such models. In the latter, a transport equation for the laminar kinetic energy is included and the transition process is seen as a transfer of energy from the stream wise non-turbulent velocity fluctuations to the fully turbulent 3-dimensional velocity fluctuations.

It is well known that there are number of researchers, including our group in Mississippi State, who have developed successful models using the LKE concept. This research proposes a description of the transition process based on a modification of this concept. Instead of the non-turbulent velocity fluctuations approach embedded in the LKE concept, this research proposes the introduction of a new variable that represents the wall-normal turbulent velocity fluctuation, which is responsible for the initiation of transition [23, 25].

Background and Methodology

Wang and Perot [24] argue that the full set of RANS equations are equally valid in the pretransitional, transitional and fully turbulent regions, which means that transitional as well as turbulent fluctuation may be modeled through the Reynolds stress tensor. The exact form of the Reynolds stress transport equation for incompressible flow is:

$$\frac{D}{Dt}\overline{u_i' u_j'} = -\nu \frac{\partial \overline{u_i' u_j'}}{\partial x_k^2} - \left(\overline{u_i' u_k'}\bar{s}_{kj} + \overline{u_j' u_k'}\bar{s}_{ki}\right) + \overline{p'\left(\frac{\partial u_i'}{\partial x_j} + \frac{\partial u_j'}{\partial x_i}\right)} - 2\nu \overline{\frac{\partial u_i'}{\partial x_k}\frac{\partial u_j'}{\partial x_k}} - \frac{\partial}{\partial x_k}\left[\overline{u_i' u_j' u_k'} + \left(\overline{p' u_i'}\delta_{jk} + \overline{p' u_j'}\delta_{ik}\right)\right] \tag{3.1}$$

The first two terms in (3.1), viscous diffusion and production, do not need any modeling if equation (3.1) is solved, but the pressure strain, dissipation, turbulence transport and pressure transport terms require modeling, and none of them can be neglected for fully turbulent flows. In theory, these terms, also non negligible in the transition region where fluctuations are relatively small, have the capabilities to control the transition process as well.

Of particular interest are the production term, $-\left(\overline{u_i' u_k'}\bar{s}_{kj} + \overline{u_j' u_k'}\bar{s}_{ki}\right)$, which transfers energy from the mean to the fluctuating flow, and the pressure strain term, $\overline{p'\left(\frac{\partial u_i'}{\partial x_j} + \frac{\partial u_j'}{\partial x_i}\right)}$, which serves to redistribute energy among the normal Reynolds stress components and modify the shear stress components. The pressure strain term is usually modeled as a "return to isotropy" that tends to redistribute the energy from high energy components to lower energy components. Moreover, this term is expressed as the sum of a rapid part, which incorporates interactions between turbulent eddies and the mean velocity field, and a slow part that incorporates inter-eddy interactions.

In [25], Walters summarizes the production of Reynolds stress components with the following steps: 1) transfer of energy from the mean flow to $\overline{u'u'}$ via interaction of $\overline{u'v'}$ with the mean strain rate; 2) transfer of energy from $\overline{u'u'}$ to $\overline{v'v'}$ and $\overline{w'w'}$ due to

the action of pressure strain; and 3) generation of turbulent shear stress $\overline{u'v'}$ via the interaction of $\overline{v'v'}$ with the mean strain rate.

Large eddy simulations by Voke and Yang [7] show that in the pretransitional region, step 2 does not occur. The shear sheltering effect apparently inhibits the redistribution of energy, which is caused by the pressure strain term in the fully turbulent region. Their results also show evidence of a positive contribution of the pressure strain term to the $\overline{u'u'}$ component very close to the wall, but it suppresses rather than increases the wall-normal component $\overline{v'v'}$. This behavior is further evident in more recent DNS and LES simulations [8-10], i.e, no peak in either $\overline{v'v'}$ or $\overline{w'w'}$ occurs within the pretransitional region of the boundary layer where the Reynolds stress budgets are clearly dominated by the production and dissipation terms.

Assuming that the pressure strain terms are negligible in the pretransitional region, the following set of simplified (approximate) equations is obtained from (3.1):

$$\frac{D}{Dt}\overline{u'u'} \approx \overline{u'v'}\frac{\partial \overline{u}}{\partial y} - \varepsilon_{11} + Transport \tag{3.2}$$

$$\frac{D}{Dt}\overline{u'v'} \approx \overline{v'v'}\frac{\partial \overline{u}}{\partial y} - \varepsilon_{12} + Transport \tag{3.3}$$

$$\frac{D}{Dt}\overline{v'v'} \approx -\varepsilon_{22} + Transport \tag{3.4}$$

$$\frac{D}{Dt}\overline{w'w'} \approx -\varepsilon_{33} + Transport \tag{3.5}$$

From equations (3.4) and (3.5), it is clear that the wall-normal ($\overline{v'v'}$) and spanwise ($\overline{ww}$) Reynolds stress components do not exhibit appreciable growth in the prestransitional

boundary layer. In addition to that, following [11], the freestream turbulence enters the boundary layer, either at the leading edge or through diffusive transport of low frequency modes farther downstream, which means that only the wall-normal component of this entrained turbulence leads to the growth of Klebanoff modes, and, in fact, the dependence of pretransitional energy production on wall-normal freestream fluctuations is well established [7-15].

The laminar boundary layer theory reports that the peak velocity gradient $\frac{\partial \bar{u}}{\partial y}$ varies as $\mathrm{Re}_x^{1/2}$. With negligible dissipation and diffusion, it is expected from (3.4) and (3.3) that the wall-normal Reynolds stress component $\overline{v'v'}$ remains approximately constant in the streamwise direction, which further leads $\overline{u'v'}$ to an approximate streamwise growth rate $\overline{u'v'} \sim \mathrm{Re}_x^{1/2}$. Likewise the streamwise Reynolds stress component, in the absence of significant dissipation or diffusive transport, will exhibit a growth rate of $\overline{u'u'} \sim \mathrm{Re}_x$. This linear streamwise growth rate behavior of pretransitional kinetic energy has been reported in previous experiments and simulations [14,15].

Finally, the transition process can be viewed as the "activation" of the pressure strain term, responsible for redistributing the energy and tending to return the fluctuations toward isotropy, leading to a rapid increase in the spanwise and especially wall-normal energy components. This process produces the well known eddy scale range and energy cascade process characteristic of high-Re turbulence.

To summarize the above discussion, Walters in [25] pointed out some key physical features in the dynamic of Reynolds stress component evolution that play an

important role in the RANS-based description of transitional boundary layer. These include: 1) production of one-dimensional streamwise fluctuation energy in the pretransitional region by entrained freeestream turbulence interacting with the mean strainrate; 2) minimal generation of three-dimensional (normal and spanwise) fluctuations in the pretransitional region, due to suppression of the pressure strain mechanism found in turbulent flow; and 3) transition initiation due to an increase in magnitude of the pressure strain term, followed by a rapid grow of three-dimensional fluctuations more indicative of fully turbulent flow.

Proposed transition concept

This section discusses the transition concept that will be used for the two models in chapters V and VI. The concept is based on the description of the transition process outlined in the previous section, and it is presented as an alternative to the LKE approach.

Assuming that the pretransitional region develops due to a suppression of the pressure-strain terms in the Reynolds stress transport equation, transition is initiated with the activation of these terms due to nonlinear instability mechanisms, which results in a transfer of energy from streamwise to the wall normal (and spanwise) components and leads to a rapid rise in turbulence production. In most LKE models, such as [5] for example, this transfer of energy is made from the LKE to the turbulent kinetic energy trough some terms included in the respective transport equations. The versions of the models presented here include the initiation of the transition process by the rapid increase of energy in the fully turbulent, three-dimensional velocity fluctuations which will be represented by the variable v^2. This modeling approach, initially introduced by Lopez

and Walters in [23], leads to slow growth of fluctuating energy in the pretransitional region and relaxation towards a fully turbulent model result downstream of transition.

The motivation for using the variable v^2 comes from several references in the open literature. As discussed above, the LES results of Voke and Yang [7] show a positive contribution of the pressure strain term to the streamwise Reynolds stress component in the pretransitional region, presumably a wall reflection effect, which works to suppress rather than increase the wall-normal component. This inhibits growth of the shear stress component and causes relatively low production of turbulent kinetic energy. Other studies, [8-10], show the same behavior, and report no peak in $\overline{v'v'}$ or $\overline{w'w'}$ within the pretransitional region of the boundary layer. Furthermore, these studies have demonstrated that only the wall-normal component of this entrained freestream turbulence leads to the growth of Klebanoff modes, and that the onset of transition coincides with a sudden increase in wall normal energy. In fact, [7] showed that pure streamwise disturbances at the inflow are ineffective at forcing transition, while wall-normal disturbances are virtually as effective as full isotropic disturbances. These considerations have led to the adoption of the $k - v^2 - \omega$ framework as an alternative to the $k - k_L - \omega$ model approach in [5] for development of a phenomenological transition-sensitive model.

CHAPTER IV

A PHYSICS-BASED CORRECTION OF THE $k_T - k_L - \omega$ MODEL

Introduction

The single-point physics-based $k_T - k_L - \omega$ transition model initially developed by Walters and Laylek [4] and further refined by Walters and Cokljat [5] incorporates an additional transport equation for laminar kinetic energy (k_L) to a modified form of a two-equation eddy viscosity turbulence model. Following [5], for low freestream turbulence intensity (less than 1%), the small velocity fluctuation behaves as self-sustained instabilities better known as Tollmien-Schlichting waves [58]. As the freestream turbulence intensity increases, the instability increases with the high amplitude streamwise fluctuations and further increase in this fluctuation leads to transition through the breakdown of the streamwise fluctuations. This transition process is known as bypass transition. In the model, the laminar-to-turbulent transition process itself is represented by a transfer of energy from the laminar kinetic energy k_L to the turbulent kinetic energy k_T. The variable k_T is assumed to represent the energy of the fully turbulent fluctuations that display the characteristics of fully turbulent flow, such as strong three-dimensionality, multiple length and time-scales, energy cascading, and significant viscous dissipation. The initiation of the transition process in the model is based on local (single-point) flow conditions. The transition location is determined by ratio of turbulent production

timescale to the molecular diffusion time-scale; when this ratio reaches a critical point the transition process is initiated.

Model equations

The complete presentation of the model equations is not included in this section; they can be found in [5]. However, reference [5] contains several typographical errors that have been corrected [59] and will be outlined in this section. One additional change, not yet reported in the open literature, will be made in this section to the $k_T - k_L - \omega$ model presented in [5]. This last modification corrects the behavior of the production of laminar kinetic energy away from the wall.

The general form of the model equations in their incompressible form is given by:

$$\frac{Dk_T}{Dt} = P_{k_T} + R_{BP} + R_{NAT} - \omega k_T - D_T + \frac{\partial}{\partial x_j}\left[\left(\nu + \frac{\alpha_T}{\sigma_k}\right)\frac{\partial k_T}{\partial x_j}\right] \tag{4.1}$$

$$\frac{Dk_L}{Dt} = P_{k_L} - R_{BP} - R_{NAT} - D_L + \frac{\partial}{\partial x_j}\left[\nu \frac{\partial k_L}{\partial x_j}\right] \tag{4.2}$$

$$\begin{aligned}\frac{D\omega}{Dt} &= C_{\omega 1}\frac{\omega}{k_T}P_{k_T} + \left(\frac{C_{\omega R}}{f_W} - 1\right)\frac{\omega}{k_T}(R_{BP} + R_{NAT}) - C_{\omega 2}\omega^2 f_W^2 \\ &+ C_{\omega 3} f_\omega \alpha_T f_W^2 \frac{\sqrt{k_T}}{d^3} + \frac{\partial}{\partial x_j}\left[\left(\nu + \frac{\alpha_T}{\sigma_\omega}\right)\frac{\partial \omega}{\partial x_j}\right]\end{aligned} \tag{4.3}$$

The first typographical correction made to [5] is the third term in the right hand side of the omega equation ($-C_{\omega 2}\omega^2$ in [5]).

Equation (11) in [5] defines the damping function f_W as

$$f_W = \frac{\lambda_{eff}}{\lambda_T} \tag{4.4}$$

but the correct formulation for f_W includes the exponent $2/3$ as in the original version of Walters and Leylek [4], thus the correct form is

$$f_W = \left(\frac{\lambda_{eff}}{\lambda_T} \right)^{2/3} \tag{4.5}$$

Finally, the intermittency damping function defined in equation (16) in [5] as

$$f_{INT} = \min \left(\frac{k_L}{C_{INT}\, k_{TOT}}, 1 \right) \tag{4.6}$$

should be corrected to

$$f_{INT} = \min \left(\frac{k_T}{C_{INT}\, k_{TOT}}, 1 \right) \tag{4.7}$$

The previous 3 corrections are just typographical errors in [5]. These corrections should be made in order to reproduce the results presented in [5].

This research has found that a deeper modification has to be made to the $k_T - k_L - \omega$ transitional model described in [5]. The production of k_L is defined as the interaction of Reynolds stresses that are associated with the pretransitional velocity fluctuations and mean shear, and is governed by the large-scale near-wall turbulent fluctuations.

The production of laminar kinetic energy P_{k_L} is defined in [5] in equations (17)-(22) as

$$P_{k_L} = \nu_{T,l} S^2 \tag{4.8}$$

where

$$\nu_{T,l} = \min \left\{ f_{\tau,1} C_{11} \left(\frac{\Omega \lambda_{eff}^2}{\nu} \right) \sqrt{k_{T,l}} \lambda_{eff} + \beta_{TS} C_{12} \left(\frac{d^2 \Omega}{\nu} \right) d^2 \Omega, \frac{0.5(k_L + k_{T,l})}{S} \right\}. \tag{4.9}$$

The limit is applied to ensure satisfaction of the realizability constraint for the total Reynolds stress contribution. The production term is comprised of two parts: the first addresses the development of Klebanoff modes and the second addresses self-excited (i.e., natural) modes ([5])

Note that as the model term is currently expressed, the second term is proportional to the wall distance raised to a power of 4. This formulation works well and describes correct physical dependence for boundary layer flows (wall-bounded flows), but the entire term could be eventually dominated by the distance from the wall for non-boundary layer flows. In fact the formulation can be completely incorrect for fully turbulent free shear flows, as evidenced by the results in this chapter. To correct this, the term should be made proportional to a length scale that scales with the wall distance in near-wall flows, and scales with the turbulent integral length scale in farfield flows.

To limit the production of natural modes in zones far from the wall in fully turbulent flows where this mechanism is not active, the second term in the “large-scale” eddy viscosity should be modified. The proposed modification to equation (4.9) is

$$\nu_{T,l} = \min\left\{ f_{\tau,1} C_{11} \left(\frac{\Omega \lambda_{eff}^2}{\nu} \right) \sqrt{k_{T,l}}\, \lambda_{eff} + \beta_{TS} C_{12} \left(\frac{d_{eff}^2 \Omega}{\nu} \right) d_{eff}^2 \Omega, \frac{0.5(k_L + k_{T,l})}{S} \right\} \tag{4.10}$$

Note that instead of the wall distance term d, the d_{eff} term is used and it is defined as

$$d_{eff} = \frac{\lambda_{eff}}{C_\lambda} \tag{4.11}$$

where $\lambda_{eff} = \min(dC_\lambda, \lambda_T)$ and C_λ, λ_T are identical to those given in [5].

Numerical results

The original version of the $k_T - k_L - \omega$ model presented in [5] (with the typographical errors corrected) and the version with the "large-scale" eddy viscosity modified by equation (4.10) have been tested using a round jet flow.

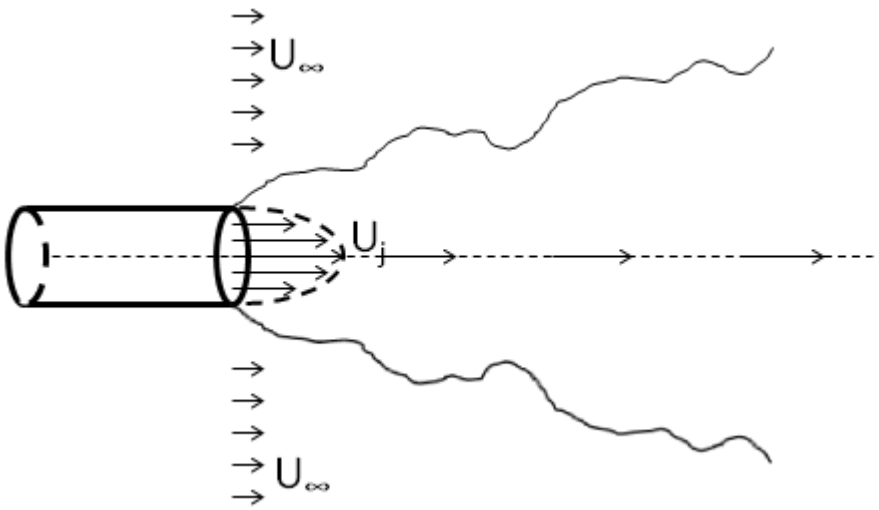

Figure 4.1 Sketch of a round jet flow

Figure 4.1 shows a schematic of the round jet flow in three dimensions. The fluid travels inside of a circular pipe (from left to right in figure 4.1) until it reaches the outlet of the pipe (jet exit) and it is dispersed in an open space. The flow field is symmetric with respect to the centerline of the domain in all directions.

Figure 4.2 shows the axisymmetric two-dimensional domain and mesh used to perform the simulations. Only half of physical domain was used in the calculations, taking the centerline of the jet as a symmetry axis. In the jet exit, the velocity was $56.2\, m/s$ and turbulence intensity less than 0.58%. In experimental studies, usually the flow is manipulated to transition to turbulent before the exit of the jet.

Two grids were used in this study. In the first one the length of the channel before the exit is 3H. The fully turbulent SST $k-\omega$ model was run in this domain and profiles of velocity, turbulent kinetic energy and specific dissipation rate were taken at a distance 1.5H from the inlet of the channel. In the second mesh, the length of the channel before the exit is 1.5H. The profiles obtained from the SST model were used as inlet conditions for the $k_T - k_L - \omega$ transitional model to ensure a fully turbulent flow.

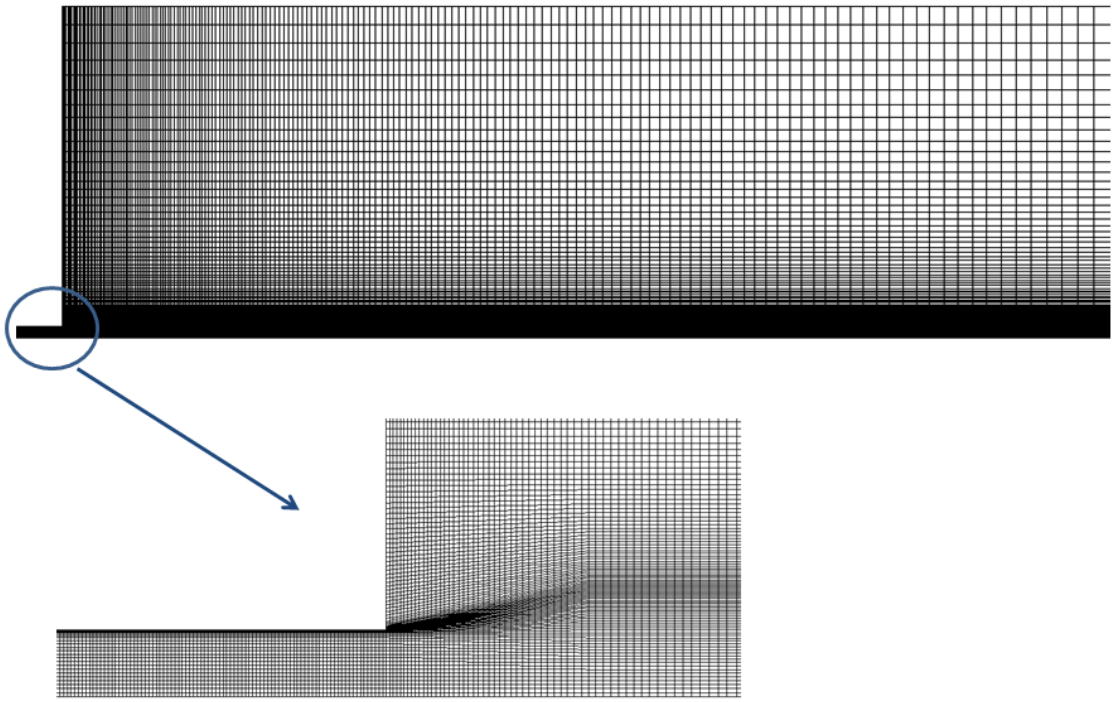

Figure 4.2 Mesh used for the fully turbulent jet flow simulations

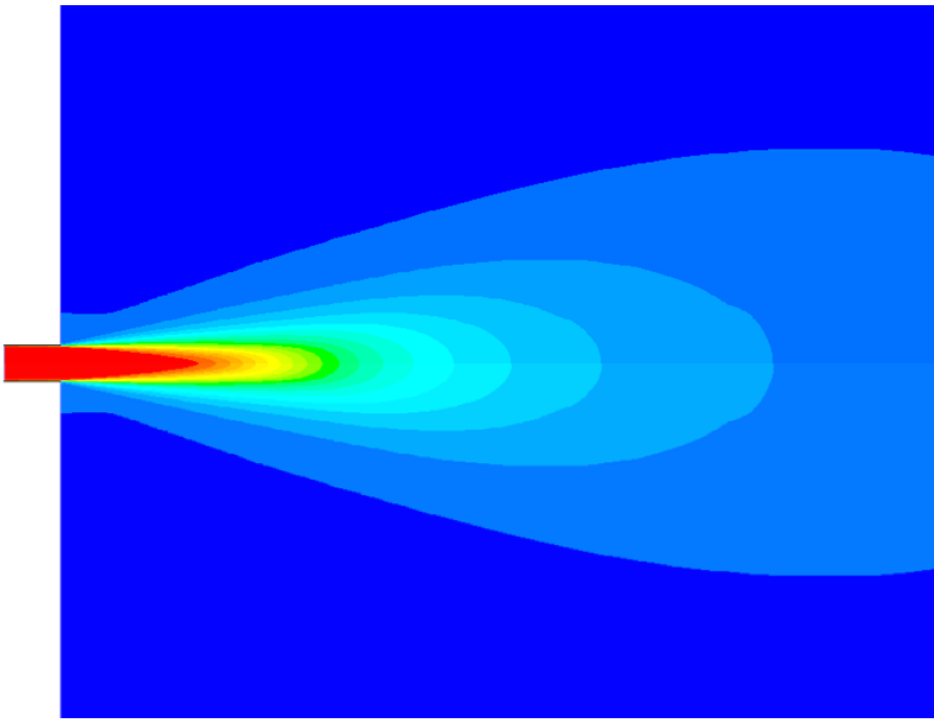

Figure 4.3 Contours of velocity in the streamwise direction computed with the $k_T - k_L - \omega$ model for the round jet flow

Figure 4.3 shows the contours of velocity computed with the $k_T - k_L - \omega$ model, using the domain and mesh presented in figure 4.2. The maximum velocity is reached at the exit of jet, and decreases as the flow moves downstream. The velocity did not show any alteration by the change made to "large-scale" eddy viscosity. On the other hand, the production of laminar kinetic energy (and hence the laminar kinetic energy itself), show significant changes that will be highlighted here.

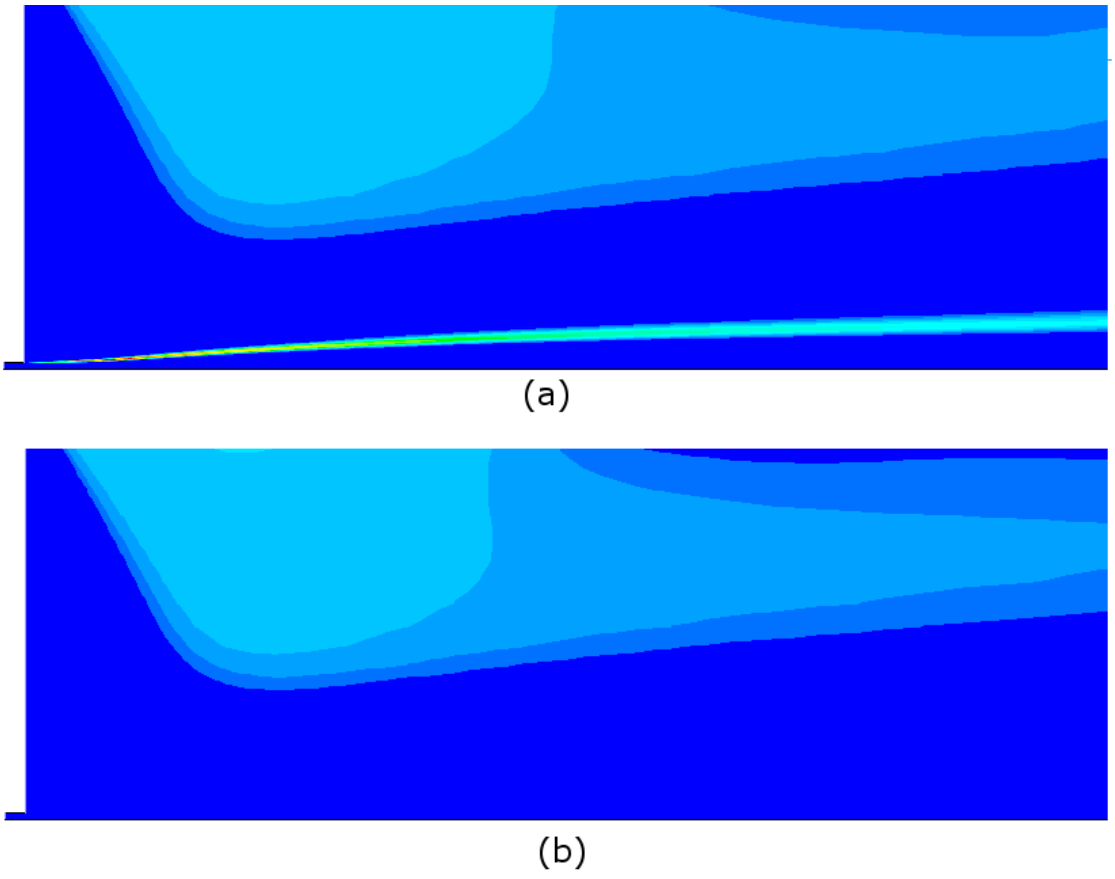

Figure 4.4 Contours of laminar kinetic energy.

(a) original model (with typographical error corrected), (b) model with modified "large-scale" eddy viscosity

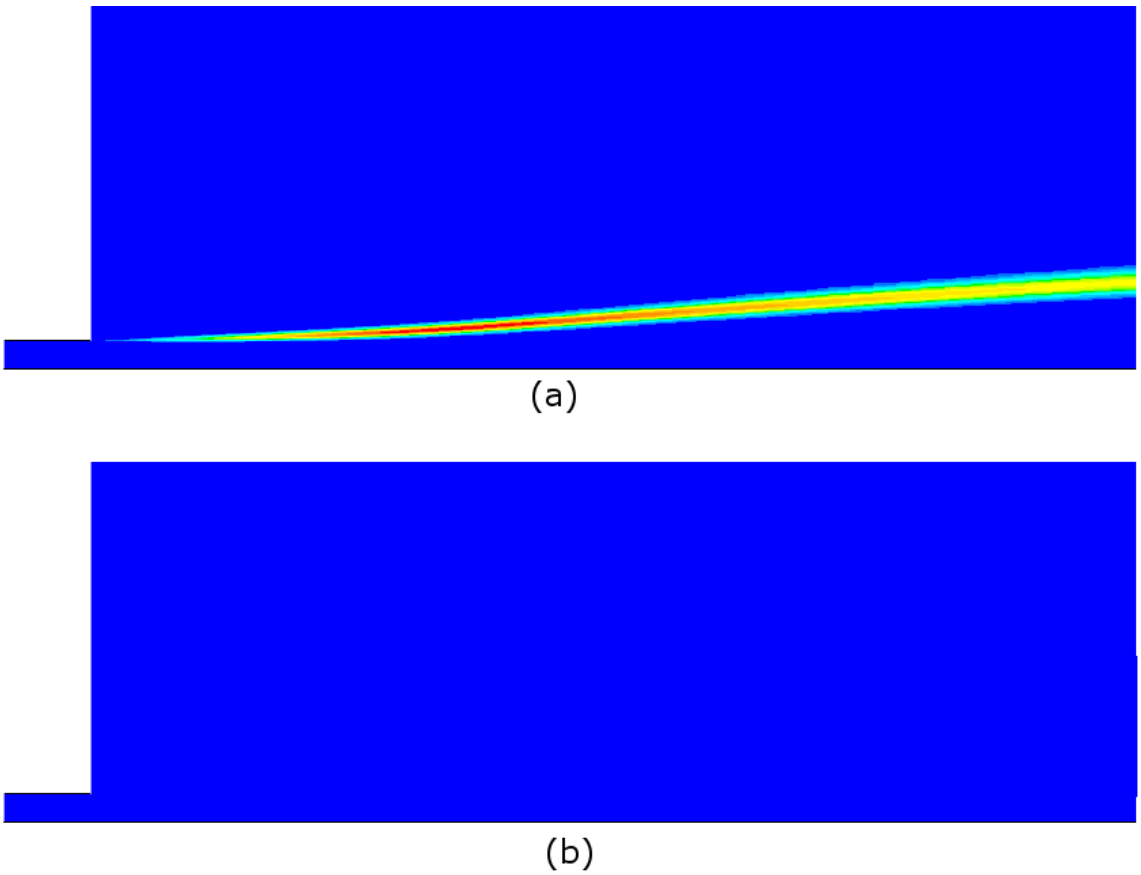

Figure 4.5 Close-up view of contours of laminar kinetic energy.

(a) original model (with typographical error corrected), (b) model with modified "large-scale" eddy viscosity

Figures 4.4 and 4.5 show the contours of laminar kinetic energy for the fully turbulent jet flow. It is clear from the figures that the levels of laminar kinetic energy increase after the outlet of the jet for the original version of the $k_T - k_L - \omega$ model. This is clearly an incorrect behavior, which is corrected with the modification of the "large-scale" eddy viscosity as demonstrated by figures 4.4(b) and 4.5(b). The maximum value of laminar kinetic energy for the original model was 43.3, and it was reached after the outlet of the jet, while the modified version reported a maximum of 10.0. However all

figures were plotted using the same scales (minimum value of 0.0 and maximum value of 43.3) for comparison purposes

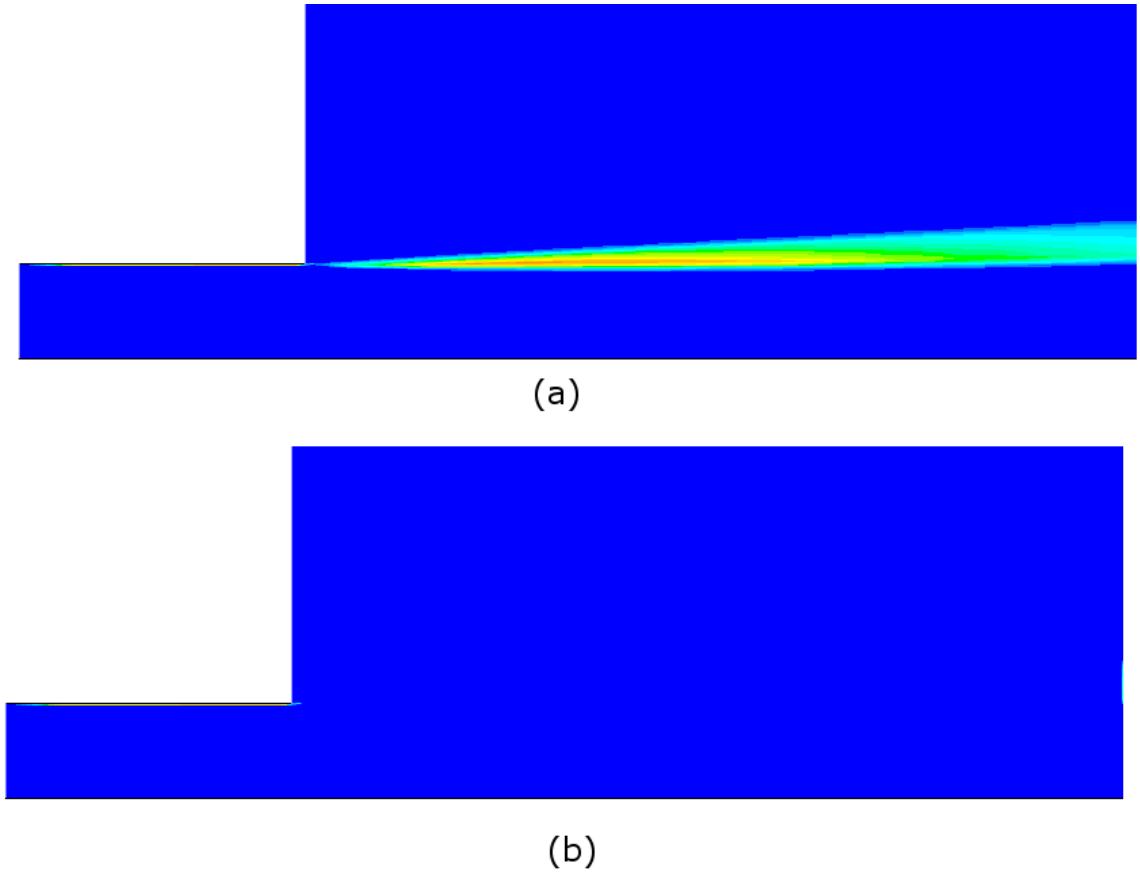

Figure 4.6 Contours of production of laminar kinetic energy.

(a) original model (with typographical error corrected), (b) Model with modified "large-scale" eddy viscosity.

Figure 4.6 shows the contours of the production of laminar kinetic energy that one more time confirm the heavy production of laminar kinetic energy in fully turbulent zones, where it should decay rather than increase. Again, figure 4.6(b) shows that the modification in equations 4.10 and 4.11 effectively corrects this issue.

Conclusions

A modification to the $k_T - k_L - \omega$ model developed by Walters and Cokljat in [5] was proposed and successfully tested in a fully turbulent jet flow. The modification to the "large-scale" eddy viscosity described in this chapter is not a typographical error of the original version of the model and the results have demonstrated that influences and corrects some issues on the physical mechanism of production of laminar kinetic energy for regions far from the wall.

CHAPTER V

A MODIFIED VERSION OF THE $k_T - k_L - \omega$ MODEL

Introduction

The $k_T - k_L - \omega$ model

The laminar kinetic energy concept is currently one of the most commonly used approaches to develop RANS models with transitional capabilities. It was first introduced by Mayle and Schulz in [6]. In general, the laminar kinetic energy represents the energy of velocity fluctuations in the pretransitional region. These fluctuations are not a result of the cascade of scale, but they generate as a consequence of the penetration of free-stream disturbances into the boundary layer [62]. Unlike turbulent kinetic energy, the laminar kinetic energy is dominated only by the stream-wise velocity fluctuations.

The single-point physics-based $k_T - k_L - \omega$ transition model initially developed by Walters and Laylek [4] and further refined by Walters and Cokljat [5] is one of the most successful transitional models that use the laminar kinetic energy concept. In [5], the model was tested for a variety of cases that demonstrated the ability of the model to predict transitional flows. The model has been further tested by researchers with satisfactory results. Wang and Walters [64] demonstrated the ability of the model to predict transitional flows over marine propeller systems, where fully turbulent models are usually used, leading in some cases to accuracy degradation. Bernardini et al [63]

demonstrated that the $k_T - k_L - \omega$ model performs well versus the SST $\gamma - \mathrm{Re}_\theta$ model [1] for boundary layer separation on a turbine blade for different values of Reynolds number.

Several modifications have been developed over the years. Chitta et al [65] incorporated sensitivity to high curvature domains to the transitional $k_T - k_L - \omega$ model through the addition of one transport equation to the system. Tuner [62] proposed several modifications for the effective length scale and the shear sheltering damping function to correct some apparent issues of the $k_T - k_L - \omega$ model when tested on the F1 Valeo-CD airfoil. Alam et al [66] used the $k_T - k_L - \omega$ model to build a transition-sensitive hybrid RANS/LES model with promising advantages over others transitional hybrid models.

A general form of the equations is given in the previous chapter. A detailed expression for each term in equations (4.1)-(4.3) is given in [5]. Note that [5] contains some typographical errors that were corrected in the previous chapter.

The shear stress transport (SST) $k - \omega$ model

The Shear-Stress Transport (SST $k - \omega$) model developed by Menter [48] is based on the transport of the principal shear stress to facilitate the prediction of adverse pressure-gradient-dominant flows. The model combines the advantages of the $k - \omega$-based model near the wall and the $k - \varepsilon$ model for free shear flows. It is one of the most used fully turbulent models for research purposes or industrial applications [61].

The general form of the equations is given by

$$\frac{Dk}{Dt} = P_k - \beta^* k\omega + \frac{\partial}{\partial x_j}\left[(\nu + \sigma_k \nu_T)\frac{\partial k}{\partial x_j}\right] \tag{5.1}$$

$$\frac{D\omega}{Dt} = \alpha S^2 - \beta\omega^2 + \frac{\partial}{\partial x_j}\left[(\nu + \sigma_\omega \nu_T)\frac{\partial \omega}{\partial x_j}\right] + 2(1 - F_1)\sigma_{\omega 2}\frac{1}{\omega}\frac{\partial k}{\partial x_j}\frac{\partial \omega}{x_j} \tag{5.2}$$

and the kinematic eddy viscosity is defined by

$$\nu_T = \frac{a_1 k}{\max(a_1\omega, SF_2)} \tag{5.3}$$

where a_1 is a constant and S is the strain rate magnitude. The functions F_1 and F_2 are the blending functions that make the transition from a $k-\omega$ based model near the wall to a $k-\varepsilon$ model for free shear flows. For a complete description of the terms in the equations see [48].

A new model formulation

The model presented in this section is a modification of the transitional model developed by Walters and Cokljat in [5]. The new version incorporates the new variable v^2 to control the transition process as described in chapter III. The model uses a $k - v^2 - \omega$ framework instead of the typical $k_T - k_L - \omega$ representation. In this new formulation the turbulent kinetic energy k represents the energy of both fully turbulent and pre-transitional velocity fluctuations and the specific dissipation rate ω has the same definition as in [5]. With the definition for k given previously, k_L can be defined as $k_L \approx k - v^2$.

For simplicity the equations are presented in their incompressible forms. The model equations have the compact form:

$$\frac{Dk}{Dt} = P_k - D_k + \frac{\partial}{\partial x_j}\left[\left(\nu + \frac{\alpha_T}{\sigma_k}\right)\frac{\partial k}{\partial x_j}\right] \tag{5.4}$$

$$\frac{Dv^2}{Dt} = P_{v^2} + R_{BP} + R_{NAT} - D_{v^2} + \frac{\partial}{\partial x_j}\left[\left(\nu + \frac{\alpha_T}{\sigma_k}\right)\frac{\partial v^2}{\partial x_j}\right] \tag{5.5}$$

$$\frac{D\omega}{Dt} = P_\omega + \left(\frac{C_{\omega R}}{f_W} - 1\right)\frac{\omega}{v^2}(R_{BP} + R_{NAT}) - C_{\omega 2}\omega^2 f_W^2 + \beta^* 2(1 - F_1^*)\sigma_{\omega 2}\frac{1}{\omega}\frac{\partial k}{\partial x_j}\frac{\partial \omega}{x_j} + \frac{\partial}{\partial x_j}\left[\left(\nu + \frac{\alpha_T}{\sigma_k}\right)\frac{\partial v^2}{\partial x_j}\right] \tag{5.6}$$

As a result of the change of variables, note that equation (5.4) does not include the transitions terms R_{BP} and R_{NAT} as in [5]. In the k equation, those terms were used to represent the transfer of energy from the non-turbulent pretransitional fluctuations (k_L) to the fully turbulent fluctuations (k_T). In this new version, v^2 is suppressed in pretransitional region. Transition initiates when the value of the term R_{BP} becomes non-negligible, representing "activation" of the pressure strain terms, followed by the growth of three-dimensional, fully turbulent fluctuations (v^2). Equation (5.6) now incorporates a cross diffusion terms as in the SST $k-\omega$ model very similar to the one in equation (5.2) that will ensure the correct prediction of the boundary layer wake region, where the original model in [5] shows weaknesses evidenced in [22].

The definitions of the following terms are similar to the version of the model in [5]. The production terms are expressed as:

$$P_k = \nu_T S^2, \quad P_{v^2} = \nu_{T,s} S^2, \quad P_\omega = \left(C_{\omega 1}\frac{\omega}{v^2}\nu_{T,s}\right)S^2 \tag{5.7}$$

The turbulent viscosity ν_T used in the momentum equation is the sum of the small and large scale contributions

$$\nu_T = \nu_{T,s} + \nu_{T,l} \tag{5.8}$$

The small-scale eddy viscosity and the effective small-scale turbulence are expressed as

$$\nu_{T,s} = f_\nu f_{INT} C_\mu \sqrt{\nu_S^2}\lambda_{eff} \quad \text{and} \quad \nu_S^2 = f_{SS} f_W \nu^2 \tag{5.9}$$

The effective (wall limited) turbulent length scale λ_{eff} and the damping function f_W are defined as

$$\lambda_{eff} = \min(C_\lambda d, \lambda_T) \quad , \quad \lambda_T = \frac{\sqrt{\nu^2}}{\omega} \tag{5.10}$$

$$f_W = \left(\frac{\lambda_{eff}}{\lambda_T}\right)^{2/3} \tag{5.11}$$

The viscous wall effect is incorporated as:

$$f_\nu = 1 - \exp\left(-\frac{\sqrt{\mathrm{Re}_T}}{A_\nu}\right) \quad , \quad \mathrm{Re}_T = \frac{f_W^2 \nu^2}{\nu\omega} \tag{5.12}$$

The shear sheltering effect responsible for inhibiting the production of three dimensional velocity fluctuations in the pretransitional region is expressed as

$$f_{SS} = \exp\left[-\left(\frac{C_{SS}\nu\Omega}{\nu^2}\right)^2\right] \tag{5.13}$$

The turbulent viscosity coefficient and the intermittency damping function for the turbulence production are defined as

$$C_{\mu} = \frac{1}{A_0 + A_S\left(\frac{S}{\omega}\right)} \quad , \quad f_{INT} = \min\left(\frac{v^2}{C_{INT}\,k}, 1\right) \tag{5.14}$$

The large scale eddy viscosity from the equation (5.8) is defined as

$$\begin{aligned} \nu_{T,l} = \min\Bigg\{ & f_{\tau,1} C_{11}\left(\frac{\Omega\,\lambda_{eff}^2}{\nu}\right)\sqrt{v_l^2}\,\lambda_{eff} \\ & + \beta_{TS} C_{12}\left(\frac{d_{eff}^2\,\Omega}{\nu}\right) d_{eff}^2\,\Omega, \frac{0.5(k - v_S^2)}{S}\Bigg\}. \end{aligned} \tag{5.15}$$

Here, the limit is applied to satisfy the realizability constraint for the total Reynolds stress contribution. Note that the second part of this term is slightly different from the corresponding term in [5]. Here, instead of the wall distance term d, the term d_{eff} is used and it is defined as

$$d_{eff} = \frac{\lambda_{eff}}{C_{\lambda}} \tag{5.16}$$

this will limit the production of natural modes in zones far from the wall in fully turbulent flows, where this mechanism should not be produce. A description of this modification is discussed in chapter IV and [26].

v_l^2 is the large-scale turbulence contribution, and it is given by

$$v_l^2 = v^2 - v_S^2 \tag{5.17}$$

Other terms in (5.15) are defined as

$$f_{\tau,1} = 1 - \exp\left[- C_{\tau,1} \frac{v_l^2}{\lambda_{eff}^2 \Omega^2} \right] \tag{5.18}$$

$$\beta_{TS} = 1 - \exp\left(- \frac{\max(\mathrm{Re}_{\Omega} - C_{TS,crit}, 0)^2}{A_{TS}} \right) \quad , \quad \mathrm{Re}_{\Omega} = \frac{d^2 \Omega}{\nu} \tag{5.19}$$

The near-wall dissipation terms for k and v^2 are expressed as

$$D_k = 2\nu \frac{\partial \sqrt{k}}{\partial x_j} \frac{\partial \sqrt{k}}{\partial x_j} \quad , \quad D_{v^2} = 2\nu \frac{\partial \sqrt{v^2}}{\partial x_j} \frac{\partial \sqrt{v^2}}{\partial x_j} \tag{5.20}$$

The effective diffusivity α_T in the turbulent transport term is defined by

$$\alpha_T = f_v \beta^* \sqrt{v_S^2} \lambda_{eff} \tag{5.21}$$

The cross diffusion term in the ω equation is similar to the one in the fully turbulent SST k-ω model. The term is included to improve the behavior of the model in the wake region and in separated shear layers, where the SST k-ω model has proven to be effective [22],[27]. The blending function F_1^* is defined as

$$F_1^* = 1 - [(1 - F_1) f_{SS}] \tag{5.22}$$

in which the shear-sheltering damping function inhibits the fully turbulent effects of the F_1 function in the pretransitional region of the boundary layer. The F_1 function is defined similar to the SST k-ω model

$$F_1 = \tanh\left\{ \left\{ \min\left[\max\left(\frac{\sqrt{v^2}}{\omega d}, \frac{500 \nu \beta^*}{d^2 \omega} \right), \frac{4 \sigma_{\omega 2} k}{CD_{k\omega} d^2} \right] \right\}^4 \right\} \tag{5.23}$$

with

$$CD_{k\omega} = \max\left(2\rho\sigma_{\omega 2}\frac{1}{\omega}\frac{\partial k}{\partial x_j}\frac{\partial \omega}{\partial x_j}, 10^{-10}\right) \tag{5.24}$$

The terms representing the natural and bypass transition are defined as

$$R_{NAT} = C_{R,NAT}\beta_{NAT}(k - v^2)\Omega, \quad R_{BP} = C_R\beta_{BP}(k - v^2)\omega / f_W \tag{5.25}$$

As discussed in [5], transition is initiated when the characteristic time-scale for turbulence production is smaller than the viscous diffusion time scale of pretransitional fluctuations. This process is controlled by the transition initiation terms β_{NAT} and β_{BP}. The expressions for these two terms are

$$\beta_{NAT} = 1 - \exp\left(-\frac{\phi_{NAT}}{A_{NAT}}\right), \quad \beta_{BP} = 1 - \exp\left(-\frac{\phi_{BP}}{A_{BP}}\right) \tag{5.26}$$

$$\phi_{NAT} = \max\left[\left(\mathrm{Re}_{\Omega} - \frac{C_{NAT,crit}}{f_{NAT,crit}}\right), 0\right], \quad f_{NAT,crit} = 1 - \exp\left(-C_{NC}\frac{\sqrt{k}\,d}{\nu}\right) \tag{5.27}$$

$$\phi_{BP} = \max\left[\left(\frac{v^2}{\nu\Omega} - C_{BP,crit}\right), 0\right] \tag{5.28}$$

To include heat transfer effects, the turbulent heat flux vector can be modeled using a turbulent thermal diffusivity α_θ

$$-\overline{u_i T} = \alpha_\theta \frac{\partial T}{\partial x_i} \tag{5.29}$$

$$\alpha_\theta = f_W\left(\frac{v^2}{k}\right)\frac{\nu_{T,s}}{\mathrm{Pr}_\theta} + (1 - f_W)C_{\alpha,\theta}\sqrt{v^2}\lambda_{eff} \tag{5.30}$$

Model constants are given in Table 5.1.

Table 5.1 Model constants

$A_0 = 4.04$	$C_{TS,crit} = 1000$	$C_{\omega 3} = 0.3$
$A_S = 2.12$	$C_{R,NAT} = 0.02$	$C_{\omega R} = 1.15$
$A_\nu = 3.8$	$C_{11} = 3.4 * 10^{-6}$	$C_\lambda = 2.495$
$A_{BP} = 0.2$	$C_{12} = 1.0 * 10^{-10}$	$\beta^* = 0.09$
$A_{NAT} = 200$	$C_R = 0.32$	$\mathrm{Pr}_\theta = 0.85$
$A_{TS} = 200$	$C_{\alpha,\theta} = 0.035$	$\sigma_k = 1$
$C_{BP,crit} = 1.5$	$C_{SS} = 3.0$	$\sigma_\omega = 1.17$
$C_{NC} = 0.1$	$C_{\tau,1} = 4360$	$\sigma_{\omega 2} = 1.856$
$C_{NAT,crit} = 1450$	$C_{\omega 1} = 0.44$	
$C_{INT} = 0.95$	$C_{\omega 2} = 0.92$	

Boundary conditions

The boundary conditions follow the ideas of [5]. At solid boundaries the no slip condition enforces

$$k = v^2 = 0 \tag{5.31}$$

and a zero normal gradient condition is used for ω

$$\frac{\partial \omega}{\partial \eta} = 0 \tag{5.32}$$

where η is the coordinate normal to the wall.

At the inlet, the values for k and ω are calculated exactly as in other k-ω type models. The turbulence kinetic energy is usually obtained based on the inlet turbulence intensity Tu_∞, assuming isotropic freestream turbulence

$$Tu_{\infty} = \frac{\sqrt{\frac{2}{3}k}}{U_{\infty}} \tag{5.33}$$

The value of ω is chosen to match the available freestream information. For example, if the turbulent length scale or decay rate is known, then ω is chosen to appropriately reproduce the freestream conditions. Since a good representation for v^2 is given by $v^2 \approx k - k_L$ and the appropriate inlet boundary condition for k_L is $k_L = 0$ [5], then it is suggested to use $v^2 = k$ will be used at the inlet.

Test cases

The model was implemented as a User-Defined Function (UDF) in the commercial finite volume CFD solver ANSYS FLUENT version 14.0 [60]. The pressure-based solver option was used with the SIMPLE method for pressure-velocity coupling. This approach has been well demonstrated to be appropriate for incompressible single-phase flows. All results presented in this document used a second-order upwind-based spatial discretization scheme. The test cases selected include standard boundary layer cases along with an airfoil test case in order to check the behavior of the model for transitional boundary layers. The model is expected to behave qualitatively equal to the $k_T - k_L - \omega$ model in these cases. Two free shear flows cases are included as well, to demonstrate the improvements in accuracy due to the modifications presented in this document, for regions of separated shear layer flow.

Boundary layer test cases

The model was initially tested and calibrated on boundary layer cases. The new model was expected to have a similar behavior for transitional boundary layers to its baseline model. Flat plate cases, with and without pressure gradients, were chosen, as well as an airfoil test case, to test the model on transitional flows. A fully turbulent backward facing step flow test case was also included.

Flat plate

The transition prediction behavior of the model was initially tested in zero-pressure and variable pressure gradient flat plate boundary layers, with different freestream turbulence intensities. The test cases chosen match the T3A, T3B, T3A- and T3C2 validation cases from the classic ERCOFTAC database [18]. The T3 test cases were developed specifically for validation of transition models and have become a recognized standard in the research community.

For each of the flat plate test cases, the computational domain was constructed to match the experimental geometry. A symmetry plane was applied at the bottom of the domain, upstream of the leading edge. This was done to allow a natural stagnation and boundary layer initiation. The other boundaries were set as velocity inlet, pressure outlet, wall, and symmetry planes, as appropriate. The extent of the domain in the vertical (y) direction was chosen to be far enough from the plate to ensure negligible acceleration of the freestream due to the finite plate thickness and boundary layer development.

The meshes, shown in Figure 5.1, consisted of block-structured quadrilaterals clustered in the near-wall and leading edge regions, and triangular elements far from the wall for the pressure gradient case. The first near-wall cell was placed such that y^+ was

less than one over the entire plate surface for all cases considered. The number of grid cells in the two-dimensional meshes was 30,196 and 24000. The top wall for the second geometry is contoured in order to produce a varying (favorable and adverse) streamwise flow acceleration. The countered top of the geometry is built to match the experimental pressure distribution on the plate and it is also responsible for producing a non-zero streamwise velocity gradient, which is negligible for the ZPG test cases

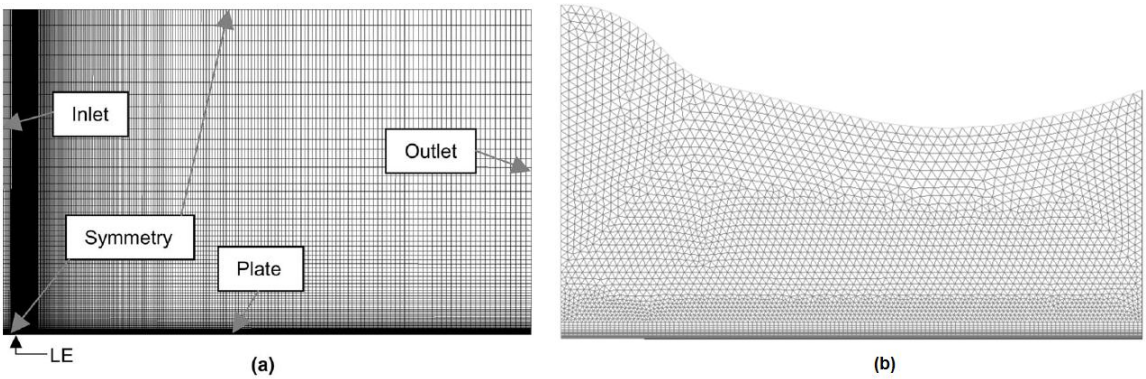

Figure 5.1 Meshes used for flat plate test cases.

(a) ZPG flat plate T3A-, T3A, T3B. (b) Pressure gradient flat plate T3C2

The inlet conditions were identical to those reported in [5], and were found to reproduce the correct freestream decay of turbulent kinetic energy, in agreement with the experimental data. The inlet values for the dimensionless turbulence variables are listed in Table 5.2.

Table 5.2 Leading edge freestream conditions for flat plate test cases

Test case	**Tu(%)**	μ_T/μ
T3A-	0.874	8.73
T3A	3.3	12.0
T3B	6.5	100.0
T3C2	3.0	11.0

The effective turbulent viscosity used to determine the inlet value of ω is defined as:

$$\mu_T = \rho\beta^* \frac{v^2}{\omega} \tag{5.31}$$

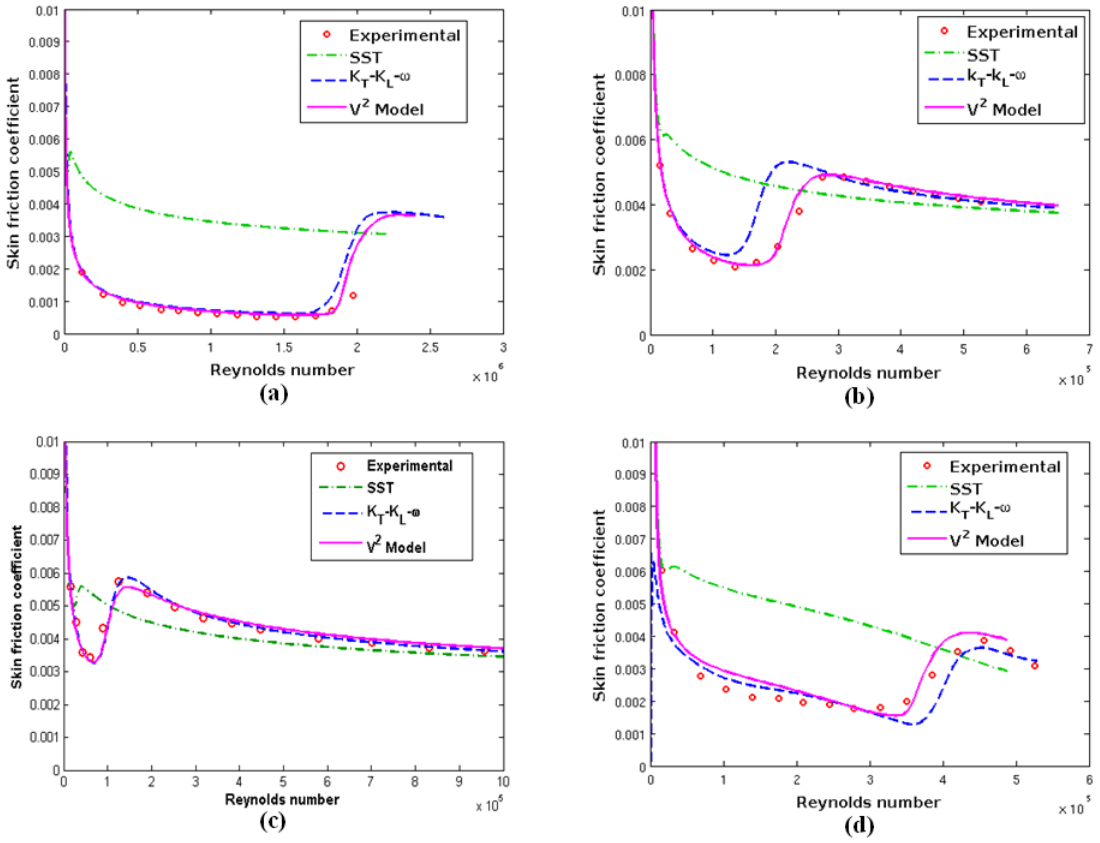

Figure 5.2 Skin friction coefficient for flat plate test cases.

(a) T3A-, (b) T3A, (c) T3B, (d) T3C2

Figure 5.2 shows the skin friction coefficient versus dimensionless downstream distance predicted by the new model (v^2 Model) compared with the experimental data

[18], the fully turbulent SST $k-\omega$ model [21] and the $k_T - k_L - \omega$ transitional model [5]. First, it is apparent that the v^2 model predicts very well the transition location in all 4 cases. For the ZPG cases, the shear stress levels in the laminar and transitional region show excellent agreement with the experimental data, while a small overprediction is apparent in the pretransitonal region for the T3C2 case. All cases show a smooth transition rather than a sudden jump in shear stress levels. Figure 5.2 shows clearly that the SST $k-\omega$ model is incapable of predicting transition, which is a very important feature in all the cases above. This is expected since this model was developed to be applied solely to fully turbulent flows. There is also a slight improvement on the transition location of the v^2 model compared with the transitional $k_T - k_L - \omega$ model. The levels of shear stress are almost the same in both models in the pretransitional and fully turbulent regions.

Figure 5.3 and 5.4 show the velocity and total kinetic energy profiles of the presented v^2 model and the $k_T - k_L - \omega$ model. The profiles of the SST model are not included due to its inability to resolve laminar and transitional flows. The profiles were obtained in the locations $\mathrm{Re}_x = 10^5$ for the laminar region, $\mathrm{Re}_x = 2.25 \times 10^5$ for the transitional region and $\mathrm{Re}_x = 5 \times 10^5$ for the turbulent region. The results in the velocity profiles are slightly better for the v^2 model in all regions, while the $k_T - k_L - \omega$ model better captures the peaks of the total kinetic energy in all three regions. In general the results of the two transitional models are very similar in all four cases, and it is concluded that the proposed model correctly inherits the transitional behavior of the baseline model, as expected.

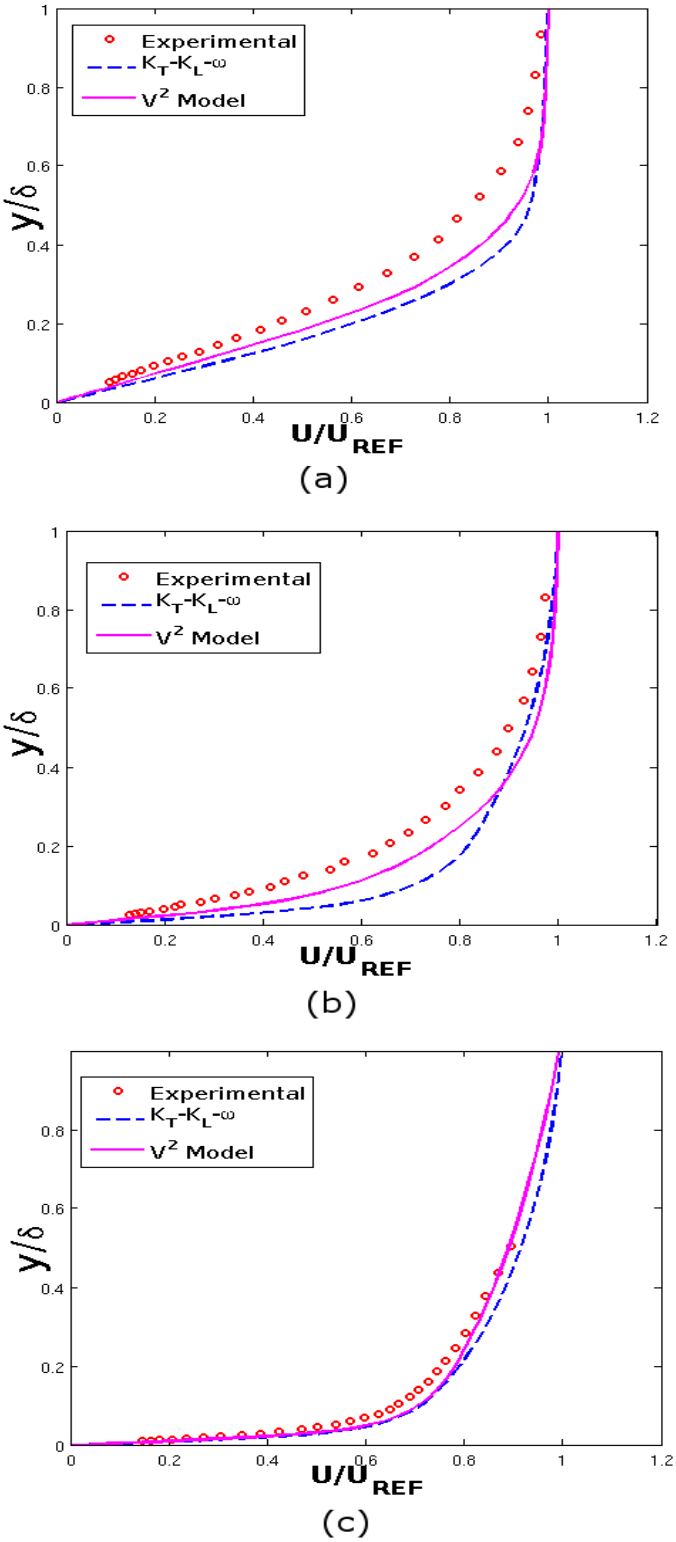

Figure 5.3 Velocity profiles in the laminar, transitional and turbulent regions respectively for the T3A case.

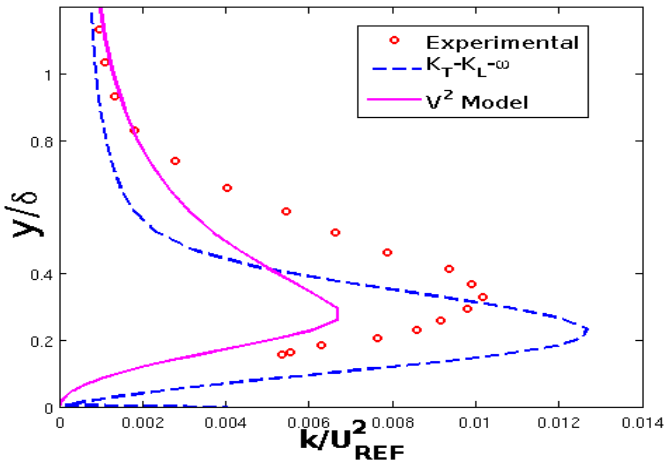

(a)

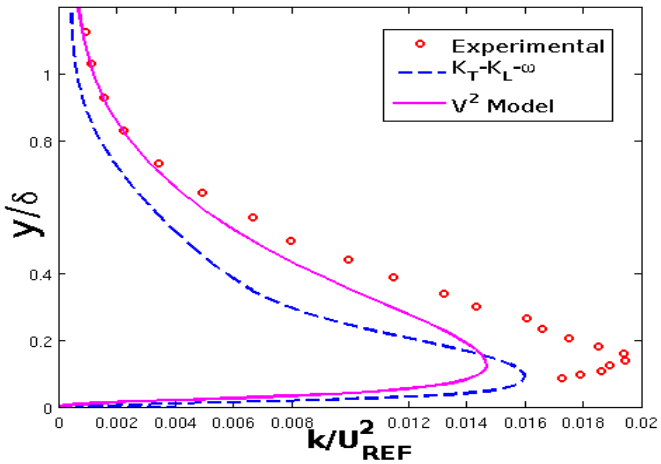

(b)

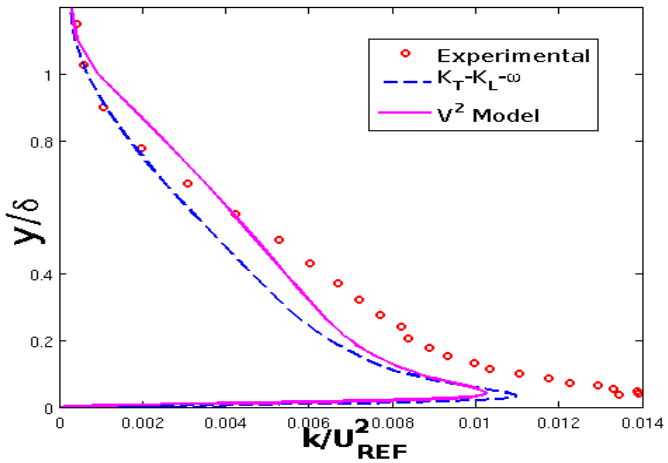

(c)

Figure 5.4 Turbulent kinetic energy profiles in the laminar, transitional and turbulent regions respectively for the T3A case.

VPI cascade

A more realistic geometry that illustrates the importance of transitional models is the airfoil test case performed at the Virginia Polytechnic Institute, and documented for the express purpose of validating CFD simulations. As shown previously, the transition in the boundary layer affects the skin friction distribution, which indirectly affects the separation or reattachment of the flow in airfoils, and it can dramatically alter the force and moment distribution of lifting bodies. The experiments were documented by Radomsky and Thole [34,35].

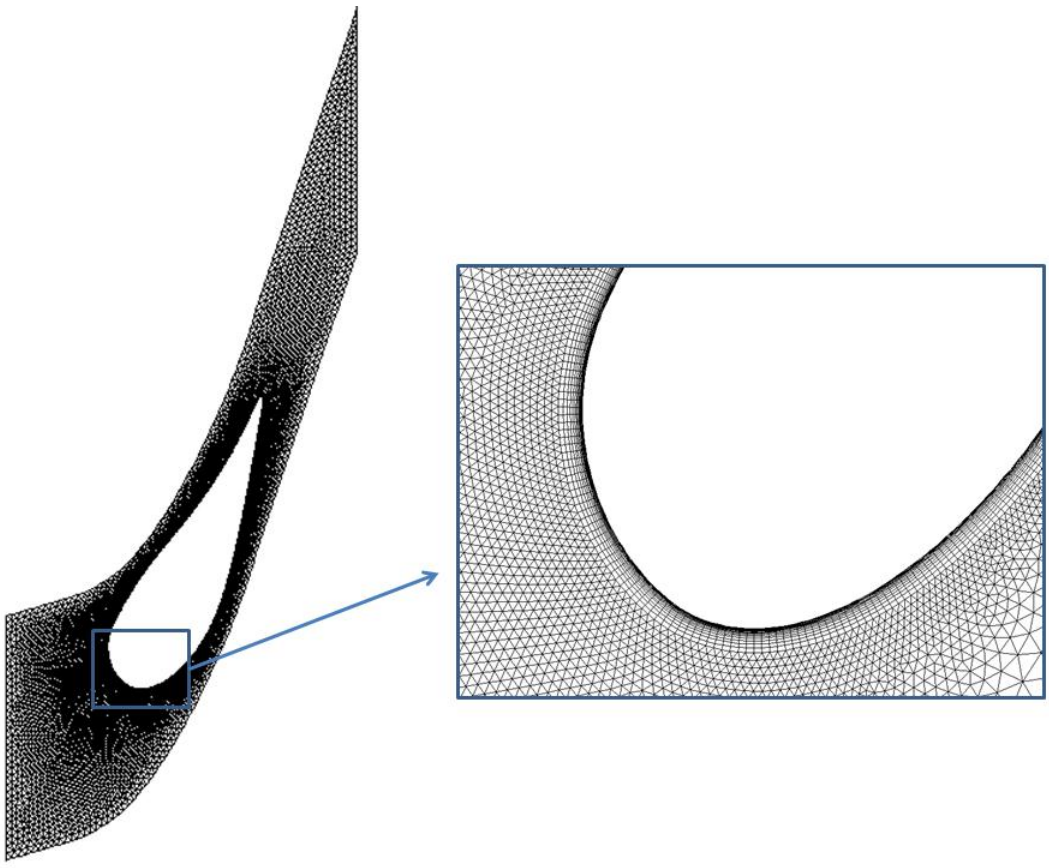

Figure 5.5 Periodic domain and mesh for the VPI cascade

The mesh and boundary conditions for this test case are the same as in [5], The hybrid mesh in figure 5.5 was built with 24,386 cells. The inlet air velocity was 5.85 m/ s, which corresponds to a Reynolds number of 230,000 based on a chord length of 59.4 cm. Two test cases, corresponding to relatively high freestream turbulence levels of 10% and 19.5%, were run. For the two cases, the specific dissipation rate was chosen to correspond to a turbulent viscosity ratio μ_T / μ of 900 and 2100, respectively.

A constant heat flux boundary condition was applied on the airfoil surface and the heat transfer coefficient was calculated using the three models previously discussed for comparison. Figure 5.6 shows heat transfer coefficient versus distance along the airfoil surface (from the stagnation point) normalized by chord length (s /C). Negative values of s indicate the pressure surface; positive values indicate the suction surface. Transition is achieved for both transitional models with relatively equal accuracy in both cases, while the SST model again fails to reproduce this result.

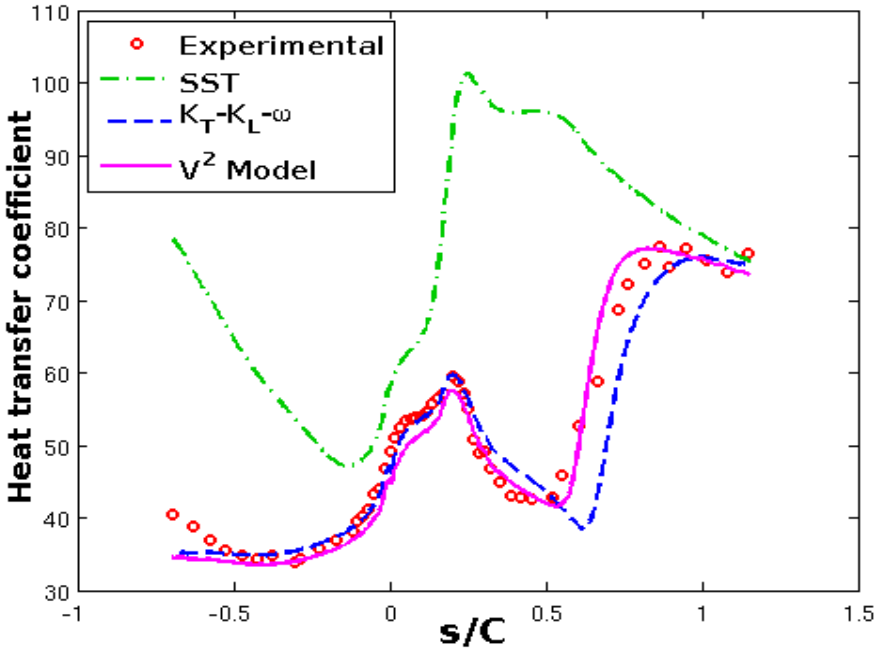

(a)

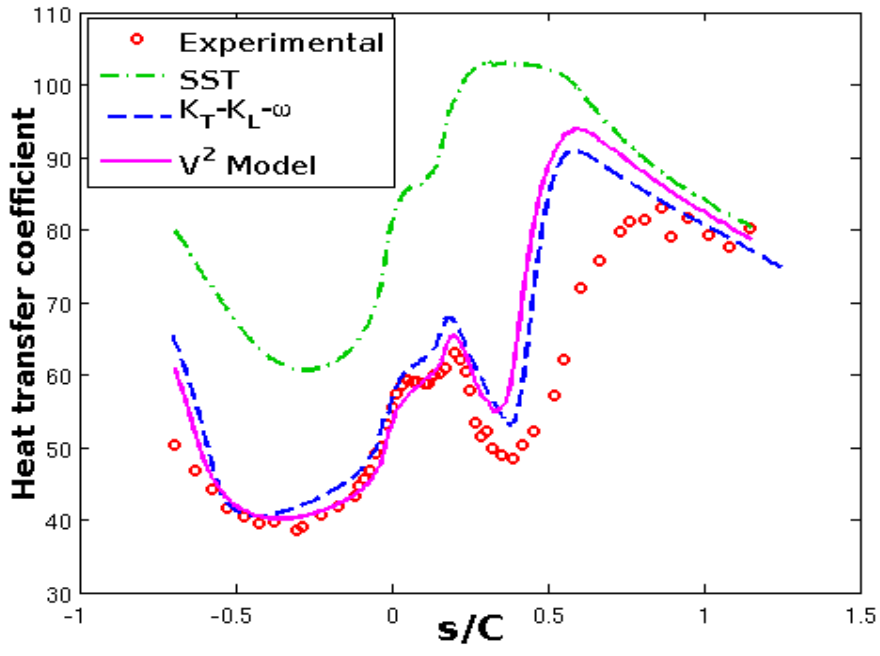

(b)

Figure 5.6 Heat transfer coefficient for the VPI test case.

(a) $Tu_{\infty} = 10\%$, (b) $Tu_{\infty} = 19.5\%$

Backward facing step

The third boundary layer test case used in this study is the backward facing step, which is a widely used benchmark test case for turbulence model validation. In this test case the flow separates at the step with a reattachment farther downstream. Figure 5.7 shows the geometry and mesh. In order to let the flow develop, the domain before the step was built to measure $100\ H$, where $H = 1.27\ cm$ is the high of the step. With an inlet velocity of $44.2\ m/s$ and $Tu_{\infty} = 3.0\%$, the flow is fully turbulent at the step location. The details of the experimental configuration are found in [36].

Figure 5.8 shows the pressure distribution and the skin friction coefficient calculated at the wall of the domain (bottom part). The flow is fully turbulent in this section of the domain and the SST model shows a slightly better performance related to the transitional models. The negative and positive peaks in the pressure coefficient are very well captured by the SST model, followed in accuracy by the proposed v^2 model. The three models show good accuracy in predicting the skin friction coefficient. The reattachment point is very well predicted by the SST model, while it occurs a little bit early for the v^2 model and much earlier for the $k_T - k_L - \omega$ model.

Figure 5.9 shows the mean stream wise velocity profiles at different locations after the step. In the recirculation zone (x/H=1.0, 2.0, 3.0), the SST model accurately predicts the velocity profiles in the boundary layer, while, in the other two models, the negative peak close to the wall is over predicted. The two transitional models behave in nearly the same form away from the wall. After reattachment, the v^2 model seems to be more accurate inside the boundary layer (but not too close to the wall) than the other models, while they have a similar behavior outside of the boundary layer.

The boundary layer experiments have demonstrated the ability of the v^2 model to predict transitional flows with reasonable accuracy, similar to its baseline model, the $k_T - k_L - \omega$ model. Furthermore, based on the previous test cases, it is clear that laminar-to-turbulent transition is an important an inherent characteristic in several fluid flow fields, however, the SST $k - \omega$ model is incapable of predicting this process. In the next subsection, the models will be tested on free shear flows where the v^2 model is expected to be superior to the $k_T - k_L - \omega$ model.

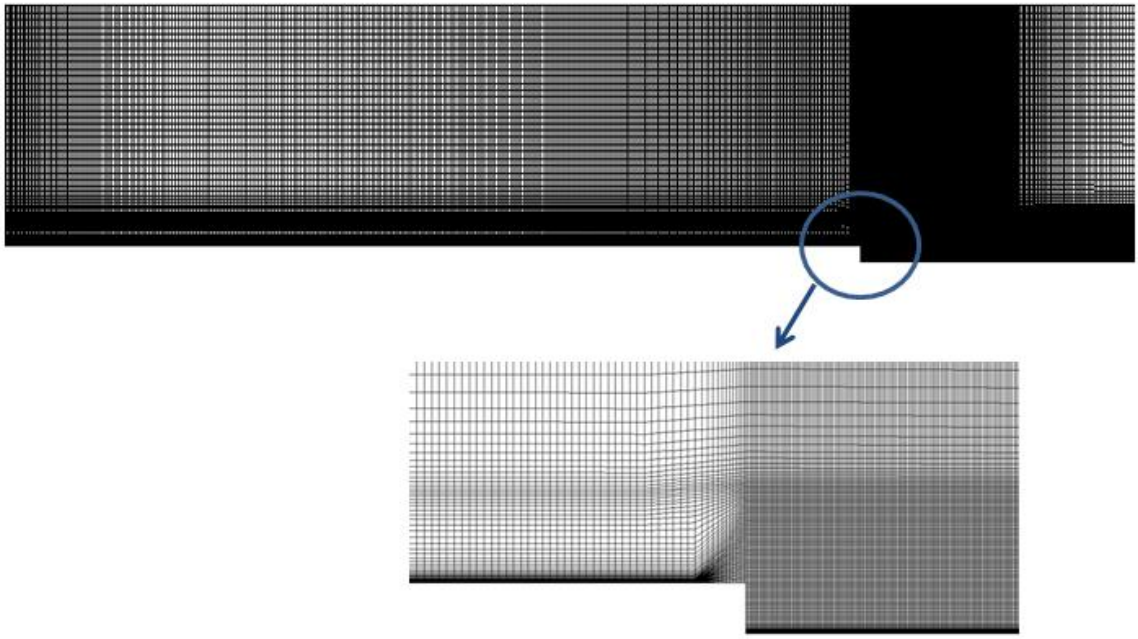

Figure 5.7 Geometry and mesh for the backward facing step

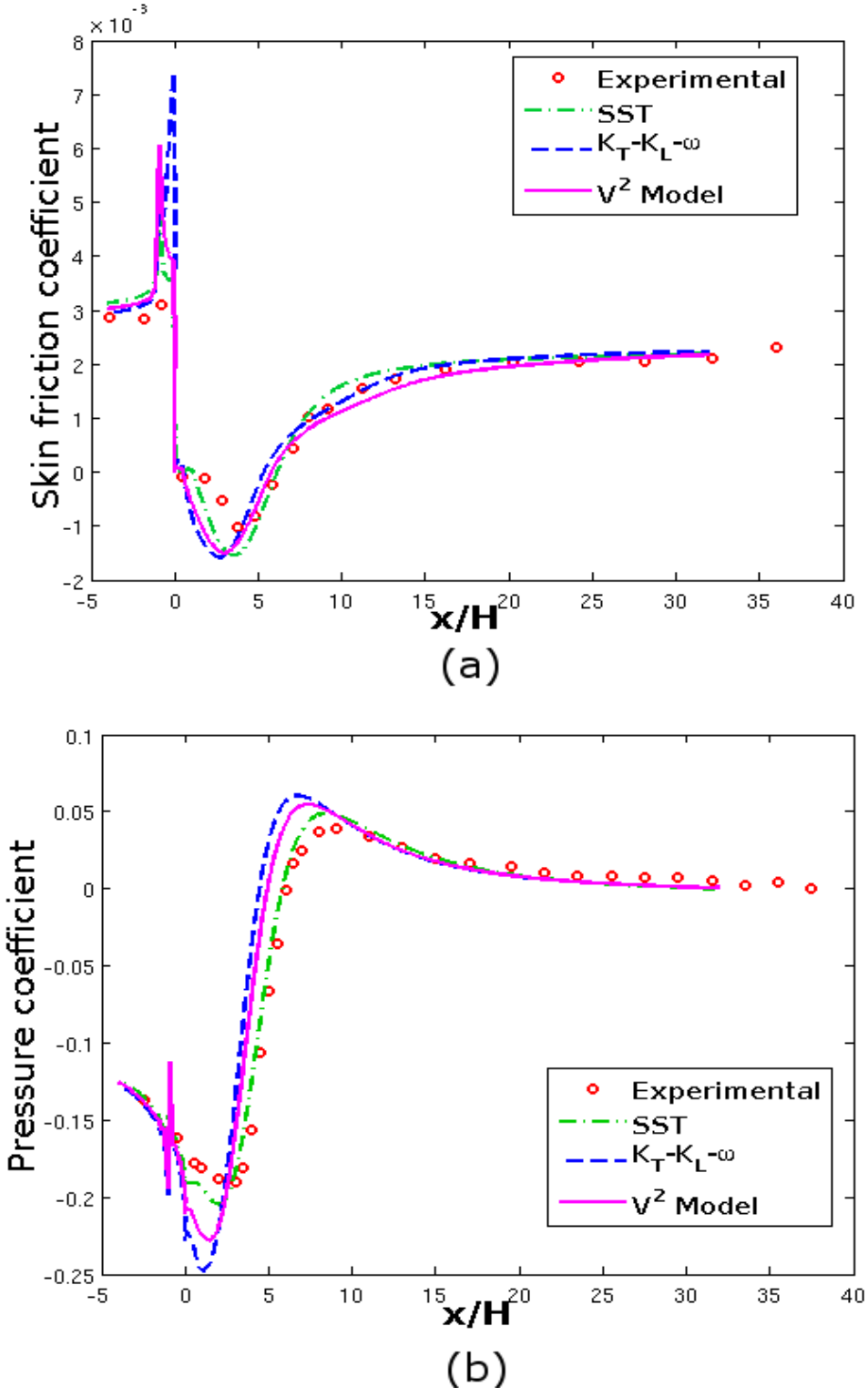

Figure 5.8 Pressure coefficient and skin friction coefficient calculated at the bottom wall.

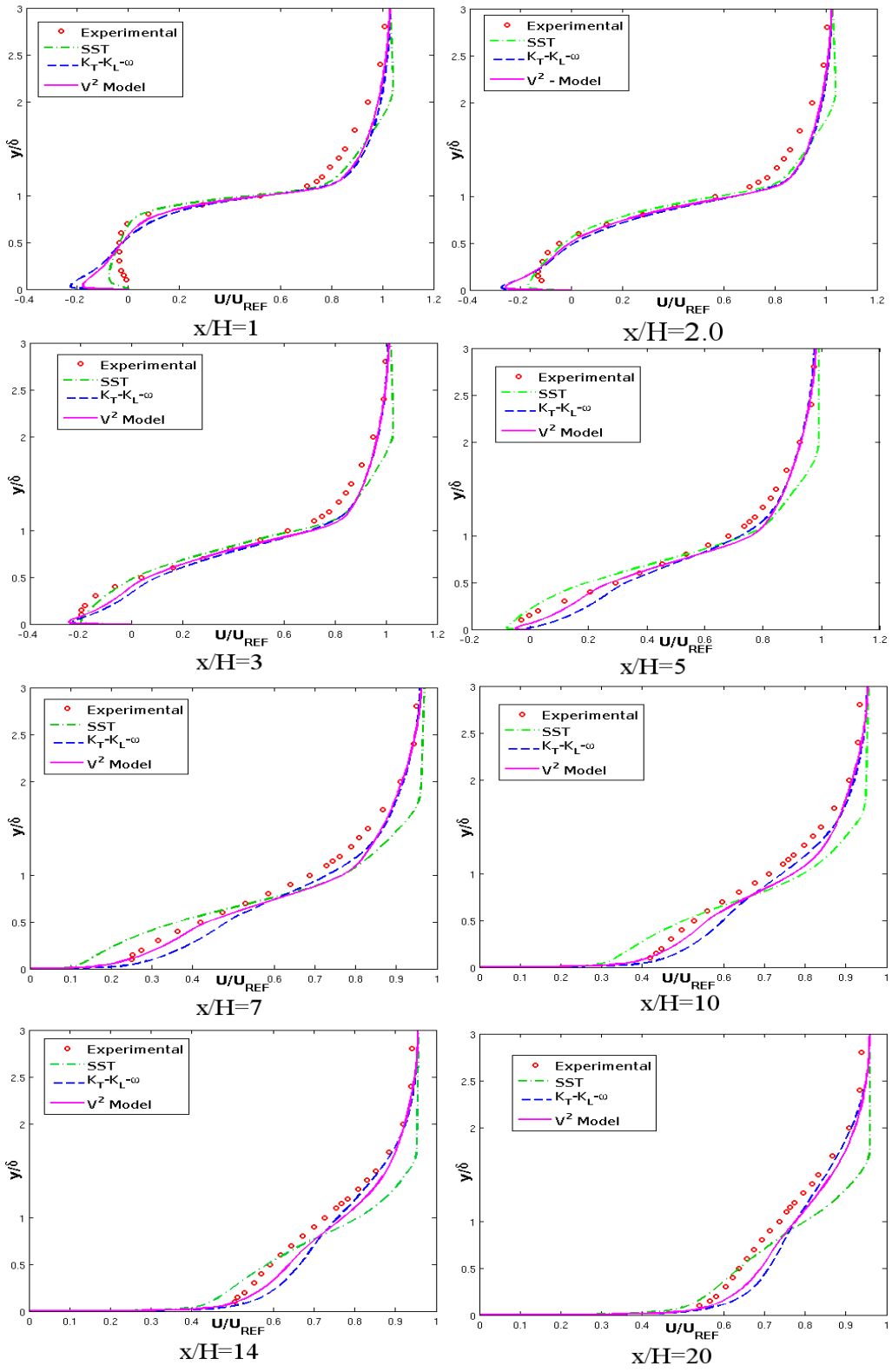

Figure 5.9 Mean velocity profiles at different streamwise stations.

Free shear flows

Up to this point, the v^2 and $k_T - k_L - \omega$ transitional models have been compared on transitional boundary layers, and so far it has been demonstrated that the v^2 model behaves qualitatively equal to its baseline model, and sometimes with minor improvements for particular test cases. In this section the models will be tested for free shear flows, where studies have demonstrated ([22]) that the $k_T - k_L - \omega$ model does not predict the characteristics of such flows well.

Round jet flow

Jets are widely used in many engineering applications such as cooling systems or aerodynamic stabilization of floating strips [71]. Their fully turbulent characteristics and capacity for high mixing process make them appealing in many processes. There are several experimental and numerical studies ([22], [27], [37]) involving axisymmetric round jet flows, in which the performance of RANS models is mixed. Of particular interest are the results of Ghahremanian and Moshfegh in [22]. They studied the behavior of several transitional and fully turbulent RANS models on a three-dimensional fully turbulent, round jet. Their results show that the $k_T - k_L - \omega$ transitional model performs poorly for this particular case. One of the key goals of this research is to correct these apparent failures in free shear flows of the $k_T - k_L - \omega$ in the new v^2 model.

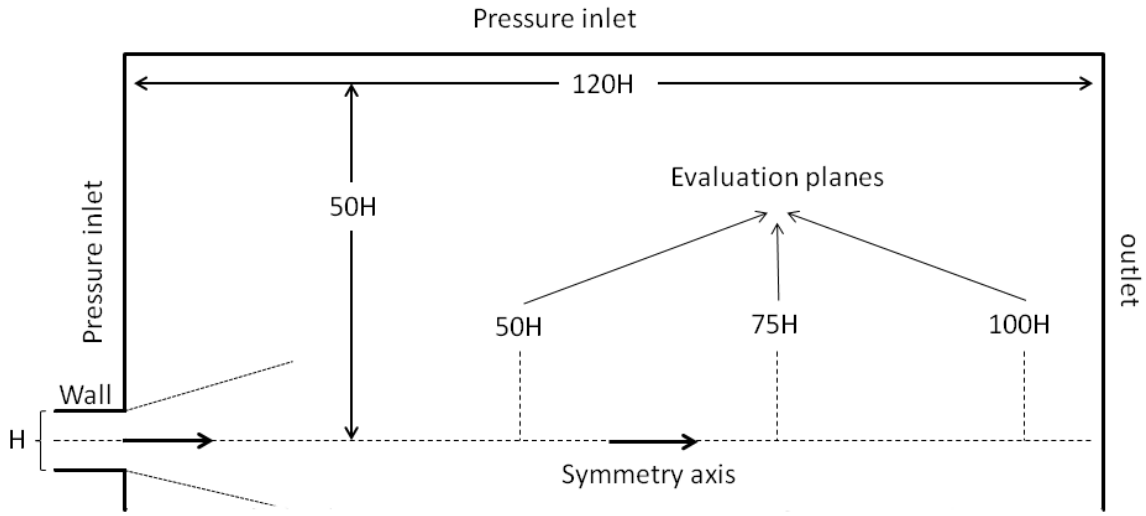

Figure 5.10 Computational domain configuration for the jet.

A sketch for the domain and the mesh used are shown in figures 5.10 and 5.11. Only half of the domain was used in the calculations, taking the centerline of the domain as a symmetry axis. The flow conditions follow the values reported in the experimental study in [37], with a jet exit velocity of $56.2\,m/s$ and turbulence intensity less than 0.58%. In the experimental studies, the flow is manipulated to transition to turbulent before the exit of the jet. Due to this, two grids were used in this study. In the first the length of the channel before the exit is 3H and the fully turbulent SST $k-\omega$ model was run in this domain and profiles of velocity, turbulent kinetic energy and specific dissipation rate were obtained at 1.5H from the inlet of the channel. In the second mesh, the length of the channel before the exit is 1.5H. The profiles obtained from the SST model were used as inlet condition for the v^2 and $k_T - k_L - \omega$ transitional models.

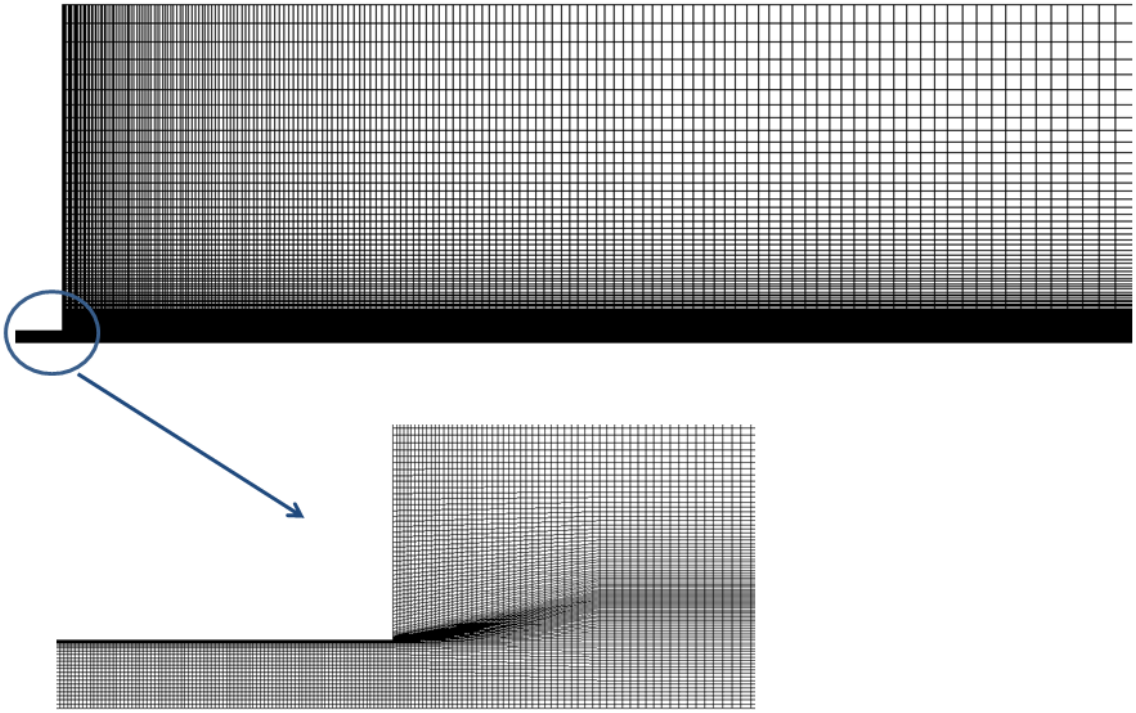

Figure 5.11 Mesh used for jet flow test case.

Figures 5.12 and 5.13 show very clearly the advantages of the new v^2 transitional model, over the existing $k_T - k_L - \omega$ model. The latter is incapable of predicting the centerline velocity decay of the jet, while the v^2 model perform nearly as well as the SST model. This behavior of the $k_T - k_L - \omega$ model was previously documented in [22], along with other results obtained from other RANS turbulent models where the SST $k - \omega$ model was clearly superior to the others. The combination of these results could suggest that the proposed v^2 model is a competitive alternative among RANS transitional models.

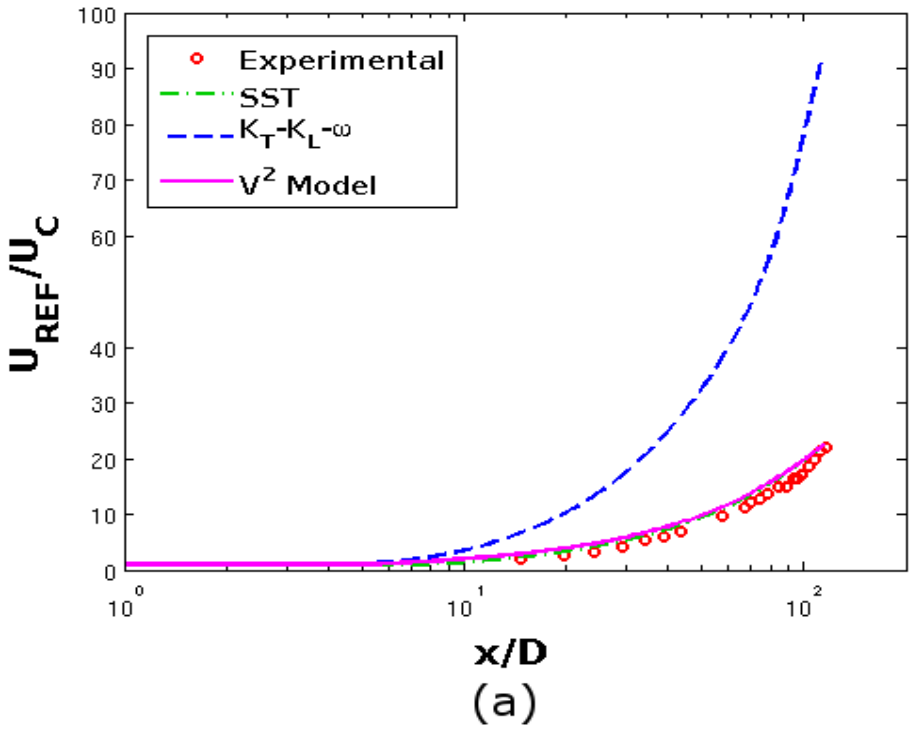

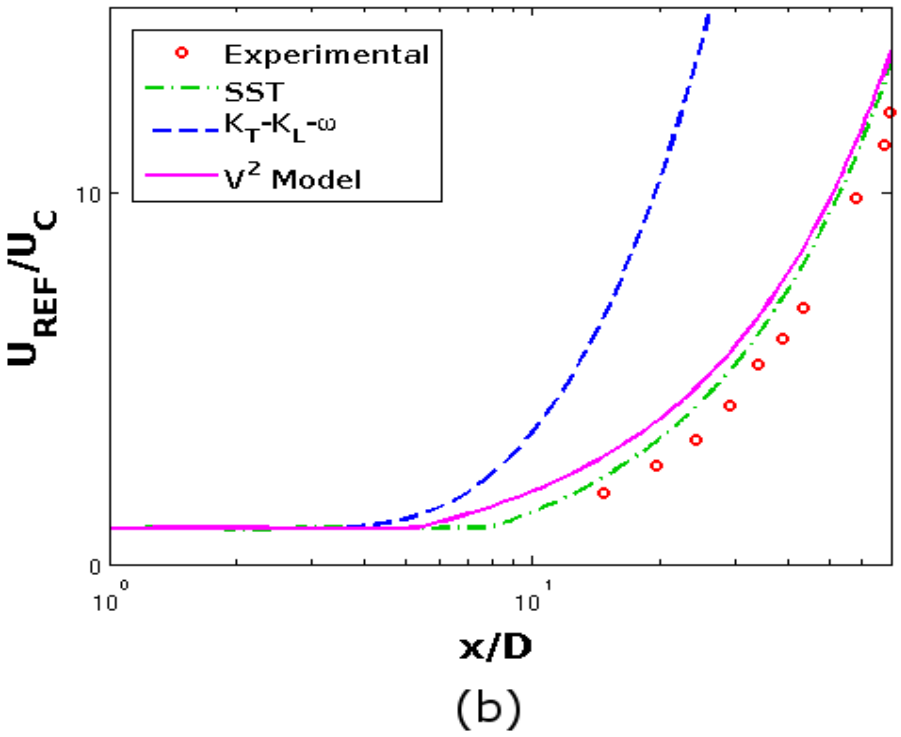

Figure 5.12 Inverse centerline velocity decay.

(a) Inverse centerline velocity decay. (b) Close-up at the exit of the channel.

Near the exit of the channel, the v^2 model predicts the virtual origin of the jet (the distance between the exit of the channel and the x-intercept of the straight line representing the inverse velocity decay) to occur too early, which causes a small deviation from the experimental data near the exit of the channel. Further downstream (about 35H) the v^2 and the SST models behave asymptotically equal.

In figure 5.14, the cross-sectional mean velocity profiles are plotted versus the nondimensional radial coordinate $\eta = y/(x - x_0)$, where x_0 represents the virtual origin predicted by each model. The results are compared with experimental data (Stationary Hot Wire (SHW), Laser-Doppler anemometry (LDA) and Flying Hot Wire (FHW)) reported in [37]. While the SST and the v^2 model produce reasonably accurate results, the $k_T - k_L - \omega$ model shows significant discrepancy away from the centerline of the yet.

The jet flow results clearly demonstrate the advantages of the proposed v^2 model compared with its baseline model. For free shear flows, the v^2 model behaves more like the SST $k - \omega$ model, while in transitional boundary layers it inherits the characteristics of the $k_T - k_L - \omega$ model.

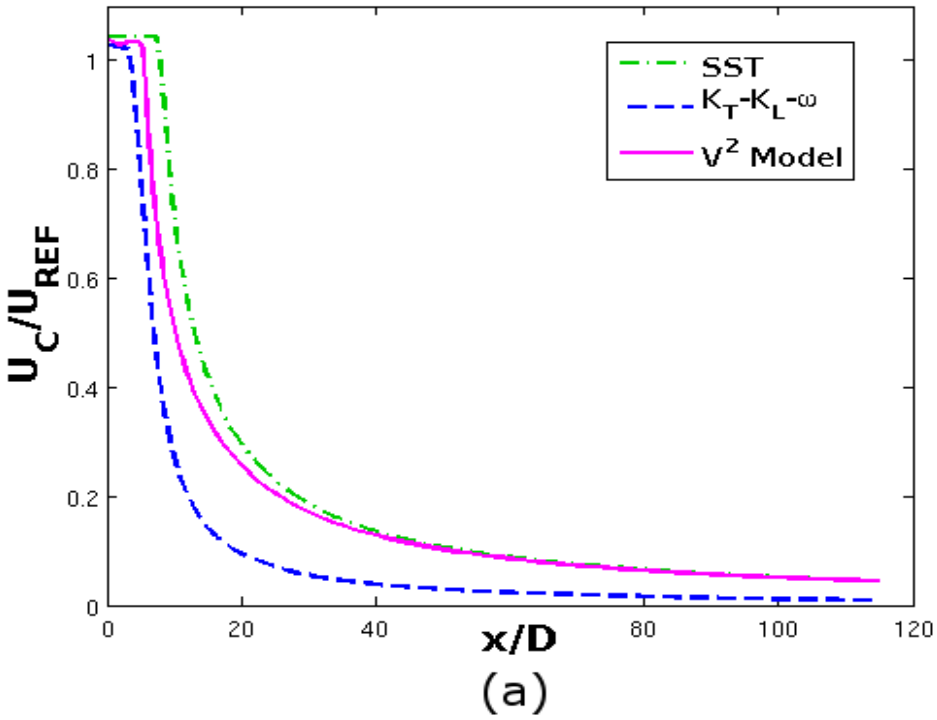

(a)

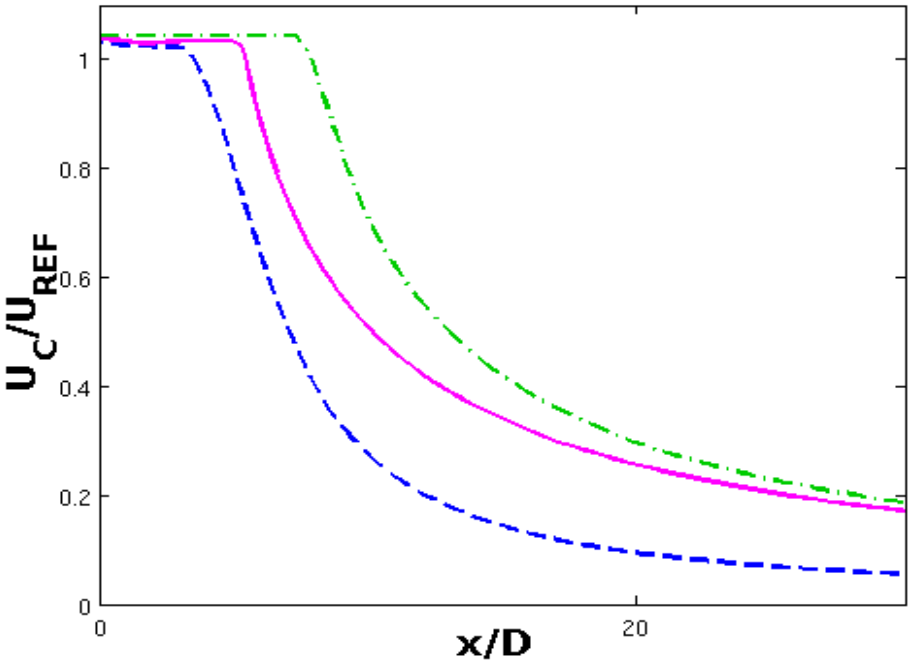

(b)

Figure 5.13 Centerline velocity decay.

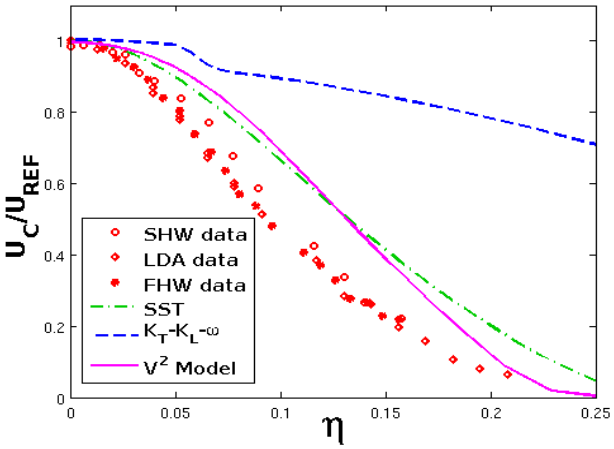

(a)

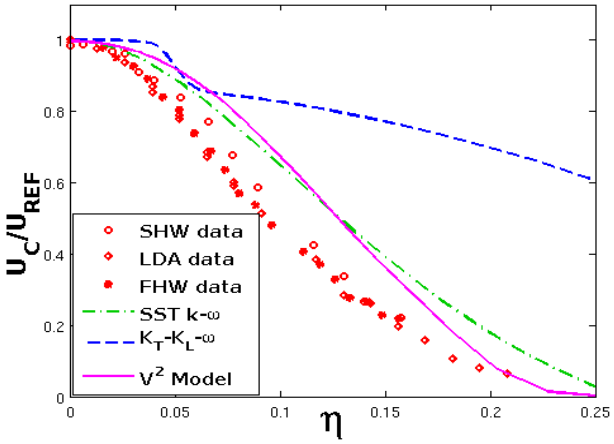

(b)

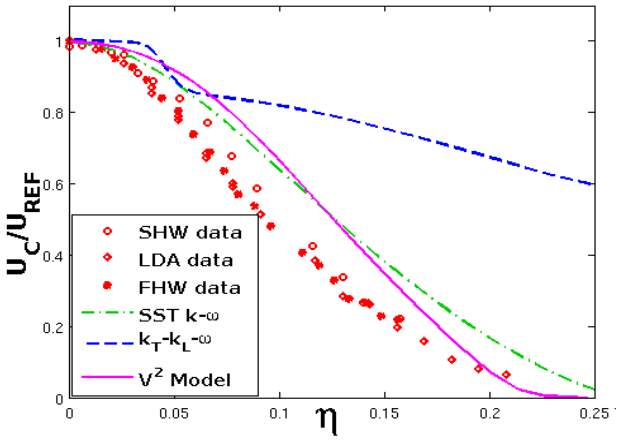

(c)

Figure 5.14 Cross-sectional mean axial velocity profiles.

(a) x/H=50, (b) x/H=75, (c) x/H=100.

Finite flat plate

In this section, a finite thin flat plate placed parallel to a uniform stream is considered. At the end of the plate a wake flow is formed and the models will be evaluated in that region. The flat plate wake is considered as an idealized configuration of flows behind two dimensional streamlined airfoils or gas turbine blade. The change from a wall bounded shear-flow type to a boundary free flow makes the test case appealing for testing turbulence models.

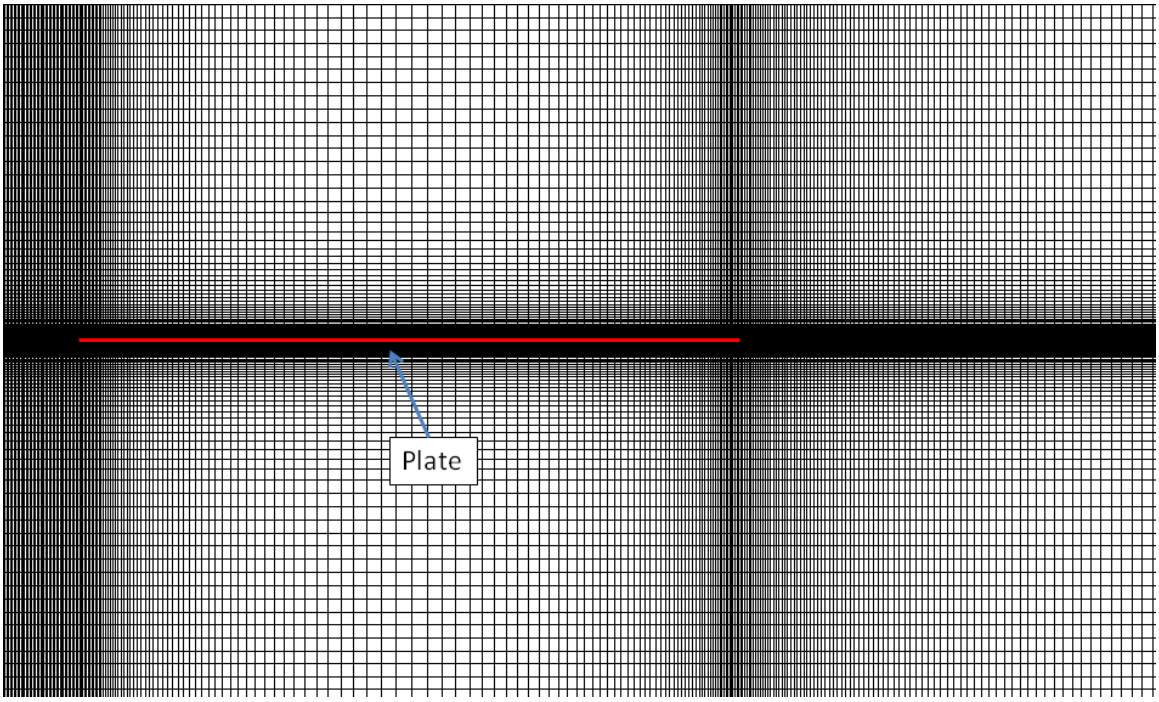

Figure 5.15 Mesh for the finite flat plate test case

Figure 5.15 shows the mesh used for the finite flat plate test case. The configuration of the domain and flow conditions match the experimental investigation in [38]. The plate was considered infinitesimally thin and the freestream velocity was

$8.6\,m/s$ while the turbulence intensity was less than 0.2%. In the experimental studies, the flow is manipulated again to make the flow transition before the flow reach the trailing edge of the plate by using of a 1.4 mm diam tripping wires on both surfaces of the plate near the leading edge. Again, two meshes were built. In the first, the length of the plate is 0.6m and it is placed with the leading edge at a distance of 0.1m from the inlet exactly as illustrated in figure 5.15. The fully turbulent SST $k-\omega$ model was run using this mesh and profiles of velocity, turbulent kinetic energy and specific dissipation rate were calculated at a distance 0.1m downstream of the leading edge of the plate. In the second mesh the length of the plate is 0.5m and the leading edge of the plate is placed exactly at the inlet of the domain. The profiles taken from the SST $k-\omega$ model were used as inlet conditions for the $k_T - k_L - \omega$ and v^2 models.

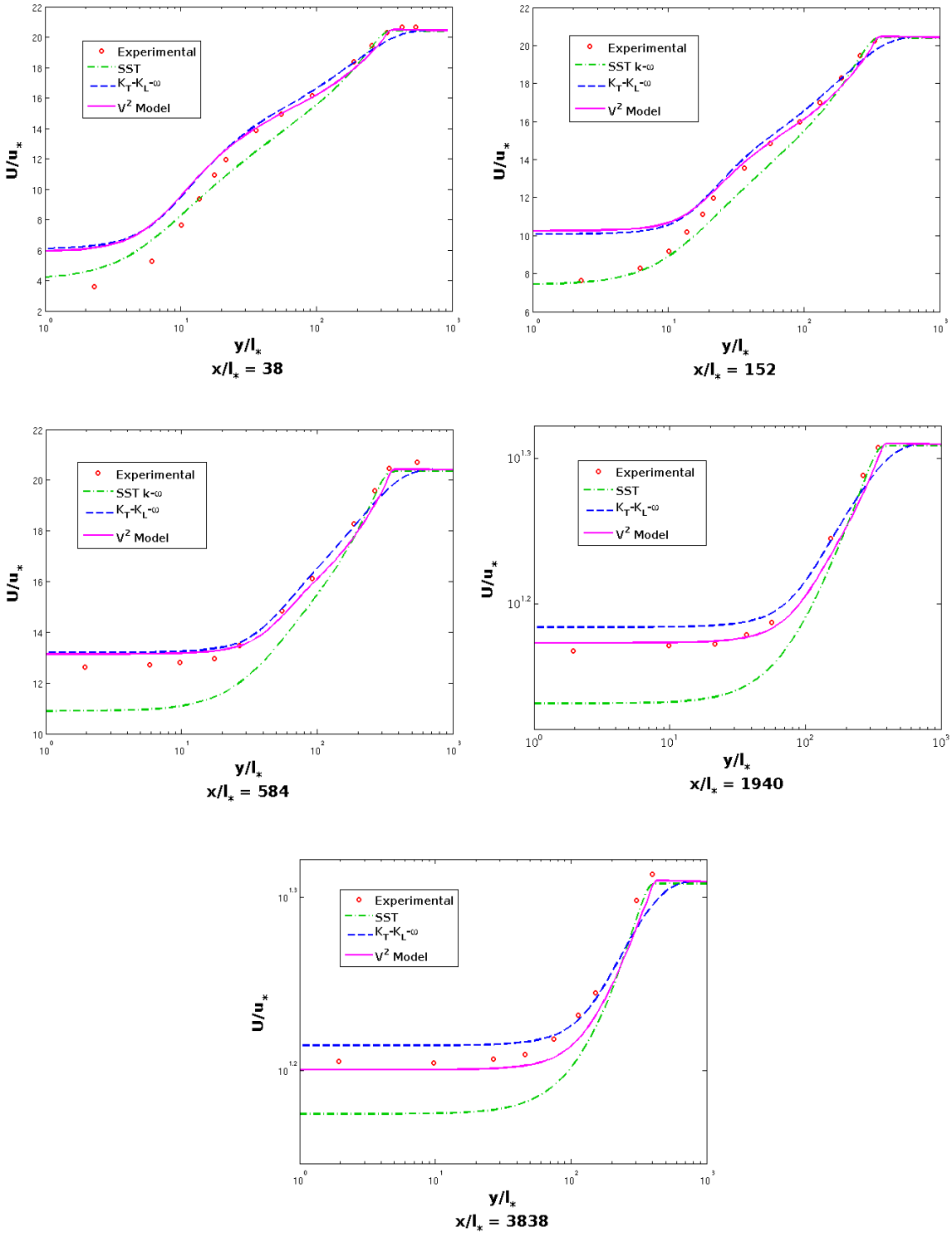

Figure 5.16 Mean velocity profiles calculated at different locations downstream in the wake region.

Figure 5.16 shows plots of the profiles of velocity normalized by the friction velocity u_* at the trailing edge of the plate, versus the vertical distance normalized by the inner-wake-layer length scale $l_* = \nu / u_*$. The friction velocity was calculated using the SST $k-\omega$ model to ensure consistent comparison across all models.

The results show good agreement of the velocity profiles calculated with the v^2 model and the experimental data. When the velocity approaches the freestream value; the SST $k-\omega$ and v^2 models reproduce the correct behavior of the flow while the $k_T - k_L - \omega$ model produces a smooth curve before reaching the freestream value, which is not characteristic of the profiles.

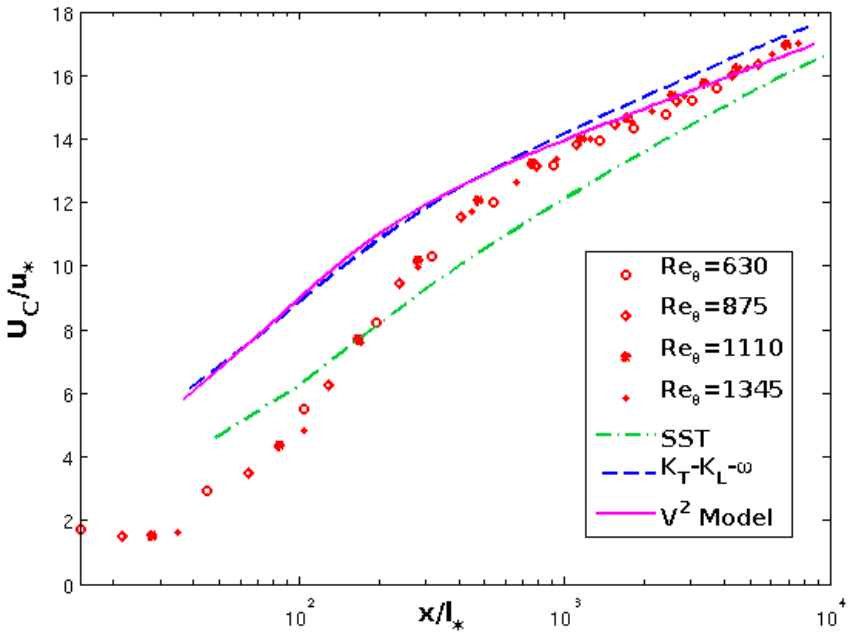

Figure 5.17 Mean centerline velocity along the wake compared with experimental data at different Reynolds numbers

In figure 5.17 the centerline velocity is compared with experimental data obtained with different freestream velocities (different momentum thickness Reynolds number in figure 5.17) reported in [38]. The SST $k-\omega$ model is more accurate near the trailing edge of the plate, but the v^2 model results are more accurate far downstream.

The results for the finite flat plate confirm the SST-like behavior of the v^2 model for free shear flows which leads to more accurate results compared to the $k_T - k_L - \omega$ model. This suggests that the v^2 model has a wider range of applications compared to the $k_T - k_L - \omega$ model, and can be more confidently applied for complex test cases that contain features of both attached boundary layers and separated shear flows.

CHAPTER VI

A SIMPLER MODEL FORMULATION FOR TRANSITIONAL FLOWS

This chapter presents a new model formulation for prediction of boundary layer transition using a linear eddy-viscosity RANS approach. It is a single-point, physics-based method that adopts the transition concept presented in the previous chapters as an alternative to the (LKE) framework. The version of the model presented here uses the SST $k-\omega$ model as the baseline, and includes the effects of transition through one additional transport equation for v^2. Here v^2 is interpreted as in the previous chapter, it represents the energy of fully turbulent, three-dimensional velocity fluctuations, while *k* represents the energy of both fully turbulent and pre-transitional velocity fluctuations. Simplicity of the formulation and ease of extension to other baseline models are two potential advantages of the new method.

The model in chapter V improves the accuracy of the $k_T - k_L - \omega$ model in [5] when the term that controls the behavior in the wake region is replaced by a SST-like term. It is valid to say that the gain in accuracy was achieved by increasing the complexity of the model.

The new transitional model presented in this chapter is an initial version of a model that is intended to be dramatically simpler in the formulation of the equations

and with less model constants than the model presented in chapter V, but with at least the same accuracy. The initial version of this model is presented in the next sections.

Model equations

For simplicity the equations are presented in their incompressible forms. The model equations have the compact form:

$$\frac{Dk}{Dt} = P_k - D_k + \frac{\partial}{\partial x_j}\left[\left(\nu + \frac{\nu_T}{\sigma_k}\right)\frac{\partial k}{\partial x_j}\right] \tag{6.1}$$

$$\frac{Dv^2}{Dt} = P_{v^2} + R_{v^2} - D_{v^2} + \frac{\partial}{\partial x_j}\left[\left(\nu + \frac{\nu_T}{\sigma_{v^2}}\right)\frac{\partial v^2}{\partial x_j}\right] \tag{6.2}$$

$$\frac{D\omega}{Dt} = P_\omega - D_\omega + 2F_T(1-F_1)\sigma_{\omega 2}\frac{1}{\omega}\frac{\partial k}{\partial x_j}\frac{\partial \omega}{x_j} + \frac{\partial}{\partial x_j}\left[\left(\nu + \frac{\nu_T}{\sigma_k}\right)\frac{\partial v^2}{\partial x_j}\right] \tag{6.3}$$

where P denotes production, D denotes destruction, and R_{v^2} is the transition term that represents the activation of pressure strain terms during transition. The model terms are defined such that, in fully turbulent regions of the flowfield, $v^2 \rightarrow k$ and a form similar to the SST $k-\omega$ model is recovered. Transition initiates when the value of the term R_{v^2} becomes non-negligible, representing "activation" of the pressure strain terms and a change in structure of the fluctuating velocity field from Klebanoff modes to three-dimensional, energetic turbulence.

The production terms are expressed as:

$$P_k = \nu_T S^2, \quad P_{v^2} = F_T\left(\frac{v^2}{k}\right)P_k, \quad P_\omega = F_T\sqrt{\beta^*}\gamma\sqrt{\frac{v^2}{k}}\omega S \tag{6.4}$$

Note that the production of v^2 includes the multiplier F_T, which represents the suppressive effect of the near-wall shear layer on the pressure strain terms. This term also appears in the generation term for specific dissipation rate, ω, since transition is expected to be accompanied by a rapid reduction in turbulence length and time scales. The turbulent viscosity is modified to adopt a velocity scale based on the "fully turbulent" energy, v^2, and a wall-limited length scale:

$$\nu_T = C_\mu \sqrt{v^2} L_T \tag{6.5}$$

$$L_T = \min\left(\frac{\sqrt{k}}{\omega}, C_L \beta^* d\right) \tag{6.6}$$

The eddy viscosity coefficient introduces a realizability constraint similar to the SST $k-\omega$ model:

$$C_\mu = \frac{A_1}{\max\left(A_1, \frac{S}{\omega}\right)} \tag{6.7}$$

Note the simplicity in the formulation of the turbulent viscosity ν_T defined by equations (6.5)-(6.7) compared with the same term in the v^2 model (defined in equations (5.8)-(5.19)) of chapter V.

The near-wall damping function F_T controls the initiation of transition:

$$F_T = \max(F_{T1}, F_{T2}) \tag{6.8}$$

$$F_{T1} = 1 - \exp\left[-\left(\frac{\sqrt{v^2} d}{C_{T1}\nu}\right)^2\right] \tag{6.9}$$

$$F_{T2} = 1 - \exp\left[-\left(\frac{v^2}{C_{T2}\nu S}\right)^2\right] \tag{6.10}$$

Note that the arguments in equations (6.8, 6.9) have similarities with the analogous terms in the previous physics-based model discussed in chapter V. Again, activation of the pressure strain terms and transition initiation is expected to occur when the viscous diffusion time scale becomes large relative to the time scale associated with the breakdown instability. The reader is referred to [5] for more details.

The destruction terms include isotropic and near-wall components:

$$D_k = \beta^* \omega k + f_k \tag{6.11}$$

$$D_{v^2} = \beta^* \omega k + f_{v^2} \tag{6.12}$$

$$D_\omega = \beta \omega^2 + f_\omega \tag{6.13}$$

$$f_\alpha = F_W \frac{2\nu\alpha}{d^2}, \qquad \alpha = k, v^2, \omega \tag{6.14}$$

$$F_W = \exp\left(-C_W \sqrt{\frac{d\omega^2}{\nu}}\right) \tag{6.15}$$

The pressure-strain analog that drives the transitional behavior in the model is expressed in a form similar to a basic "return-to-isotropy" model:

$$R_{v^2} = C_{T3}\psi (k - v^2) \tag{6.16}$$

$$\psi = F_T \left(S + C_\psi \omega \frac{k}{v^2}\right) \tag{6.17}$$

The form of Eq. (6.17) indicates that both slow and rapid parts are included. Note that, when F_T= 1, the model will tend to enforce that $v^2 \rightarrow k$. In fact, in any region of the

flowfield for which F_T= 1 and $v^2 = k$, the solutions for v^2 and k will remain identical, which follows the conceptual description outlined above, i.e. all fluctuating energy is assumed to be classical three-dimensional turbulence.

The new model constants introduced in the transition-sensitive formulation were calibrated to best fit the experimental data of the 4 different flat plate test cases presented in this chapter and discussed in the next section, they are:

$$C_L = 2.495\ ;\ C_{T1} = 100\ ;\ C_{T2} = 3.5\ ;\ C_{T3} = 0.008$$

$$C_W = 0.3\ ;\ C_\psi = \frac{7}{8}$$

All other constants take the same values as in the SST k-ω model. Note the number of constants (without including the ones in the original SST k-ω) used in the formulation of this new model compared with the number of constants in table 1 for previous model. The simplicity of the new model is clear compared with the description of the model in chapter V.

The wall boundary conditions are different for the SST k-ω model: the new model will use $k = \omega = v^2 = 0$. The dissipation increases near the wall due to (6.14) rather than enforcing a large value of ω at the wall. Equations (6.14,6.15) ensure that the dissipation is asymptotically correct to leading order as $y \to 0$. The inlet values are calculated similar than in the model in chapter V, using equation (5.33) and $k = v^2$. For ω instead of using (5.34), it is correct to use

$$\mu_T = \rho \frac{v^2}{\omega} \tag{6.18}$$

Test cases

This section presents 6 test cases already discussed in chapter V. The flat plate geometry without and with pressure gradient is used in order test the ability of the model to predict the transition process. The correct behavior in the transition zone is the most challenging part in this case because the baseline model used is a fully turbulent model in contrast to the transitional model used in chapter V. The backward facing step test case is used to check the SST-like behavior of the new model in the fully turbulent region.

Flat plate

In this section the test cases are identical to the flat plate test cases discussed in chapter V. Again the T3A-, T3A, T3B and T3C2 validation cases from the classic ERCOFTAC database are considered. They were developed specifically for validation of transition models and have become a recognized standard in the research community.

Figure 6.1 shows the skin friction coefficient predicted by the new model, which will be identified as "Simpler v^2 Model", compared with experimental data. Although this is only a preliminary version of the model, some key features are apparent. First, the transition location is relatively well predicted in most of the cases, and moves upstream as freestream turbulence intensity increases. Due to this, the new model shows a slightly earlier transition initiation for the T3B test case. Second, the wall shear stress in both the laminar (pretransitional) and fully turbulent regions predicted by the model is in good agreement with the expected values indicated by the experimental data. The transition occurs too fast for the T3A- case, but for the other cases, the transition is smooth, rather than sudden and nearly discontinuous. All of these aspects are positive and important characteristics of RANS single-point models for transition prediction.

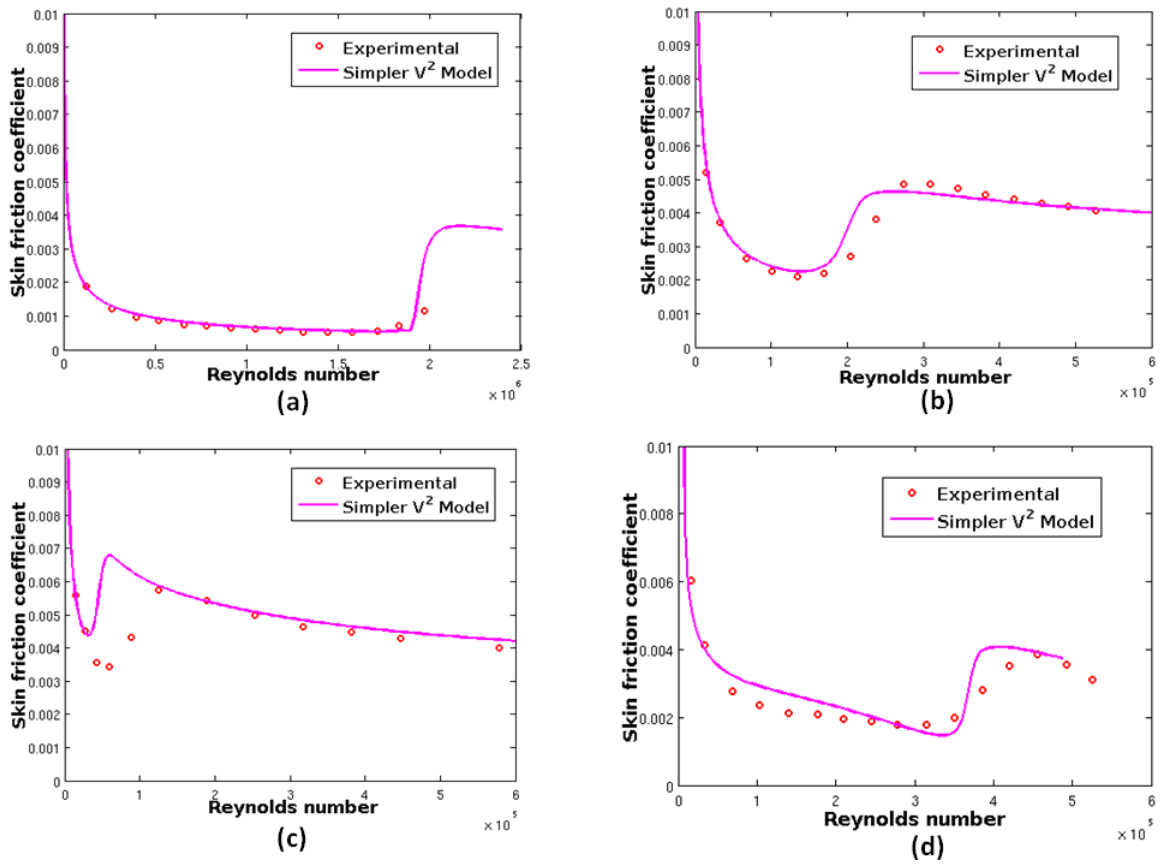

Figure 6.1 Skin friction coefficient calculated with the new model compared against experimental data.

(a) T3A-, (b)T3A, (c)T3B, (d)T3C2.

VPI cascade

The configuration for this test case is identical to the description presented for the same test case in chapter V. For completeness of the section, the configuration of the test case is included in this section.

Figure 5.15 shows the domain and hybrid two-dimensional mesh used. The inlet air velocity was 5.85 m/s, which corresponds to a Reynolds number of 230,000 based on a chord length of 59.4 cm. Due to the limitation of this initial version of the model, just

one test case was performed. Inlet conditions matched the freestream turbulence level of 10% and turbulent viscosity ratio μ_T / μ of 900.

A constant heat flux boundary condition was applied on the airfoil surface and the heat transfer coefficient was calculated in the simulation and compared with experimental data.

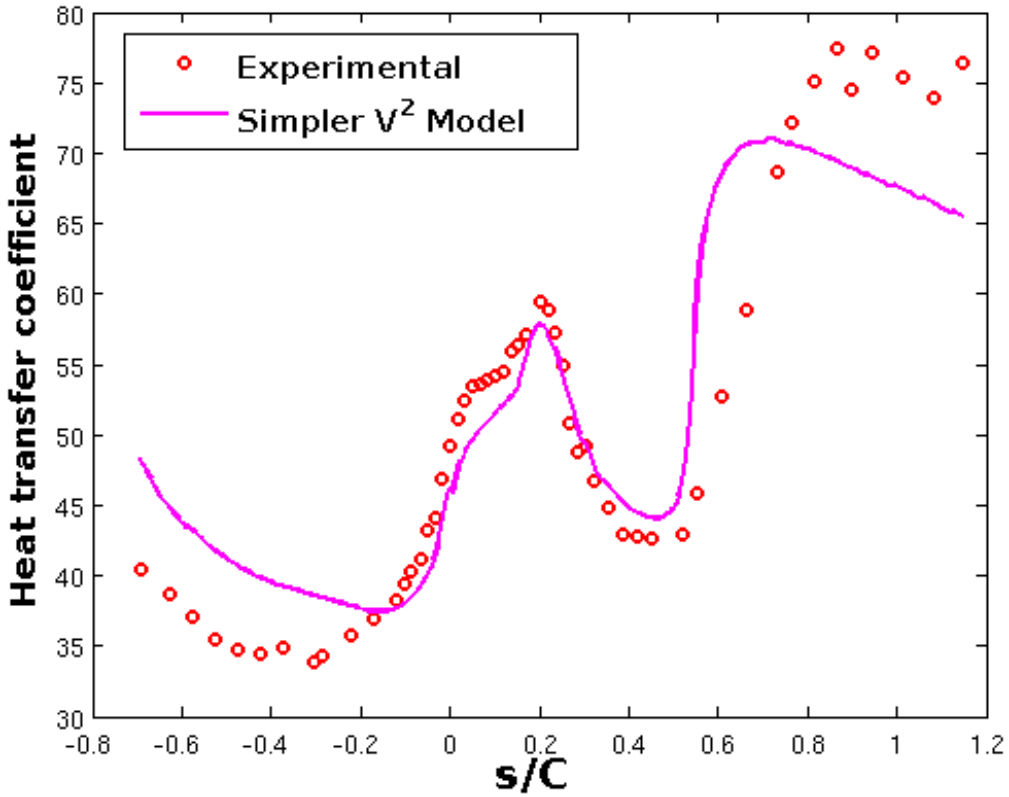

Figure 6.2 Heat transfer coefficient calculated along the surface of the airfoil for $Tu_{\infty} = 10\,\%$.

Figure 6.2 shows heat transfer coefficient versus distance along the airfoil surface (from the stagnation point) normalized by chord length (*s*/*C*). Negative values of *s* indicate the pressure surface; positive values indicate the suction surface. It is apparent

that the simpler v^2 model can predict the transition location with reasonable accuracy for this case. In the transition zone, the levels of heat transfer coefficient increase very fast, which indicates that transition is not smooth as suggested by the experimental data. Besides that, the heat transfer coefficient does not reach the desired values in the fully turbulent region.

Despite the lack of accuracy in some parts of the domain shown in figure 6.2, it is worthwhile to highlight the transitional behavior demonstrated by the model over the airfoil test case. This result in addition to the ones on the flat plate with and without pressure gradient demonstrate the potential of the new model to achieve high levels of accuracy for the prediction of transitional flows using a much simpler model form.

Backward facing step

The simpler v^2 model uses the fully-turbulent shear stress transport model proposed by Menter in [48], therefore this new model is expected to behave similar to the SST $k-\omega$ model in fully turbulent regions. The primary challenge for the proposed simpler v^2 model is the correct incorporation of the transition process. Nevertheless, the model has to be tested for fully turbulent flows to demonstrate that the inclusion of transitional capabilities does not affect the benefits of the baseline model in fully turbulent regions.

The backward facing step test case was chosen to test the hypothesis described in the previous paragraph. Again the same domain configuration, mesh and initial conditions as in chapter V were used to test the new model. The details were described in chapter V and also in [36]. The length of the domain prior the step is long enough to

guarantee transition and fully developed flow characteristics before the step. The flow is fully turbulent before it reaches the step, where it separates and then reattachment occurs farther downstream. These characteristics make the test case a good test case for fully turbulent validations.

Figure 6.2 shows the pressure coefficient and skin friction coefficient predicted by the model and compared with experimental data. The results are very accurate and, as expected, show similar behavior as the fully turbulent SST $k-\omega$ model. This confirms that in fully turbulent regions, $v^2 \rightarrow k$ and the solutions for v^2 and k tend to be identical and a similar version of the SST model is effectively recovered.

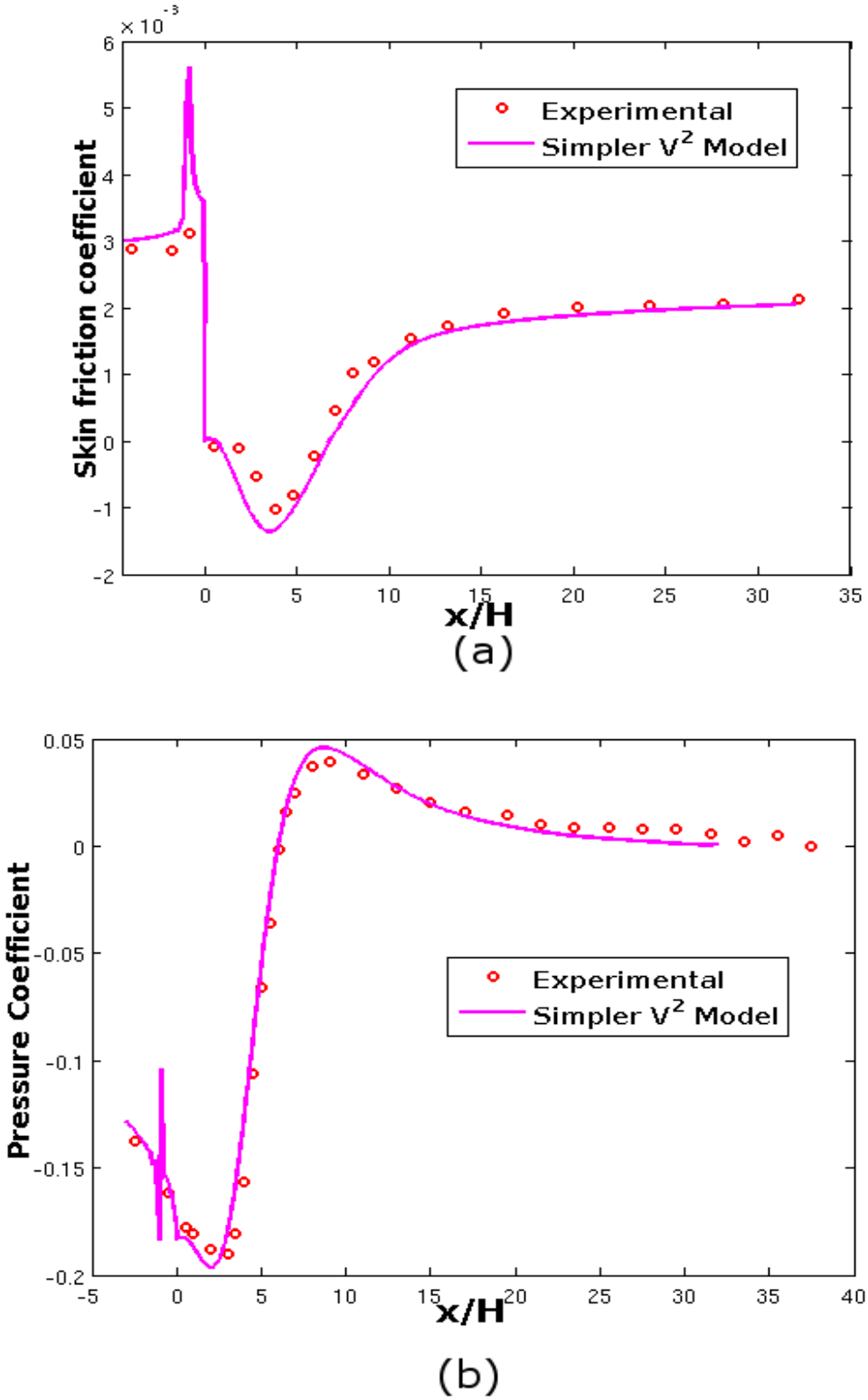

Figure 6.3 Skin and pressure coefficient calculated at the bottom wall.

CHAPTER VII

CONCLUSIONS

In this study, a new methodology for the description of the transition process in turbulence models for use in CFD simulations has been proposed as an alternative to the laminar kinetic energy approach. This new methodology has been used to further develop two physics-based, single-point, linear eddy-viscosity RANS transitional models. The first one uses the existing $k_T - k_L - \omega$ transitional model presented in [5] as a baseline, along with a transformation of variables to a $k - \omega - v^2$ form. The term that controls the behavior in the wake region was modified in the baseline model to accurately capture the physics of fully turbulent free shear flows. The model formulation was tested for several boundary layer and free shear flow test cases. The simulations show accurate results, qualitatively equal to the baseline model on transitional boundary layer test cases, and substantially improve over the baseline model for free shear flows. The second model uses the SST $k - \omega$ fully turbulent model and again the effects of transition are included through one additional transport equation for v^2. An initial version of the model is presented here.

The major contributions and findings are summarized as follows:

- The introduction of the new variable v^2 seems to represent better the description of the transition process described in this research and initially introduced by Walters in [25]
- Even though the v^2 model is intended to be qualitatively equal to the baseline model when predicting the transition process, the transition location predicted by the new model is slightly better for the majority of the test cases presented
- The cross-diffusion term from the SST $k-\omega$ model effectively incorporates the benefits of the SST $k-\omega$ model on the wake region into the new v^2 model
- The new v^2 model now has a wider range of applications than its baseline model
- The simpler v^2 model confirms that the new methodology for the transition process may be potentially incorporated into other fully turbulent models
- The initial results of the simpler v^2 model suggest there is a good potential in the model for a future version, without sacrificing the simplicity of the model.

In general, theoretical and practical advantages of the new methodology for the description of the transition process have been shown. It was effectively incorporated in an existing transition model, and a good potential to easily include transitional characteristics to fully turbulent models has been demonstrated with the simpler v^2

model. Further investigation and development of the simpler v^2 model will provide a robust model with a very simple formulation.

REFERENCES

[1] Menter, F.R., Langtry, R.B., Likki, S.R., Suzen, Y.B., Huang, P.G., and Volker, S., 2006, "A Correlation-Based Transition Model Using Local Variables – Part I: Model Formulation," ASME J. Turbomach., 128, 413-422.

[2] Langtry, R.B., and Menter, F.R., 2005, "Transition Modeling for General CFD Applications in Aeronautics", AIAA Paper 2005-522, Reno, Nevada.

[3] Menter, F.R., Langtry, R., and Volker, S., 2006, "Transition Modelling for General Purpose CFD Codes," Flow, Turbulence and Combusion, Vol. 77, pp.277-303,.

[4] Walters, D.K., and Leylek, J.H., 2004, "A New Model For Boundary Layer Transition Using a Single-Point RANS Approach," J. Turbomach., 126, pp. 193-202.

[5] Walters, D.K., and Cokljat, D., 2008, "A Three-Equation Eddy-Viscosity Model for Reynolds-Averaged Navier- Stokes Simulations of Transitional Flow," J. Fluids Eng., 130 (121401).

[6] Mayle, R.E. and Schulz, A., 1997, "The Path to Predicting Bypass Transition," J. Turbomach, 119, 405-411.

[7] Voke, P.R. and Yang, Z., 1995, "Numerical Study of Bypass Transition," Physics of Fluids, 7, 2256-2264.

[8] Jacobs, R.G. and Durbin, P.A., 2001, "Simulations of Bypass Transition," Journal of Fluid Mechanics, 428, 185-212.

[9] Brandt, L., Schlatter, P. and Henningson, D.S., 2004, "Transition in Boundary Layers Subject to Free-Stream Turbulence," Journal of Fluid Mechanics, 517, 167-198.

[10] Zaki, T.A. and Durbin, P.A., 2005, "Mode Interaction and the Bypass Route to Transition. Journal of Fluid Mechanics, 531, 85–111.

[11] Andersson, P., Brandt, L., Bottaro, A. and Henningson, D.S., 2001, "On the Breakdown of Boundary Layer Streaks," Journal of Fluid Mechanics, 428, 29-60.

[12] Brandt, L., Schlatter, P. and Henningson, D.S., 2004, "Transition in Boundary Layers Subject to Free-Stream Turbulence," Journal of Fluid Mechanics, 517, 167-198.

[13] Lardeau, S., Li, N. and Leschziner, M.A., 2007, "Large Eddy Simulation of Transitional Boundary Layers at High Free-Stream Turbulence Intensity and Implications for RANS Modeling," ASME Journal of Turbomachinery, 129, 311-317.

[14] Volino, R.J. and Simon, T.W., 1997, "Boundary Layer Transition Under High Free-Stream Turbulence and Strong Acceleration Conditions: Part 2 -- Turbulent Transport Results," ASME Journal of Heat Transfer, 119, 427-432.

[15] Leib, S.J., Wundrow, D.W. and Goldstein, M.E., 1999, "Effect of Free-Stream Turbulence and Other Vortical Disturbances on a Laminar Boundary Layer," Journal of Fluid Mechanics, 380, 169-203.

[16] Matsubara, M. and Alfredsson, P.H., 2001, "Disturbance Growth in Boundary Layers Subjected to Free-Stream Turbulence," Journal of Fluid Mechanics, 430, 149-168.

[17] Andersson, P., Berggren, M. and Henningson, D.S., 1999, "Optimal Disturbances and Bypass Transition in Boundary Layers," Physics of Fluids, 11, 134-150.

[18] Coupland, J., 1990, ERCOFTAC Special Interest Group on Laminar to Turbulent Transition and Retransition: T3A and T3B Test Cases.

[19] Schlatter, P. and Orlu, R., 2010," Assessment of Direct Numerical Simulation Data of Turbulent Boundary Layers," J. Fluid Mech, 659, 116-126.

[20] Dhakal, T.P., Walters, D.K., 2011, "A Three-Equation Variant of the SST k-omega Model Sensitized to Rotation and Curvature Effects," J. Fluids Eng., 133 (111201).

[21] Menter, F. R., 1992, "Improved Two-Equation $k-\omega$ Turbulence Models for Aerodynamic Flows," NASA Technical Memorandum, 103975, Ames Research Center, Moffett Field.

[22] Ghahremanian, S., Moshfegh, B., 2014, "Evaluation of RANS Models in Predicting Low Reynolds, Free, Turbulent Round Jet," J. Fluids Eng., 136 (011201).

[23] Lopez, M., Walters, D.K., 2012, "Laminar-to-Turbulent Boundary Layer Prediction Using an Alternative to the Laminar Kinetic Energy Approach," Proceedings, ASME 2012 International Mechanical Engineering Congress & Exposition. Paper No. IMECE2012-89433

[24] Wang, C., Perot, B., 2002, "Prediction of turbulent transition in boundary layers using the turbulent potential model," J. Turbul., **3**, N22.

[25] Walters, D.K., 2009, "Physical Interpretation of Transition-Sensitive RANS Models Employing the Laminar Kinetic Energy Concept", ERCOFTAC Bulletin, Vol 80, pp. 67-71.

[26] Walters, D.K., Lopez, M., 2014, "A Physics-based Correction of the $k_T - k_L - \omega$ model". In preparation

[27] Heschl, C., Inthavong, K., Sanz, W., Tu, J., 2013, "Evaluation and Improvements of RANS Turbulence Models for Linear Diffuse Flows", J. Computers & Fluids, 71, 272-282.

[28] Hirsch, C., 2007, "Numerical Computation of Internal & External Flows", 2nd ed., DCW industries, Calif.

[29] Wilcox, D.C., 1998, "Turbulence Modeling for CFD", 2nd ed., DCW industries, Calif.

[30] Bredberg, J. 2001. "On Two Equation Eddy-Viscosity Models," Department of thermo and fluid dynamics, Chalmers University of technology.

[31] Abu-Ghannam, B. J., and Shaw, R., 1980 "Natural Transition of Boundary Layers The Effects of Turbulence, Pressure Gradient, and Flow History", J. Mech. Eng SCi, 22, pp 213-228.

[32] Mayle, R.E, 1991, "The Role of Laminar-Turbulent Transition in Gas Turbine Engines", ASME J. Turbomach., 113, pp. 509-537.

[33] Dhawan, S., and Narasimha, R., 1958, "Some Properties of Boundary layer During the Transition From Laminar to Turbulent Flow Motion", J. Fluid mech., 3, pp. 418-436.

[34] Radomsky, R. W., and Thole, K. A., 2000, "Flowfield Measurements for a Highly Turbulent Flow in a Stator Vane Passage," ASME J. Turbomach., 122, pp. 255-262.

[35] Radomsky, R. W., and Thole, K. A., 2001, "Detailed Boundary-Layer Measurements on a Turbine Stator Vane at Elevated Freestream Turbulence Levels," ASME Paper No. 2001-GT-0169.

[36] Driver, D.M., and Seegmiller, H.L, 1985, "Features of a Reattaching Turbulent Shear Layer in Divergent Channel Flow," *AIAA J.*, Vol. 23, p 163.

[37] Hussein, H.J., Capp, S.P., and George, W. K., 1994, "Velocity Measurements in a High-Reynolds Number, momentum-conserving, axisymmetric, turbulent jet," J. Fluid Mech. Vol 258, pp. 31-75.

[38] Hayakawa, M., Lida, S., 1992, "Behavior of turbulence in the near wake of a thin flat plate at low Reynolds number," Physics of fluids, Vol 4, No. 10.

[39] Davidson, D.L., 2002, "The Role of Computational Fluid Dynamics in process industries," Bridge, 32(4), pp 9-14.

[40] Moin, P., K. Mahesh, 1998, "Direct Numerical Simulation: a Tool in Turbulence Research," Annual review of fluid mechanics, 30(1), pp. 539-578.

[41] Spalart, P.R. R., et al., 2006, "A new Version of Detached-eddy Simulation, Resistant to Ambiguous Grid Densities," Theoretical and Computational Fluid Dynamics, **20**(3), pp. 181-195

[42] Shur, M.L., et al., 2008, "A hybrid RANS-LES Approach with Delayed-DES and Wall Modelled LES Capabilities," International Journal of Heat and Fluid Flow, **29**(6), pp. 1638-1649.

[43] Walters, D.K., et al., 2012, "Investigation of a Dynamic Hybrid RANS/LES Modelling Methodology for Finite-Volume CFD Simulations," Flow, turbulence and combustion, 91(3), pp. 643-667

[44] Alam, M.F., D.K. Walters, and D.S. Thompson, "Evaluation of a Dynamic Hybrid RANS/LES Modeling Methodology for Attached and Separated Flows," ASME Journal of Fluids Engineering, in review.

[45] Spalart, P.R., 2000, "Strategies for Turbulence Modeling and Simulations," International Journal of Heat and Fluid Flow, 21(3), pp. 252-263.

[46] Lilly, D.K., 1992 "A proposed modification of the Germano subgrid scale closure method," Physics of Fluids A: Fluid Dynamics, 4, pp. 633.

[47] Hirsch, C. and B. Tartinville, 2009 "Reynolds-Averaged Navier-Stokes Modelling for Industrial Applications and Some Challenging Issues," International Journal of Computational Fluid Dynamics, 23(4), pp. 295-303.

[48] Menter, F.R., 1994, "Two-equation eddy-viscosity turbulence models for engineering applications," AIAA journal, 32(8), pp. 1598-1605.

[49] Kalitzin, G., X. Wu, and P.A. Durbin, 2003, "DNS of fully turbulent flow in a LPT passage," International Journal of Heat and Fluid Flow, 24(4), pp. 636-644.

[50] Savill, A.M., 2002 "By-pass transition using conventional closures," Closure strategies for turbulent and transitional flows, 17, pp. 464-492.

[51] Wilcox, D.A., 1994 "Simulation of transition with a two-equation turbulence model," AIAA journal, 32(2), pp. 247-255.

[52] Rumsey, C.L., 2007 “Apparent transition behavior of widely-used turbulence models,” International Journal of Heat and Fluid Flow, 28(6), pp. 1460-1471

[53] Abid, R., 1993, “Evaluation of two-equation turbulence models for predicting transitional flows,” International Journal of Engineering Science, 31(6), pp.831-840.

[54] Edwards, J.R., et al., 2001, “Development of a one-equation transition/turbulence model,” AIAA journal, 39(9), pp. 1691-1698.

[55] Abu-Ghannam, B.J. and R. Shaw, 1980, “Natural Transition of Boundary Layers: the Effects of Turbulence, Pressure gradient, and Flow History,” Journal of Mechanical Engineering Science, 2(5), pp. 213-228

[56] Suzen, Y.B. and P.G. Huang, 2000 “Modeling of flow transition using an intermittency transport equation,” Journal of fluids engineering, 122(2), pp. 273-284.

[57] Steelant, J. and E. Dick, 2001 “Modeling of laminar-turbulent transition for high freestream turbulence,” Journal of fluids engineering, 123(1), pp. 22-30.

[58] Schlichting, H., and Gersten, K., 2000, “Boundary Layer Theory”, 8th ed.,Springer-Verlag, Berlin.

[59] Furst, J., 2012, “Numerical Simulations of Transitional Flows with Laminar Kinetic Energy,” 18th International conference engineering mechanics, pp. 309-315.

[60] *User Guide FLUENT 6.3*, Centerra Resource Park, 10 Cavendish Court, Lebanon, NH 03766, USA.: FLUENT Inc..

[61] Menter, F.R., 2009, “Review of Shear Stress Transport Turbulence Model experience From an Industrial Prospective,” International Journal of Fluid Mechanics, 23:4, pp. 305-316.

[62] Turner, C., 2012, “Laminar Kinetic Energy Modeling for Improved Laminar-Turbulent Transition Prediction,” Dissertation, school of mechanical, aerospace and civil engineering, University of Manchester.

[63] Bernardini, C, et al., 2012, “Turbine Blade Boundary Layer Separation Suppression via synthetic Jet: an Experimental and Numerical study,” Journal of thermal science, 21(5), pp. 404-412.

[64] Wang, X., Walters, D.K., 2012 “Computational Analysis of Marine-Propeller Performance Using Transition-Sensitive Turbulence Modeling,” Journal of Fluids Engineering, 134.

[65] Chitta, V., Dhakal, T., Walters, D.K., 2013 "Development and Application of a New Four-Equation Eddy-Viscosity Model for Flows With Transition, Curvature and Roration Effects," ASME Proceedings 4th International Symposium on Turbukent Flows.

[66] Alam, M. F., Walters, D. K., and Thompson, D. S., "A Transition-Sensitive Hybrid RANS/LES Modeling Methodology for CFD Applications," 51st AIAA Aerospace Sciences Meeting, AIAA Paper 2013-0995, January 2013.

[67] W. P. Jones, B.E. Launder., 1972, "The Prediction of Laminarization with a two-equation model of turbulence," Int. J. Heat and mass transfer, 15, pp. 301-314.

[68] S-H. Peng and L. Davidson., "New Two-equation Eddy-viscosity Transport Model for Turbulent Flow Computation," AIAA Journal, 38, pp. 1196-1205.

[69] C.G. Speziale, R. Abid, and E.C. Anderson. 1992 "Critical Evaluation of Two-equation Models for Near-wall Turbulence," AIAA Journal, 30, pp. 324-331.

[70] D.C. Wilcox., 1998 "Reassessment of the Scale Determining Equation for Advanced Turbulence Models," AIAA Journal, 26, pp. 1299-1310.

[71] C. Krame, H.J. Gerhardt, M. Knoch, 1984, "Applications of jet flows in industrial Flow Circuits," Journal of Wind Engineering and Industrial Aerodynamics, 16, pp. 173-188.

APPENDIX A

FLUENT SOURCE CODE FOR MODELS OF CHAPTERS V AND VI

FLUENT source code for model in chapter V

```
#include "udf.h"
 #include "turb.h"


/*USER DEFINED SCALARS*/
#define K 0
#define W 1
#define V2 2
#define SRT_K 3
#define SRT_V2 4


/*USER DEFINED MEMORIES*/
#define MU_T 3
#define ALPHA_T 4
#define DSRTK_DX 5
#define DSRTV2_DX 6
#define L_T 7
#define L_EFF 8
#define F_WALL 9
#define F_NU 10
#define F_SS 11
#define C_MU 12
#define V2_S 13
#define V2_L 14
#define MU_TS 15
#define MU_TL 16
#define F_OMEGA 17
#define R_BP 18
#define PROD_V2 19
#define PROD_K 20
#define RE_T 21
#define RE_ROT 22
#define F_INT 23
#define B_TS 24
#define F_TAU 25
#define MU_TL0 26
#define MU_TL1 27
#define PHI_BP 28
#define BETA_BP 29
#define DK_DW 30
#define F_1 31
#define RT_K_GRAD_SQR 32
#define RT_V2_GRAD_SQR 33
#define D_W_K 34
#define D_W_V2 35
#define F_NAT_CRIT 37
#define PHI_NAT 38
#define BETA_NAT 39
#define R_NAT 40

/* MODEL CONSTANTS */
#define A_0 4.04
```

```
#define A_S 2.12
#define A_NU 3.8
#define A_BP 0.2
#define A_NAT 200.
#define A_TS 200.
#define C_BP_CRIT 1.5
#define C_NC 0.1
#define C_NAT_CRIT 1450.0
#define C_INT 0.95
#define C_TS_CRIT 1000.0
#define C_R_NAT 0.02
#define C_R1 0.32
#define C_ALP_THE 0.035
#define C_SS 3.0
#define C_TAU 4360.0
#define C_W1 0.44
#define C_W2 0.92
#define C_W3 0.3
#define C_WR 1.15
#define C_L 2.495
#define C_MU_STD 0.09
#define Pr_T 0.85
#define SIG_K 1.0
#define SIG_W 1.17
#define TINY 1.e-12


/* ========================== Properties ================================= */

DEFINE_TURBULENT_VISCOSITY(mod_mu_t, c, t)
{
 return C_UDMI(c,t,MU_T);
}

DEFINE_DIFFUSIVITY(user_diffusivity, c, t, eqn)
{
real diff;
switch(eqn)
 {
 case K:
   diff = C_MU_L(c,t) + C_UDMI(c,t,ALPHA_T)/SIG_K;
   break;
 case W:
   diff = C_MU_L(c,t) + C_UDMI(c,t,ALPHA_T)/SIG_W;
   break;
 case V2:
   diff=  C_MU_L(c,t) + C_UDMI(c,t,ALPHA_T)/SIG_K;
   break;
 default:
   diff = C_MU_L(c,t) + C_UDMI(c,t,MU_T);
 }
return diff;
}

DEFINE_PRANDTL_T(user_pr_t, c, t)
{
```

```
 real DIFF_NRG = (1.-
C_UDMI(c,t,F_WALL))*0.035*C_R(c,t)*sqrt(C_UDMI(c,t,V2))*C_UDMI(c,t,L_EFF) +
(C_UDMI(c,t,V2)/C_UDMI(c,t,K))*C_UDMI(c,t,F_WALL)*C_UDMI(c,t,MU_TS)/0.85;
 return (C_UDMI(c,t,MU_T)+0.00085*C_MU_L(c,t))/(DIFF_NRG+0.001*C_MU_L(c,t));
}

/*============================== Adjust Functions
================================*/
DEFINE_ADJUST(adjust_fn_kw_sst, domain)
{
Thread *t;
cell_t c;


real arg_1, cd_kw, d_eff, re_rot1;

thread_loop_c(t,domain)
 {
 if (&C_UDSI_G(0,t,K)[0] != NULL)
  {
  begin_c_loop(c,t)
   {
   C_UDMI(c,t,K) = MAX(C_UDSI(c,t,K),0.5*(C_UDMI(c,t,K)+1.e-18));
   C_UDMI(c,t,V2) = MAX(C_UDSI(c,t,V2),0.5*(C_UDMI(c,t,V2)+1.e-18));
   C_UDMI(c,t,W) = MAX(C_UDSI(c,t,W),0.5*(C_UDMI(c,t,W)+1.e-18));


/*====================== Determine "anisotropic" dissipation
components=========================*/


   C_UDSI(c,t,SRT_K)=sqrt(C_UDMI(c,t,K));
   C_UDSI(c,t,SRT_V2)=sqrt(C_UDMI(c,t,V2));



C_UDMI(c,t,DSRTK_DX)=C_UDSI_G(c,t,SRT_K)[0]*C_UDSI_G(c,t,SRT_K)[0]+C_UDSI_G(c,t,SR
T_K)[1]*C_UDSI_G(c,t,SRT_K)[1];

C_UDMI(c,t,DSRTV2_DX)=C_UDSI_G(c,t,SRT_V2)[0]*C_UDSI_G(c,t,SRT_V2)[0]+C_UDSI_G(c,t
,SRT_V2)[1]*C_UDSI_G(c,t,SRT_V2)[1];


#if RP_3D
   C_UDMI(c,t,DSRTK_DX) +=C_UDSI_G(c,t,SRT_K)[2]*C_UDSI_G(c,t,SRT_K)[2];
   C_UDMI(c,t,DSRTV2_DX) +=C_UDSI_G(c,t,SRT_V2)[2]*C_UDSI_G(c,t,SRT_V2)[2];
#endif


   C_UDMI(c,t,RT_K_GRAD_SQR) = 0.5*C_UDMI(c,t,DSRTK_DX) +
0.5*C_UDMI(c,t,RT_K_GRAD_SQR);
   C_UDMI(c,t,RT_V2_GRAD_SQR) = 0.5*C_UDMI(c,t,DSRTV2_DX) +
0.5*C_UDMI(c,t,RT_V2_GRAD_SQR);

   C_UDMI(c,t,D_W_K) = 2.*(C_MU_L(c,t)/C_R(c,t))*C_UDMI(c,t,RT_K_GRAD_SQR);
   C_UDMI(c,t,D_W_V2) = 2.*(C_MU_L(c,t)/C_R(c,t))*C_UDMI(c,t,RT_V2_GRAD_SQR);
```

```
/*////////////////////////////////////////////////////////////////////////////*/

   C_UDMI(c,t,L_T) = sqrt(C_UDMI(c,t,V2))/C_UDMI(c,t,W);
   C_UDMI(c,t,L_EFF) = MIN(C_L*C_WALL_DIST(c,t),C_UDMI(c,t,L_T)); /*Effective
Turbulence Length Scale*/
   C_UDMI(c,t,F_WALL) = pow(C_UDMI(c,t,L_EFF)/C_UDMI(c,t,L_T),0.666667);

   C_UDMI(c,t,RE_T) =
pow(C_UDMI(c,t,F_WALL),2.0)*C_UDMI(c,t,V2)*C_R(c,t)/(C_MU_L(c,t)*C_UDMI(c,t,W));

   C_UDMI(c,t,F_NU) = 1.0 - exp(-sqrt(C_UDMI(c,t,RE_T))/A_NU);
   C_UDMI(c,t,F_SS) = exp(-
pow(C_SS*C_MU_L(c,t)*Rotationrate_Mag(c,t)/(C_UDMI(c,t,V2)*C_R(c,t)),2.0));
   C_UDMI(c,t,C_MU) = 1.0/(A_0+A_S*(Strainrate_Mag(c,t)/C_UDMI(c,t,W)));
/*Turbulent viscosity coefficient*/

   C_UDMI(c,t,F_INT) = MIN(C_UDMI(c,t,V2)/(C_INT*C_UDMI(c,t,K)),1.0);


   C_UDMI(c,t,V2_S) = C_UDMI(c,t,F_SS)*C_UDMI(c,t,F_WALL)*C_UDMI(c,t,V2);
/*Effective "small-scale" turbulence*/
   C_UDMI(c,t,MU_TS) =
C_R(c,t)*C_UDMI(c,t,F_NU)*C_UDMI(c,t,F_INT)*C_UDMI(c,t,C_MU)*sqrt(C_UDMI(c,t,V2_S)
)*C_UDMI(c,t,L_EFF);/*"small-scale" eddy viscosity*/

   C_UDMI(c,t,V2_L) = C_UDMI(c,t,V2) - C_UDMI(c,t,V2_S); /*Effective "large-scale"
turbulence*/

   d_eff = C_UDMI(c,t,L_EFF)/C_L;


   re_rot1=d_eff*d_eff*Rotationrate_Mag(c,t)*C_R(c,t)/C_MU_L(c,t);
   C_UDMI(c,t,RE_ROT) =
C_WALL_DIST(c,t)*C_WALL_DIST(c,t)*Rotationrate_Mag(c,t)*C_R(c,t)/C_MU_L(c,t);
   C_UDMI(c,t,B_TS) = 1.0 - exp(-pow(MAX(C_UDMI(c,t,RE_ROT) -
C_TS_CRIT,0.0),2.0)/A_TS);
   C_UDMI(c,t,F_TAU) = 1.0 - exp(-
C_TAU*C_UDMI(c,t,V2_L)/(pow(C_UDMI(c,t,L_EFF)*Rotationrate_Mag(c,t),2.0)+TINY));


C_UDMI(c,t,MU_TL0)=C_R(c,t)*(0.0000034)*C_UDMI(c,t,F_TAU)*C_R(c,t)*Rotationrate_Ma
g(c,t)*pow(C_UDMI(c,t,L_EFF),3.0)*sqrt(C_UDMI(c,t,V2_L))/C_MU_L(c,t);
   C_UDMI(c,t,MU_TL1)=0.5*C_R(c,t)*(MAX(C_UDMI(c,t,K)-
C_UDMI(c,t,V2_S),0))/(Strainrate_Mag(c,t)+TINY);
   C_UDMI(c,t,MU_TL) = MIN(C_UDMI(c,t,MU_TL0)+C_R(c,t)*C_UDMI(c,t,B_TS)*(1.e-
10)*re_rot1*pow(d_eff,2.0)*Rotationrate_Mag(c,t),C_UDMI(c,t,MU_TL1)); /*"Large-
scale" eddy viscosity*/

   C_UDMI(c,t,ALPHA_T) =
C_R(c,t)*C_UDMI(c,t,F_NU)*C_MU_STD*sqrt(C_UDMI(c,t,V2_S))*C_UDMI(c,t,L_EFF);

   C_UDMI(c,t,F_OMEGA) = 1.0 - exp(-0.41*pow(C_UDMI(c,t,F_WALL),4.0));
```

```
   C_UDMI(c,t,PHI_BP) =
MAX(C_UDMI(c,t,V2)*C_R(c,t)/(Rotationrate_Mag(c,t)*C_MU_L(c,t)+TINY) -
C_BP_CRIT,0.0);

   C_UDMI(c,t,BETA_BP) = 1.0 - exp(-C_UDMI(c,t,PHI_BP)/A_BP);
   C_UDMI(c,t,R_BP) = C_R1*C_R(c,t)*C_UDMI(c,t,BETA_BP)*MAX(C_UDMI(c,t,K)-
C_UDMI(c,t,V2),0.0)*C_UDMI(c,t,W)/C_UDMI(c,t,F_WALL);

   C_UDMI(c,t,F_NAT_CRIT) = 1.0 - exp(-
C_NC*C_R(c,t)*sqrt(C_UDMI(c,t,K))*C_WALL_DIST(c,t)/C_MU_L(c,t));
   C_UDMI(c,t,PHI_NAT) = MAX(C_UDMI(c,t,RE_ROT)-
C_NAT_CRIT/(C_UDMI(c,t,F_NAT_CRIT)+TINY),0.0);
   C_UDMI(c,t,BETA_NAT) = 1.0 - exp(-C_UDMI(c,t,PHI_NAT)/A_NAT);
   C_UDMI(c,t,R_NAT) = C_R(c,t)*C_R_NAT*C_UDMI(c,t,BETA_NAT)*MAX(C_UDMI(c,t,K)-
C_UDMI(c,t,V2),0.0)*Rotationrate_Mag(c,t);


    C_UDMI(c,t,MU_T)=C_UDMI(c,t,MU_TS) + C_UDMI(c,t,MU_TL);  /*Eddy viscosity*/

    /*Production of V2 and K*/
    C_UDMI(c,t,PROD_V2) =
C_UDMI(c,t,MU_TS)*Strainrate_Mag(c,t)*Strainrate_Mag(c,t);
    C_UDMI(c,t,PROD_K) = C_UDMI(c,t,MU_T)*Strainrate_Mag(c,t)*Strainrate_Mag(c,t);



     /* SST terms */
   C_UDMI(c,t,DK_DW) = C_UDSI_G(c,t,V2)[0]*C_UDSI_G(c,t,W)[0] +
C_UDSI_G(c,t,V2)[1]*C_UDSI_G(c,t,W)[1];
#if RP_3D
   C_UDMI(c,t,DK_DW) += C_UDSI_G(c,t,V2)[2]*C_UDSI_G(c,t,W)[2];
#endif
   C_UDMI(c,t,DK_DW) *= MAX(C_UDSI(c,t,V2),0.)/C_UDMI(c,t,V2);
   C_UDMI(c,t,DK_DW) *= MAX(C_UDSI(c,t,W),0.)/C_UDMI(c,t,W);

   cd_kw = MAX(2.*C_R(c,t)*1.856*C_UDMI(c,t,DK_DW)/C_UDMI(c,t,W),1.e-10);

   arg_1 = MAX( sqrt(C_UDMI(c,t,V2))/(C_UDMI(c,t,W)*C_WALL_DIST(c,t)) ,
500.*0.09*(C_MU_L(c,t)/C_R(c,t))/(C_WALL_DIST(c,t)*C_WALL_DIST(c,t)*C_UDMI(c,t,W))
);
   arg_1 = MIN( arg_1 ,
4.*C_R(c,t)*1.856*C_UDMI(c,t,K)/(cd_kw*C_WALL_DIST(c,t)*C_WALL_DIST(c,t)) );

   C_UDMI(c,t,F_1) = tanh(pow(arg_1,4.));

   C_UDMI(c,t,F_1)= 1.0 - ((1.0-C_UDMI(c,t,F_1))*C_UDMI(c,t,F_SS));




   }
  end_c_loop(c,t)
  }
 else
  {
```

```
  begin_c_loop(c,t)
   {
   C_UDMI(c,t,K) = MAX(C_UDSI(c,t,K),1.e-16);
   C_UDMI(c,t,W) =
MAX(C_UDSI(c,t,W),0.1*(C_MU_L(c,t)/C_R(c,t))/(C_WALL_DIST(c,t)*C_WALL_DIST(c,t)));
   C_UDMI(c,t,V2) = MAX(C_UDSI(c,t,V2),1.e-16);


   C_UDMI(c,t,MU_T) = C_R(c,t)*C_UDMI(c,t,K)/C_UDMI(c,t,W);
   }
  end_c_loop(c,t)
  }
 }
}


/* ------------------------- Sources --------------------------- */

DEFINE_SOURCE(k_source, c, t, dS, eqn)
{
 real S;

 S = C_UDMI(c,t,PROD_K);
 S -= C_R(c,t)*C_UDMI(c,t,W)*MIN(C_UDMI(c,t,K),C_UDMI(c,t,V2));
 S -= 2.0*C_MU_L(c,t)*C_UDMI(c,t,DSRTK_DX)*(C_UDSI(c,t,K)/C_UDMI(c,t,K));

 dS[eqn] =-C_R(c,t)*C_UDMI(c,t,W) -
2.0*C_MU_L(c,t)*C_UDMI(c,t,DSRTK_DX)*(1.0/C_UDMI(c,t,K));

 return S;
}

DEFINE_SOURCE(omega_source, c, t, dS, eqn)
{
real S,PWC;

 PWC = C_W1*C_UDMI(c,t,PROD_V2)*C_UDMI(c,t,W)/C_UDMI(c,t,V2);

 real f_sst =0.09*2.*(1.-
C_UDMI(c,t,F_1))*C_R(c,t)*1.856*C_UDMI(c,t,DK_DW)/C_UDMI(c,t,W);
 real a_0 = PWC + (C_WR/C_UDMI(c,t,F_WALL)-
1.)*(C_UDMI(c,t,R_BP)+C_UDMI(c,t,R_NAT))*C_UDMI(c,t,W)/C_UDMI(c,t,V2) +
MAX(f_sst,0.);
 real a_1 = - C_R(c,t)*C_W2*C_UDMI(c,t,W)*C_UDMI(c,t,F_WALL)*C_UDMI(c,t,F_WALL) +
MIN(f_sst,0.)/C_UDMI(c,t,W);

 S = a_0 + a_1*C_UDSI(c,t,W);
 dS[eqn] = a_1;
 return S;

}

DEFINE_SOURCE(V2_source, c, t, dS, eqn)
{
 real S;

 S = C_UDMI(c,t,PROD_V2);
```

```
 S += C_UDMI(c,t,R_BP)+C_UDMI(c,t,R_NAT);
 S -= C_R(c,t)*C_UDMI(c,t,W)*C_UDMI(c,t,V2);

 S -= 2.0*C_MU_L(c,t)*C_UDMI(c,t,DSRTV2_DX)*(C_UDSI(c,t,V2)/C_UDMI(c,t,V2));


 dS[eqn] = - C_R(c,t)*C_UDMI(c,t,W) -
2.0*C_MU_L(c,t)*C_UDMI(c,t,DSRTV2_DX)*(1.0/C_UDMI(c,t,V2));


 return S;
}
```

FLUENT source code for the model in chapter VI

```
#include "udf.h"
 #include "turb.h"


/*USER DEFINED SCALARS*/
#define K 0
#define W 1
#define V2 2
#define RT_K 3
#define RT_V2 4


/*USER DEFINED MEMORIES*/
#define MU_T 3
#define L_T 4
#define SIG_K 5
#define SIG_W 6
#define F_1 7
#define BETA 8
#define CD_KW 9
#define GAMMA 10
#define PROD_K 11
#define DK_DW 12
#define F_EPS_W 13
#define DRTV2_DX 14
#define FT 15
#define L_TT 16
#define DRTK_DX 17


/* MODEL CONSTANTS */
#define BETA_STAR 0.09
#define BETA_1 0.075
#define BETA_2 0.0828
#define SIG_K_1 0.85
#define SIG_K_2 1.0
```

```
#define SIG_W_1 0.5
#define SIG_W_2 0.856
#define GAMMA_1 0.555
#define GAMMA_2 0.44
#define A_1 0.31
#define CR_V2 1
#define CT1 0.0010
#define CT2 100.0
#define CT3 3.5

/* ========================== Properties ================================ */
DEFINE_TURBULENT_VISCOSITY(mod_mu_t, c, t)
{
 return C_UDMI(c,t,MU_T);
}

DEFINE_DIFFUSIVITY(user_diffusivity, c, t, eqn)
{
real diff;
switch(eqn)
 {
 case K:
   diff = C_MU_L(c,t) + C_UDMI(c,t,MU_T)*C_UDMI(c,t,SIG_K);
   break;
 case W:
   diff = C_MU_L(c,t) + C_UDMI(c,t,MU_T)*C_UDMI(c,t,SIG_W);
   break;
 case V2:
   diff=  C_MU_L(c,t) + C_UDMI(c,t,MU_T)*C_UDMI(c,t,SIG_K);
   break;
 default:
   diff = C_MU_L(c,t) + C_UDMI(c,t,MU_T);
 }
return diff;
}

DEFINE_PRANDTL_T(user_pr_t,c,t)
{
  real pr_t, lam_eff, lam_t, fw, nu_t, alpha_t;

  nu_t=C_UDMI(c,t,MU_T)/C_R(c,t);
  lam_t=sqrt(C_UDMI(c,t,V2))/(0.03*C_UDMI(c,t,W)+1.e-16);

lam_eff=MIN(2.495*C_WALL_DIST(c,t),sqrt(C_UDMI(c,t,V2))/(0.03*C_UDMI(c,t,W))+1.e-
16);
  fw=lam_eff/(lam_t+1.e-16);

  alpha_t=fw*(C_UDMI(c,t,V2)/C_UDMI(c,t,K))*(nu_t/0.85) + 0.035*(1.0-
fw)*sqrt(C_UDMI(c,t,V2))*lam_eff;

  pr_t=nu_t/(alpha_t+1.e-16);

  return pr_t;
}

/*============================ Adjust Functions ============================*/
```

```
DEFINE_ADJUST(adjust_fn_kw_sst, domain)
{
Thread *t;
cell_t c;

real arg_1, arg_2, arg_3, F_2, c_mu, f_mu, re_y, F_T1,F_T2;

thread_loop_c(t,domain)
 {
 if (&C_UDSI_G(0,t,K)[0] != NULL)
  {
  begin_c_loop(c,t)
   {
   C_UDMI(c,t,K) = MAX(C_UDSI(c,t,K),1.e-16);
   C_UDMI(c,t,W) = MAX(C_UDSI(c,t,W),1.e-16);
   C_UDMI(c,t,V2) = MAX(C_UDSI(c,t,V2),1.e-16);

   C_UDMI(c,t,DK_DW) = C_UDSI_G(c,t,K)[0]*C_UDSI_G(c,t,W)[0] +
C_UDSI_G(c,t,K)[1]*C_UDSI_G(c,t,W)[1];


  /* Other Wall destruction term*/


   C_UDSI(c,t,RT_K)=sqrt(C_UDMI(c,t,K));
   C_UDSI(c,t,RT_V2)=sqrt(C_UDMI(c,t,V2));


C_UDMI(c,t,DRTK_DX)=C_UDSI_G(c,t,RT_K)[0]*C_UDSI_G(c,t,RT_K)[0]+C_UDSI_G(c,t,RT_K)
[1]*C_UDSI_G(c,t,RT_K)[1];

C_UDMI(c,t,DRTV2_DX)=C_UDSI_G(c,t,RT_V2)[0]*C_UDSI_G(c,t,RT_V2)[0]+C_UDSI_G(c,t,RT
_V2)[1]*C_UDSI_G(c,t,RT_V2)[1];
/*////////////////////////////////////////////////////////////////////////////*/

#if RP_3D
   C_UDMI(c,t,DK_DW) += C_UDSI_G(c,t,K)[2]*C_UDSI_G(c,t,W)[2];
#endif

  /* =================SST Terms============================*/

   C_UDMI(c,t,CD_KW) =
MAX(2.*C_R(c,t)*SIG_W_2*C_UDMI(c,t,DK_DW)/C_UDMI(c,t,W),1.e-10);

   arg_1 = MAX( sqrt(C_UDMI(c,t,K))/(BETA_STAR*C_UDMI(c,t,W)*C_WALL_DIST(c,t)) ,
500.*(C_MU_L(c,t)/C_R(c,t))/(C_WALL_DIST(c,t)*C_WALL_DIST(c,t)*C_UDMI(c,t,W)) );
   arg_1 = MIN( arg_1 ,
4.*C_R(c,t)*SIG_W_2*C_UDMI(c,t,K)/(C_UDMI(c,t,CD_KW)*C_WALL_DIST(c,t)*C_WALL_DIST(
c,t)) );

   C_UDMI(c,t,F_1) = tanh(pow(arg_1,4.));

   C_UDMI(c,t,SIG_K) = C_UDMI(c,t,F_1)*SIG_K_1 +(1.-C_UDMI(c,t,F_1))*SIG_K_2;
   C_UDMI(c,t,SIG_W) = C_UDMI(c,t,F_1)*SIG_W_1 + (1.-C_UDMI(c,t,F_1))*SIG_W_2;
   C_UDMI(c,t,GAMMA) = C_UDMI(c,t,F_1)*GAMMA_1 + (1.-C_UDMI(c,t,F_1))*GAMMA_2;
   C_UDMI(c,t,BETA) = C_UDMI(c,t,F_1)*BETA_1 + (1.-C_UDMI(c,t,F_1))*BETA_2;
```

```
   arg_2 = MAX( 2.*sqrt(C_UDMI(c,t,K))/(BETA_STAR*C_UDMI(c,t,W)*C_WALL_DIST(c,t))
, 500.*(C_MU_L(c,t)/C_R(c,t))/(C_WALL_DIST(c,t)*C_WALL_DIST(c,t)*C_UDMI(c,t,W)) );

   F_2 = tanh(arg_2*arg_2);

   c_mu = A_1/MAX(A_1,Strainrate_Mag(c,t)/C_UDMI(c,t,W));
   re_y = sqrt(C_UDMI(c,t,V2))*C_WALL_DIST(c,t)*C_R(c,t)/C_MU_L(c,t);

   arg_3 = C_WALL_DIST(c,t)*C_WALL_DIST(c,t)*C_UDMI(c,t,W)*C_R(c,t)/C_MU_L(c,t);
   C_UDMI(c,t,F_EPS_W) = exp(-0.3*sqrt(arg_3));

C_UDMI(c,t,L_T)=MIN(sqrt(C_UDMI(c,t,K))/C_UDMI(c,t,W),2.495*BETA_STAR*C_WALL_DIST(
c,t));
  C_UDMI(c,t,L_TT)=C_UDMI(c,t,L_T)*c_mu; /* Length scale */
    C_UDMI(c,t,MU_T)=C_R(c,t)*sqrt(C_UDMI(c,t,V2))*C_UDMI(c,t,L_TT); /* Eddy
viscosity */

   C_UDMI(c,t,PROD_K)=C_UDMI(c,t,MU_T)*Strainrate_Mag(c,t)*Strainrate_Mag(c,t);/*
TKE Production */

   /* Transition Terms */
    F_T1=1. - exp(-
pow(sqrt(C_UDMI(c,t,V2))*C_WALL_DIST(c,t)*C_R(c,t)/(C_MU_L(c,t)*CT2),2.0));
    F_T2=1. - exp(-
pow(C_UDMI(c,t,V2)*C_R(c,t)/(C_MU_L(c,t)*Strainrate_Mag(c,t)*CT3),2.0));

   C_UDMI(c,t,FT) = MAX(F_T1,F_T2);
   }
  end_c_loop(c,t)
  }
 else
  {
  begin_c_loop(c,t)
   {
   C_UDMI(c,t,K) = MAX(C_UDSI(c,t,K),1.e-16);
   C_UDMI(c,t,W) =
MAX(C_UDSI(c,t,W),0.1*(C_MU_L(c,t)/C_R(c,t))/(C_WALL_DIST(c,t)*C_WALL_DIST(c,t)));
   C_UDMI(c,t,V2) = MAX(C_UDSI(c,t,V2),1.e-16);

   C_UDMI(c,t,CD_KW) = MAX(C_UDMI(c,t,CD_KW),1.e-10);

   C_UDMI(c,t,MU_T) = C_R(c,t)*C_UDMI(c,t,K)/C_UDMI(c,t,W);
   }
  end_c_loop(c,t)
  }
 }
}


/* ============================== Sources ==================================*/

DEFINE_SOURCE(k_source, c, t, dS, eqn)
{
 real S;

 S = C_UDMI(c,t,PROD_K);
 S -= BETA_STAR*C_R(c,t)*C_UDMI(c,t,W)*C_UDSI(c,t,K);
```

```
 S -=
2.*C_MU_L(c,t)*C_UDMI(c,t,F_EPS_W)/(C_WALL_DIST(c,t)*C_WALL_DIST(c,t))*C_UDSI(c,t,
K);

 dS[eqn] = - BETA_STAR*C_R(c,t)*C_UDMI(c,t,W) -
2.*C_MU_L(c,t)*C_UDMI(c,t,F_EPS_W)/(C_WALL_DIST(c,t)*C_WALL_DIST(c,t));

 return S;
}

DEFINE_SOURCE(omega_source, c, t, dS, eqn)
{
 real S;

 S =
C_UDMI(c,t,FT)*C_UDMI(c,t,GAMMA)*C_R(c,t)*sqrt(C_UDMI(c,t,V2)/C_UDMI(c,t,K))*Strai
nrate_Mag(c,t)*(0.3*C_UDMI(c,t,W));
 S -= C_UDMI(c,t,BETA)*C_R(c,t)*C_UDMI(c,t,W)*C_UDSI(c,t,W);
 S += C_UDMI(c,t,FT)*2.*(1.-
C_UDMI(c,t,F_1))*C_R(c,t)*SIG_W_2*C_UDMI(c,t,DK_DW)/(C_UDMI(c,t,W)*C_UDMI(c,t,W))*
C_UDSI(c,t,W);
 S -=
2.*C_MU_L(c,t)*C_UDMI(c,t,F_EPS_W)/(C_WALL_DIST(c,t)*C_WALL_DIST(c,t))*C_UDSI(c,t,
W);

 dS[eqn] = - C_UDMI(c,t,BETA)*C_R(c,t)*C_UDMI(c,t,W) -
2.*C_MU_L(c,t)*C_UDMI(c,t,F_EPS_W)/(C_WALL_DIST(c,t)*C_WALL_DIST(c,t));

 return  S;
}

DEFINE_SOURCE(V2_source, c, t, dS, eqn)
{
 real S;

 real wt =
8.0*Strainrate_Mag(c,t)+7.0*C_UDMI(c,t,W)*(C_UDMI(c,t,K)/C_UDMI(c,t,V2));

 S = C_UDMI(c,t,FT)*C_UDMI(c,t,V2)*C_UDMI(c,t,PROD_K)/C_UDMI(c,t,K);
 S -= BETA_STAR*C_R(c,t)*C_UDMI(c,t,W)*C_UDSI(c,t,V2);
 S -=
2.*C_MU_L(c,t)*C_UDMI(c,t,F_EPS_W)/(C_WALL_DIST(c,t)*C_WALL_DIST(c,t))*C_UDSI(c,t,
V2);
 S += CT1*C_UDMI(c,t,FT)*C_R(c,t)*wt*(C_UDMI(c,t,K)-C_UDSI(c,t,V2));

 dS[eqn] = - BETA_STAR*C_R(c,t)*C_UDMI(c,t,W)*sqrt(C_UDMI(c,t,V2)/C_UDMI(c,t,K)) -
2.*C_MU_L(c,t)*C_UDMI(c,t,F_EPS_W)/(C_WALL_DIST(c,t)*C_WALL_DIST(c,t))
           - CT1*C_UDMI(c,t,FT)*C_R(c,t)*wt;

 return S;
}
```